STUDY OF WETTING PHENOMENON DURING COOLING OF CURVED SURFACES USING IMPINGING WATER JETS

STUDY OF WETTING PHENOMENON DURING COOLING OF CURVED SURFACES USING IMPINGING WATER JETS

By

MUHAMMAD AKMAL,

B.Sc.

A Thesis

Submitted to the School of Graduate Studies

in Partial Fulfillment of the Requirements

for the Degree

Master of Applied Science

McMaster University

MASTER OF APPLIED SCIENCE (2004) McMaster University

(Mechanical Engineering) Hamilton, Ontario

TITLE: Study of Wetting Phenomenon during Cooling of Curved Surfaces using Impinging Water Jets

AUTHOR: Muhammad Akmal,

B.Sc. (University of Engineering and Technology, Lahore, Pakistan)

SUPERVISOR: Dr. M.S.Hamed

Department of Mechanical Engineering

NUMBER OF PAGES: xvii, 121

ABSTRACT

Wetting phenomenon during cooling of hot cylindrical specimens using Impinging Jet of water has been studied. Effect of jet velocity, jet diameter, water temperature, specimen surface temperature and surface curvature on propagation of wetting front has been analyzed. Propagation of wetting front correlated well with power function of time. Experiments were conducted at specimen surface temperatures of 250,500 and 800°C. Water temperatures of 20, 50 and 70 or 75 or 80°C were employed with Jet velocities of 5 and 7.75m/sec. Jet diameters of 3mm and 4mm were utilized during experiments. Propagation of wetting front strongly depends upon water temperature. Wetting front grows faster at low water temperature and high jet velocities. For constant water temperature, growth of wetting front is high with high jet velocities. Velocity of wetting front increases with jet diameter of 4mm when compared with that of 3mm due to increase in mass flow. The influence of jet diameter is greater for low water temperature, low surface temperature and high jet velocities. Effect of jet velocity and degree of sub-cooling on constant "a" and exponent "n" of the power relation are studied. Constant "a" is found to be linear function of jet velocity and degree of sub-cooling. Exponent "n" appears to be independent of jet velocity but weekly dependent on degree of sub-cooling.

Propagation of wetting front with time was analyzed in comparison with the transient temperature drop of material for different thermocouples embedded at stream wise locations within specimen at a distance of 1mm from surface. Temperature readings were used to predict the propagation of wetting front, which was found to be valid for a distance of 10mm from impingement point.

Effect of surface curvature was analyzed by comparing the results of present study with those reported by previous researchers. Surface curvature was found to have significant impact on propagation of wetting front.

ACKNOWLEDGEMENTS

I would like to dedicate this work to my father and mother. I would like to thank my wife for her support and encouragement that has enabled me to overcome difficult situations while undertaking this research work..

The author would like to thank the following people for their contributions to this work:

Dr.M.S.Hamed for his patience, continuous guidance, support and encouragement throughout the course of the master's work.

Dr. C.Y.Ching for his advice and suggestions during critical phases of this program. Andrew Buyers, Ron Lodewyks, Joe Verhaege and Dave Shick for their technical guidance and help.

Dr. Samir Ziada for his kind advice, trust and help during master's work.

Friends and colleagues of the Thermal Processing Laboratory (TPL) and Thermal Management Research Laboratory (TMRL) for their support and friendship.

TABLE OF CONTENTS

LIST OF FIGURES

LIST OF TABLES

NOMENCLATURE

a	constant	
D_j	Jet diameter	mm
g	acceleration due to gravity	m/s^2
$L_{s.}$	Scale factor	
R	Radius of wetting front	mm
R_e	Reynolds number, $R_e = \frac{V_j D_j}{\nu}$	
t	Time	seconds
Tw	Water Temperature	°C
Tsp	Initial specimen surface temperature.	°C
$\Delta Tsub$	Degree of subcooling	°K
V_j	Jet velocity	m/sec
ρ	specimen density	kg/m^3
ν	Kinematic viscosity	m^2/sec
k	Thermal conductivity	W/m-K

Chapter 1.

INTRODUCTION AND LITERATURE REVIEW

Efficient removal of high heat flux during different industrial processes is required for proper functioning of the components and overall systems. Methods employed to achieve this objective are the focus of research worldwide. Heat removal technologies include methods with single-phase, two-phase flow and other specialized techniques as shown below in Table 1.1.

Table 1.1. Heat Removal Technologies.

Single- phase flow cooling	**Two-phase flow cooling**	**Specialized cooling methods**
Convective Air Cooling Convective Liquid Cooling	Pool Boiling Falling Films Liquid Jet Impingement Flow boiling	Heat Pipes Thermoelectric devices.

Single-phase flow cooling, natural convection air cooling, although is reliable but limited by its low cooling capacity. Forced convection by addition of some source e.g. fan etc. can be used to enhance the heat transfer by this mode. Impinging air flows further enhance the heat transfer. But these techniques have their own limitations and are

employed in applications, where lower heat flux removal is required. For applications where high power dissipation is desired more efficient cooling technologies e.g. Liquid Cooling, Boiling or Heat Pipes is found to be useful.

Liquid cooling can achieve the desired result of high power dissipation but its use is limited due to potential problems e.g. leakage, corrosion, condensation, requirement of circulating loop etc.

High heat transfer rates can be achieved with moderate wall temperatures in cooling with two-phase flow. These include pool boiling, flow boiling and liquid film evaporation. In pool boiling with fluids, a hot material specimen is submerged in the pool of liquid and the boiling takes place at the hot surface. pool boiling is characterized by different stages i.e. free convection boiling, nucleate boiling, transition boiling and film boiling. In nucleate boiling region, high heat transfer coefficient with low temperature difference between the wall and fluid is obtained. Critical heat flux (CHF) in pool boiling limits the maximum dissipation of heat flux. Nucleate boiling followed by transition boiling accompanied by surface temperature overshoot along with the unsuitability of pool boiling for applications with space limitations make it less desired.

Falling film cooling is achieved by the flow of liquid driven by gravity and falling on a hot vertically placed specimen material. Boiling is created to enhance heat transfer over hot surfaces. Such a system requires a closed loop cooling chamber with condenser, reservoir and pump. This cooling technique has demonstrated promising results with higher convective heat transfer coefficients and higher CHF than for Pool boiling, but its

use is limited due to its lack of versatility in orientation, temperature overshoot and space requirements.

Spray cooling as the name signifies, employs slow stream of coolant over a large area and therefore provides uniform surface temperature. It operates by the continuous formation and evaporation of a thin liquid film which may lead to undesired thermal hysterisis.

Flow boiling cooling uses saturated or sub-cooled liquid flowing over the hot surface. In such systems the coolant is in direct contact with the heated surfaces or coolant moves through a channel which is directly attached to hot specimen. Higher flow velocities can lead to higher cooling rates in these systems because these enhance the coolant contact with hot specimen due to reduction in thickness of vapor layer on the specimen. Such a system requires evaporator, condenser, pump and many other components.

Heat Pipe is composed of a vacuum type envelope, a wick structure and a working fluid. It is filled with a small amount of working fluid under the vacuum conditions. It is composed of an evaporator side and a condenser side. As the heat enters the evaporator side, vapors are generated which travel towards condenser side. At condenser side a slight low temperature causes the fluid to condense giving up its latent heat of vaporization. Condensed fluid is then fed back to the evaporator side by capillary action in the wick structure. This continuous cycle has the capacity to transfer large amounts of heat with low thermal gradients. But Heat Pipes loose their lower thermal resistance at high power levels or due to continuous operation for a longer period of time.

For most cases Heat Pipes operate at fluxes below 20W/cm² [1].Thermoelectric devices like heat sink are used in applications where low heat flux removal is desired.

Liquid Jet Impingement Cooling (LJI Cooling) is characterized by the use of jets of liquid coolant at different speeds impinging on high temperature surface of material specimen. Very high cooling rate can be achieved with this technology as compared to pool boiling and falling film cooling with boiling on heated surface. Heat flux removal as high as 400MW/m² [2] has been reported through LJI Cooling. Heat transfer in this mode is influenced by jet size, Jet to material surface distance, jet type (circular, planar, slot jet, rectangular jet etc.), jet velocity, specimen material, surface temperature, surface finish, coolant type, coolant temperatures etc. Dependence of this mode of heat transfer on the abovementioned factors clearly demonstrates its flexibility, adaptability and controllability which also require further investigation and research. LJI Cooling is widely used in industry in its various forms for different applications. Figure 1.1 below shows a classification of main applications of LJI cooling:

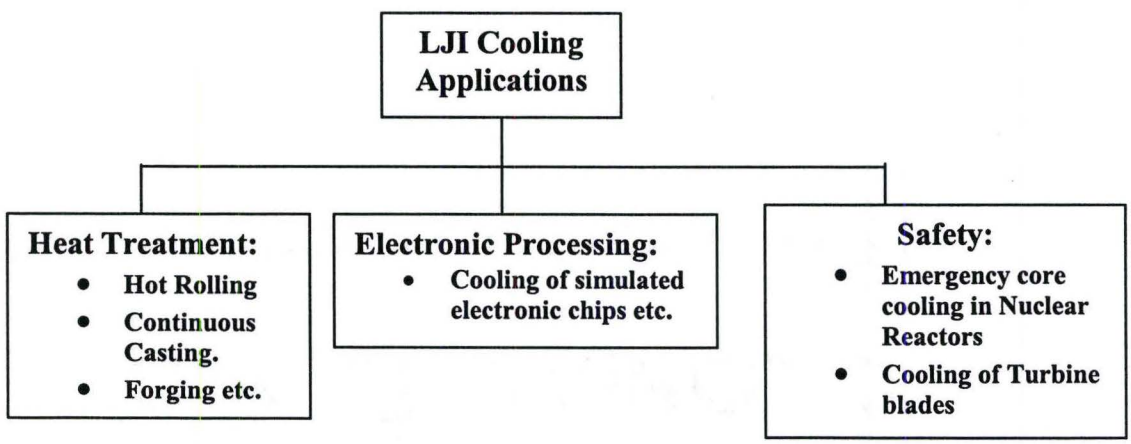

Fig.1.1. Classification of LJI cooling applications.

Keeping in view the above stated benefits of LJI Cooling in comparison with other cooling technologies and, its wide use in industrial applications have motivated this research work on the subject. Although different researchers have done commendable work in exploring various avenues of LJI Cooling on flat surfaces, but limited knowledge is available about the heat transfer from high temperature curved surfaces. As a first step in this direction, cylindrical surface was chosen and experiments were performed to investigate the effect of various parameters on cooling within the specimen and rewetting phenomenon.

1. LITERATURE REVIEW

1.1 Introduction

Liquid Jet Impingement cooling (LJI cooling), may be defined as the "Cooling of a high temperature material surface with high speed impinging Jets". A pictorial representation of LJI cooling for a high temperature stationary flat surface is given in figure 1.2. When a high temperature material surface is subjected to an evaporable coolant, the coolant undergoes different boiling stages, i.e. vapor blanket stage, nucleate boiling stage and convection stage.

As the hot material is subjected to coolant, the coolant evaporates and the resulting vapor forms a stable film on the surface. This stable film is known as the vapor blanket and from here the name come the vapor blanket stage. This blanket acts as an insulating layer on the surface preventing "surface wetting" and consequently keeping the heat transfer from the surface very low.

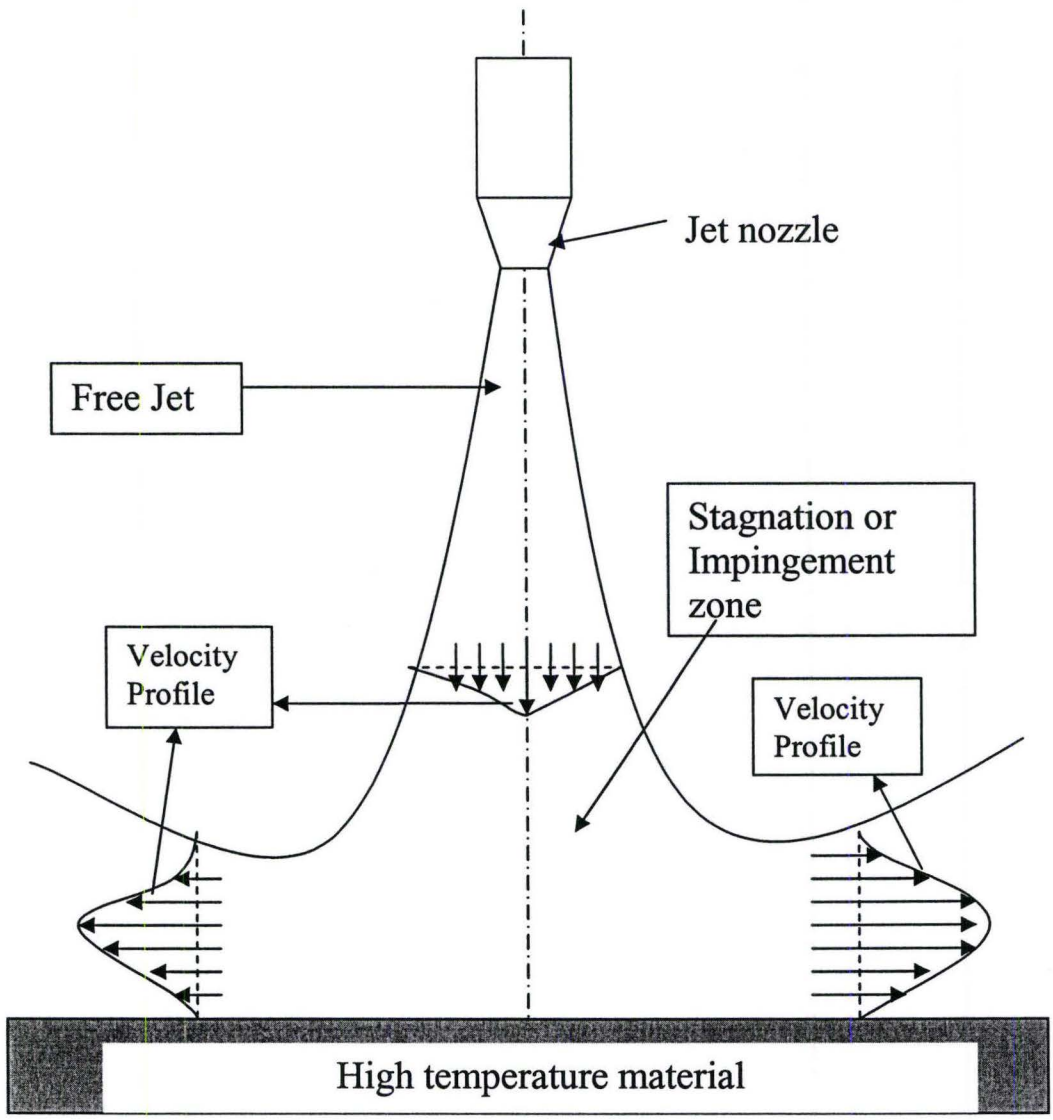

Figure 1.2-Schematic of the use of LJI cooling

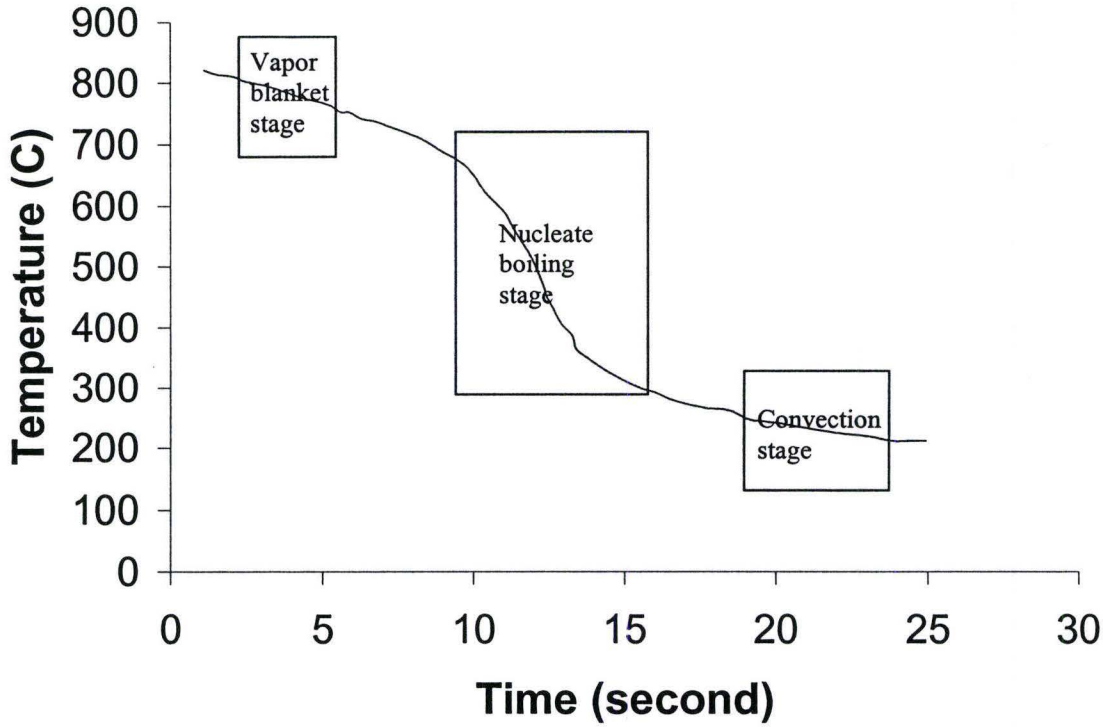

Figure: 1.3- Boiling Stages

Nucleate boiling stage starts when the surface temperature drops below a certain temperature known as the "Leidenfrost" temperature where the vapor blanket collapses and surface wetting starts. This is the stage of high heat transfer as compared to other boiling stages because of the direct contact of coolant with high temperature surface. This is the desired region of operation for many high heat flux cooling applications.

The convection stage starts when the material surface temperature decreases below the coolant's boiling temperature. Heat Transfer during this stage is due to convection only. Controlled cooling depends upon the knowledge of different stages, their occurrence and flexibility to control their occurrence.

1.2. Applications.

LJI cooling is distinguished by its ability to remove heat fluxes at high end of cooling spectrum [3]. It is extensively used in various Industrial applications where high heat flux removal coupled with desired mechanical properties is the primary concern for the final product. In material processing industry, the product quality from many manufacturing processes depends on thermal response of the material to the cooling technique employed. Product quality means the physical dimensions as well as the mechanical properties. In hot rolling, continuous casting and forging operations Jet impingement technology is employed to control cooling rates which affect solidification, phase transformation and other temperature dependent processes.

Controlled water cooling systems are used along the run out table in hot strip mills to cool hot steel strips. Such cooling process is essential for determining the final mechanical properties and flatness of steel strips. Liu and Fraser [4] have simulated this run out table operation and constructed a run out table facility at University of British Columbia. They studied the effects of cooling water temperature and impingement velocity on heat transfer from stationary steel plate.

Demand to dissipate more power densities are increasing continuously. Cooling in controlled nuclear fusion require very reliable high heat flux design necessary to avoid Loss of coolant accidents (LOCA) in nuclear reactors. In LOCA in a light-water reactor the clad surface temperature of fuel rods rapidly increases because of the release of stored energy in fuel. This heat energy can not be removed by surrounding steam. In order to avoid any damage, the emergency core cooling system injects water in the reactor core to

keep clad from overheating and re-establish cooling by rewetting the clad surface after film boiling [5]. LJI cooling plays a crucial role in safety applications. Various researchers have studied the re-wetting of hot surfaces keeping in view the loss of coolant accident.

Mitsutake and Monde [6] have based their study on hypothetical accidents in fusion reactor i.e. Ingress of coolant accident, which can destroy the vacuum vessel and consequently release the radioactive particles contained. They studied the character of surface temperature, heat flux distribution with an observation of boiling phenomenon and growth of wetting region with time.

With rapid increase of electronic chip switching frequency the power densities have reached a stage where direct cooling of chips with liquids is now under investigation by various researchers. Mudawar and Wadsworth [7] studied the use of a confined rectangular jet to cool a simulated square chip (12.7x12.7mm^2).

1.3. Classification of Impinging Jets.

Impinging jets used in various forms for different applications can be classified on the bases of specimen surface, nozzle geometry and fluid flow. These include (1) Nozzle shape (circular or planar) (2) nozzle orientation relative to the surface (vertical or inclined) (3) free jet or submerged jet (4) working fluid (water, gas, air, polymers), (5) single jet or array of jets (6) confined wall jets (7) relative motion between jet and surface. Since jet impingement is used at places where high heat flux removal is required, changing any of the above stated features have a significant effect on heat transfer produced by jets.

Present research work is on free surface round jets impinging on hot curved surface. Round jet is selected for its uniform effect on the specimen. It is well known that the heat transfer produced by jets is significantly affected by jet conditions. Therefore a brief review of jet flow field is given before proceeding further.

1.4.Flow in Round Jets.

When a jet of liquid exits a nozzle it is broken down into three regions i.e. turbulence, transition (free jet) and stagnation (impingement) regions. The turbulence region is marked by the development of a shear layer near the field, increasing the turbulence intensity of flow as it moves downstream. Centre of jet in this region is called potential core within which the uniform exit velocity is retained and flow is irrotational. With increasing distance from the exit, momentum exchange between jet and ambient causes the broadening of jet free boundary and consequently contract the potential core.

At the end of potential core, transition region starts and in this region the flow transforms itself from shear layer dominated flow to a jet flow. This region of flow is also termed as free jet because of no effect of impingement surface. Velocity profile in this region is non-uniform over the entire jet cross section and maximum velocity (at centre) decreases as distance from nozzle exit increases.

In stagnation or impingement zone, flow is affected by the target surface. Flow is decelerated in the normal direction (z-direction) and accelerated in the traverse direction (r or x direction) horizontal to the impingement surface. But flow acceleration in the horizontal direction can not continue for long because of zero momentum fluid from ambient, the accelerating flow in this region transforms itself to decelerating wall jet.

Therefore with increase in r or x directions, the velocity of jet along the surface increases from a value of zero to maximum and then dies down to zero.

Impingement or stagnation zone has been the focus of attention of various researchers. Faggini and Grassi [8] argued that at a short distance upstream of impingement point the radial velocity component of jet starts increasing while axial velocity decreases to zero due to which the liquid pressure, close to wall, assume a bell shape distribution with maximum pressure at stagnation point and approaching ambient pressure at the end of impingement region on target surface (r* from the stagnation point). Length of the impingement region "r*" is claimed by Martin in 1977 (reported and verified by Faggini [8]) to extend up to 2 to 2.5 of internal nozzle diameter.

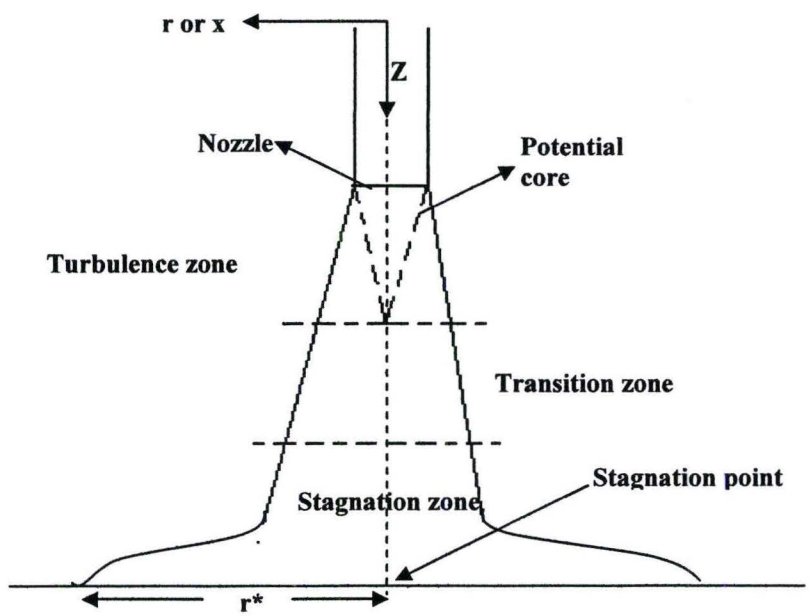

Figure 1.4: Flow regions of free jet.

Anno [9] theoretically studied the effect of jet velocity, gravity and surface tension on jet instability.

1.5.Heat Transfer by Impinging Jet:

The heat transfer produced by the impinging jet is a function of various variables and can be written in the non-dimensional form as:

$$Nu=Nu\ (R,Pr,\ Tu,\ H/D,\ r/D,\ *) \qquad (1)$$

Where: Re= Reynolds No., Pr=Prandtl No., Tu=Turbulence intensity, H/D= jet to plate distance and r/D= Lateral displacement from stagnation point, * = any other geometric factor.

Numerous investigations of heat transfer by free surface round jets impinging on hot solid surfaces of different materials of different geometries (mostly on flat surfaces) have been done by various researchers which show the effect of various parameters.

Parameters affecting the heat transfer can be divided into three categories.

In most of the Industrial applications, water is used as a preferred coolant because of its abundant availability, low cost and being environmentally friendly. Keeping in view the above discussion, liquid jet impingement cooling has a wide range of applications with a lot of potential for growth. It is governed by many parameters which give the flexibility and controllability as an added advantage.

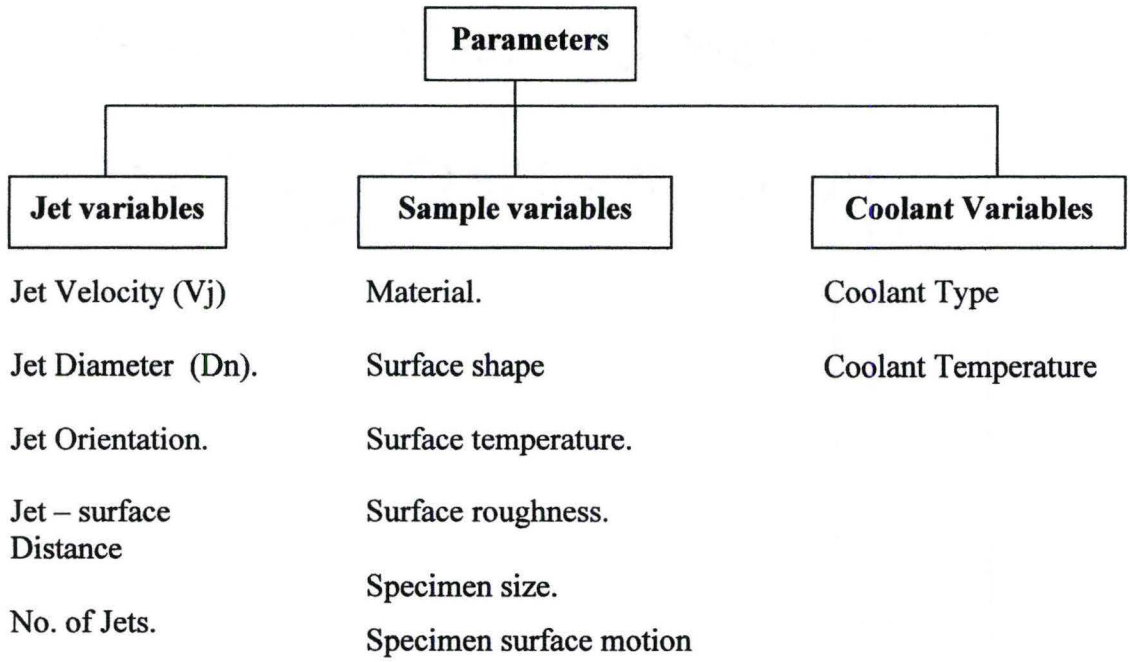

1.6. Investigations on LJI Cooling

LJI cooling has been the focus of various researchers in its various forms. Literature indicates that the versatility of LJI cooling attracted the investigators some where in 1940s-1950s. Jet Impingement cooling can be classified on the bases of work done by previous researchers. Experimental and analytical work has been done by researchers for both the steady state boiling heat transfer and transient cooling. A brief overview of investigations is given here.

1.6.1. Transient and Steady State Investigation.

The cooling effect of liquid jet impingement cooling was investigated by Nevins [10]. Water and oil were used in Jominy end quench tests. Nevins compared heat transfer

coefficients obtained from the transient cooling & steady state experiments for surface temperature of 200°C and found them to be differing by a factor of almost two. Nevins attributed this difference to the transient nature of impinging jets.

1.6.2. Steady State Investigations.

Copeland [11] investigated the steady state behavior of a saturated circular water jet impinging vertically upward on a horizontal flat nickel plated copper surface. Copeland found the net heat transfer to jet and net heat flux in nucleate boiling regime to be dependent on temperature excess, which is the difference between specimen temperature and saturation temperature, with no dependence on jet diameter, jet velocity and jet temperature. Ruch and Holman [12] confirmed the results of Copeland [11], film boiling heat flux was found to be independent of jet velocity and nozzle diameter. Jet velocity and jet diameter were instrumental in increasing the surface area of contact and consequently increasing heat transfer in nucleate boiling as well as film boiling regions.

Piggott [13] studied the factors affecting the initiation of wetting on hot rods, under steady state conditions, by impingement of a jet of water. Electrically heated rods of inconel, silica and gold materials were used and corresponding response of each material to different parameters was studied. Initiation of the wetting front, its oscillation and delay time for inconel and gold surfaces was measured. Piggott photographed several distinct regimes for both materials and found delay time to be strongly influenced by surface thermal conductivity. Piggot also found the rate of water re-wetting the surface to be strongly influenced by degree of sub-cooling of water (difference between saturation and coolant temperatures).

Pais and Chow [14] examined the effect of rotation of an array of jets about a radius arm on heat flux in jet impingement cooling on flat surface and found appreciable increase in heat flux with increase in flow rate because hot surface is wetted by a thin film of continuously replenished coolant. No effect of jet velocity, no. of jets and rate of rotation was observed. Heat flux decreased with increase in jet temperature because of reduction in sub-cooled boiling

Liu and Zhu [15] presented a simplified analytical model supported with experimental observations to predict critical heat flux of convective boiling of a saturated water jet impinging in stagnation zone. Model of maximum liquid subfilm layer based on Helmholtz instability was employed. Jet velocity and jet diameter were found to strongly affect critical heat flux in following manner:

$$q_{c,0} \propto Vj \quad \text{and} \quad q_{c,0} \propto 1/Dj \tag{2}$$

where Vj=jet velocity and Dj= jet diameter.

Liu concluded that for saturated water jet at atmospheric pressure:

$$q_{c,0} \propto (V_j/D_j)^{1/3} \tag{3}$$

Liu evaluated the following correlation and tested it against experimental data of critical heat flux:

$$\frac{q_{c,0}}{Gh_{fg}} = 0.132\left(1+\frac{\rho_v}{\rho_l}\right)^{1/3}\left(\frac{\sigma\rho_l}{G^2 d}\right)^{1/3}\left(\frac{\rho_v}{\rho_l}\right)^{1.4/3} \tag{4}$$

Since the thermal and physical properties are constant for saturated water under atmospheric pressure, the relationship between critical heat flux, jet velocity and jet diameter can be written as:

$$q_{c,0} = 0.36x10^6 (V_j/D_j)^{1/3} \quad (5)$$

Liu [16] in 2004 experimentally investigated the critical heat flux in nucleate boiling regime for a round sub-cooled water jet impinging on flat stagnation zone. Experimental observations indicated the insensitiveness of the boiling curve in the stagnation zone to sub-cooling which indicate that heat transfer in the nucleate boiling region at stagnation zone is dominated by bubble activity at the surface. Critical heat flux increases with increase in water sub-cooling due to increased liquid solid contact. Zhen-Hua Liu deduced that the above equation (5) derived for saturated water jet can be used for the sub-cooled water jet. Deduced the following empirical correlation for critical heat flux for sub-cooled liquids for pool boiling and forced convective boiling :

$$\frac{q_c}{q_{c,0}} = 1 + 11.82\left(\frac{C_{p,l}\Delta T_{sub}}{h_{fg}}\right) \quad (6)$$

1.6.3. Transient Investigations.

Akimenko [17] as reported by Ruch and Holman [12], observed the existence of a period of stable film boiling as a function of jet velocity during experimental investigation for the transient boiling of jets incident on flat plates .Ishigai et al [18] found shifting of characteristic points of boiling curve to higher heat fluxes and wall temperature with increase in sub-cooling and jet velocity. For sub-cooling higher than 55°C, no film boiling was observed for jet velocity of 2m/sec.

Miyaska et al [19] experimentally studied the effect of sub-cooling; jet velocity and stagnation pressure on critical heat flux and nucleate boiling in transient region. They provided the boiling curves for nucleate boiling regime.

Ochi et al. [20] deduced boiling heat transfer data in the region from stagnation point to radial distance of 24mm during impingement of a circular free surface jet. At stagnation point increasing the nozzle diameters decreased minimum film boiling heat flux and increases with increase in jet velocities and sub-cooling.

Tseng and Chen [21] investigated analytically and experimentally the heat transfer coefficients of jet impingement cooling on a hot rotating roll used as specimen. A thin film silicon sensor with fast response time deposited on a metal plug was used to measure the instantaneous surface temperature variations along the circumference of specimen. Finite difference scheme on the bases of measured temperatures was used to calculate temperature distribution and surface heat fluxes. At impingement zone, a peak value of 6000 W/m^2-°C and of 2000 W/m^2-°C in puddling region is reported.

Han and Chen [22], and, Chen and Kothari [23] investigated the effect of surface motion on heat transfer by impingement of round water jets with different jet velocity, jet diameter and speed of specimen surface. Surface motion stretched the water film in the direction of motion (downstream of stagnation point) and was shortened upstream. Drastic temperature drop observed at moving impingement point. Cooling zone appears to be elliptical. Increasing the moving speed results in shorter cooling zone length and smaller surface temperature drop due to decrease of surface tension & increase of

evaporation rate of water at high surface temperature and shorter residence time. They concluded that increasing the specimen speed enhances heat transfer rate.

Liu and Lien hard [2] investigated the factors limiting the heat fluxes in the stagnation zone by removing extremely high heat fluxes with high speed impinging jets. They heated the specimen to its melting point before doing experiments and concluded that heat flux removal is limited by thermal resistance of liquid, conduction resistance and material properties i.e. thermal stresses and melting point temperatures. Stagnation zone heat transfer depends upon the jet velocity.

Kumagai et al. [24] studied transient cooling on hot metal slab by jet impingement cooling. Found critical heat flux to be depending upon stream wise location and degree of sub-cooling. Critical heat flux found to be highest at stagnation point and decreases gradually with increasing distance from the impingement point for a given degree of sub-cooling.

Liu and Wang [25] proposed an analytical model supported by experimental study for film boiling heat transfer in the impingement zone for water jet impinging on flat high temperature surface. Proposed the following relationship for film boiling region:

$$q_w \alpha \left(V_s / d \right)^{1/2} \tag{7}$$

Where: q_w = wall heat flux, d is diameter of nozzle. and V_s is impingement velocity. Relationship for wall heat flux (q_w) and ΔT_{sat} found to be affected by water sub-cooling, which was expressed as:

$$q_w \alpha (\Delta T_{sat})^n \tag{8}$$

Where: n=1/2 for high water sub-cooling and n=3/4 for saturated case.

Liu examined his analytical model by comparing experimental results.

Hall [26] experimentally studied boiling heat transfer during cooling of cylindrical copper disk by sub-cooled water jet. Local measurements of boiling in the stagnation and radial flow regions are compared with correlations from steady state experiments. Visual observations were recorded for different stages of cooling as the jet impinged. Radial distribution of maximum heat flux correlated well with relations developed by Monde [27]. Minimum film boiling heat flux decreased with radial location. Minimum film boiling heat flux depends upon jet hydrodynamics.

Liu and Fraser [4] studied the effect of cooling water temperature and impingement velocity by a circular water jet on heat transfer from a steel plate. Experiments were performed at high steel temperatures of 700 to 900°C. Cooling water temperature appeared to have little effect on heat transfer in the impingement zone because of already high heat transfer rate in this region. Away from the impingement zone, water temperature significantly affects the cooling rate with respect to time. Water at low temperature tends to cool the specimen at higher rate than the water at higher temperature. Liu deduced that lower cooling water temperature lead to faster expanding impingement zone or wetting front which was evident from the cooling curves for different water temperatures.

Cooling intensity of jet is strongly affected by the impingement velocity. With increase in jet velocity for given water temperature the cooling intensity of jet is enhanced and consequently increases the velocity of wetting front.

Mitsutake and Monde [6] experimentally studied transient boiling heat transfer due to jet impingement on hot flat surface of cylindrical block. The initiation of wetting front for different materials (copper, brass and steel) was observed, they found the time after impingement of jet during which surface remained un-wetted becomes larger for materials with larger thermal inertia $(\rho c\lambda)^{1/2}$. Growth of wetting region was also observed. Solid liquid first contact was established at stagnation point of jet. Wetting region starts spreading from stagnation point to the circumference of specimen. Three heat transfer regions were identified from the centre. These regions are single phase forced convection, nucleate boiling and dry regions. An annular shape of very small width designated by Δr_b appearing to be of white color marked the occurrence of nucleate boiling regime. This annular ring then appears to spread from stagnation point to the circumference of specimen and seems to be limited in the area close to solid-liquid contact line.

Value of Δr_b appeared to depend on the degree of sub-cooling and material of block as it decreased with increase in sub-cooling and thermal conductivity of material. This fact is governed by a combination of factors, i.e. heat removed by cooling of liquid film and heat transferred by conduction in solid. An increase in cooling by liquid film reduces boiling area due to lack of heat conduction in solid. So increase in cooling by liquid film reduces boiling area because of low conduction in solid. But for a constant cooling rate by liquid, an increase in thermal conductivity supplies enough heat to enlarge boiling area.

Mitsutake and Monde compared the growth of wetting front for different materials with time for velocities (5, 10 and 15 m/sec) for sub-cooling of 50°K and found it to increase with increase of jet velocity, degree of sub-cooling and influenced by thermal conductivity of material. They approximated each curve by a tentative function of the position, r_{wet}, as power function with respect to time as given by the following equation:-

$$R_{wet} = at^n \tag{9}$$

The values of constant "a" and exponent "n" were plotted against jet velocity and degree of sub-cooling. Constant "a" has a linear relationship with jet velocity and degree of sub-cooling. Exponent "n" was found to be independent of jet velocity and thermal conductivity of material but weakly depending upon degree of sub-cooling.

Mitustake measured temperature at 8 locations within the material at depth of 1mm and 5mm from the surface. Solution of 1-D heat conduction showed that time delay between surface temperature estimated and temperature measured at plane of 1mm is very low for even a material with lowest thermal conductivity i.e. carbon steel, therefore, the temperatures measured at depth of 1mm were considered as temperature of surface. The discretized 2-D energy balance equation was used for calculation of surface heat flux using measured temperatures at different depths. Results show that peak heat flux initially existed at stagnation point and it moves outwards with decreasing value with time. Peak heat flux at a radial position occurs at place where nucleate boiling region exists.

Recently Haukson et al. [28] has experimentally investigated transient heat transfer in a steel plate by jet impingement cooling. Cooling curves were plotted for different points away from stagnation point and progression of wetting front estimated using temperature measurements and visual observations. Trends show similar effects of jet sub-cooling and flow rate on cooling and heat flux as determined by Mitsutake [6]

1.7. Objectives of Present study.

The above discussion demonstrates the enormous work done on jet impingement cooling. But due to the complexity of appearance of various regimes during heat transfer by jet impingement and its dependence on various factors, it is not yet fully explored. Mitsutake [6] has demonstrated the importance of study of wetting of hot surfaces. Haukson et. Al [28] has investigated spread of cooling effect on target surface. Most of the above stated investigative work has been done on flat surfaces. Although Piggot [13] has studied the delay time on cylindrical rods of inconel, silica and gold but spread of wetting front with time and its effect on cooling on hot cylindrical surface has yet to be investigated. Further the materials used by Piggot are not the ones frequently used in the industry.

Keeping in view the above discussion and importance of wetting of surface in jet impingement cooling, it is intended to study the wetting of hot cylindrical steel pipe instrumented with thermocouples. An effort has been made to study the wetting phenomenon, spread of wetting and cooling rate at the surface in transient mode. SS304

pipe of following thermal properties was selected because of availability of investigations on flat surface with the same material for comparison purposes as well as its wide use in industry:-

- at 100°C, K = 16.2 W/m-°K.
- at 500°C, K= 21.5 W/m-°K.
- $\rho = 8000$ Kg/m^3.
- at 100°C, C = 500 J/kg- °K.

Previous work on flat surfaces has shown that wetting of hot surfaces is greatly affected by the following parameters:

- Jet velocity.
- Jet diameter.
- Degree of sub-cooling.
- Specimen surface temperature.

Therefore during the present study an effort has been made to study the effect of the above stated factors on spread of wetting front and rate of cooling of surface.

Chapter 2.

Experimental Facility.

An experimental facility was designed to investigate the effect of jet velocity, jet diameter, water degree of sub-cool and specimen surface temperature on propagation of wetting front and specimen surface cooling rate by jet impingement cooling on a hot cylindrical stainless steel pipe. Experiments were performed in transient mode at three stages of specimen surface temperature, low temperature (250°C), medium temperature (500°C) and high temperature (800°C). Effect of jet impingement velocity is studied for two water velocities i.e. 5m/sec and 7.75m/sec. Jet diameters of 3mm and 4mm, and, water temperatures of 20, 50 and 70 or 75 or 80°C are employed during experiments, resulting in 80,50and 30 or 25 or 20°C degrees of subcooling.

Thermocouples were instrumented within the specimen at 1mm from the surface to study the effect of above stated parameters on cooling rate. Experimental facility is composed of three sections, fluid handling and water circulation section, specimen handling and instrumentation section, and high speed imaging and support structure section. Major parts of the experimental facility are shown in Figure 2.1.

2.1. Fluid handling and water circulation.

2.1.1. Water reservoir.

It is an enclosed stainless steel cylindrical tank (diameter=0.6m, height=0.9m) fed from municipality water supply by opening of 6.4cm diameter at top center of water tank.

Inlet water temperature is approximately 23°C. It has three water lines: 3.8cm nominal diameter stainless steel water pipe supply line at bottom of water reservoir, bypass line: 2.5 cm nominal diameter stainless steel water pipe on circumference of water reservoir at 78.8cm from its bottom, and, water return line: 3.8cm nominal diameter stainless steel opening at circumference of the water reservoir at 86.4cm from its bottom. Water lines along with other components are shown in figure 2.2.

Supply line supplies water to the system through a water pump. To flush the system a drain line located at bottom of water reservoir connected through a t-junction and elbow to supply line is used. Flow is controlled by a full port ball valve connected to 1.3 cm diameter hose pipe used to drain in municipality drain.

Bypass line along with bypass valve (ball valve) is instrumental in controlling the flow rate to vary the jet velocity which is one of the parameters in the present study. Bypass line is connected through a t-junction to 2.5 cm nominal diameter water line after exit from water pump.

Water return line is used to transmit water after impingement on specimen surface during experiment from collecting tank back to water reservoir where it is re-circulated. Return line is connected at one end with the bottom of collecting tank and other end to water reservoir via a hose barb assembly.

A T-type thermocouple placed on the side of water reservoir at 46 cm from its bottom is used to monitor the average temperature of the water through data acquisition system. Thermocouple is fitted with a swage lock fitting.

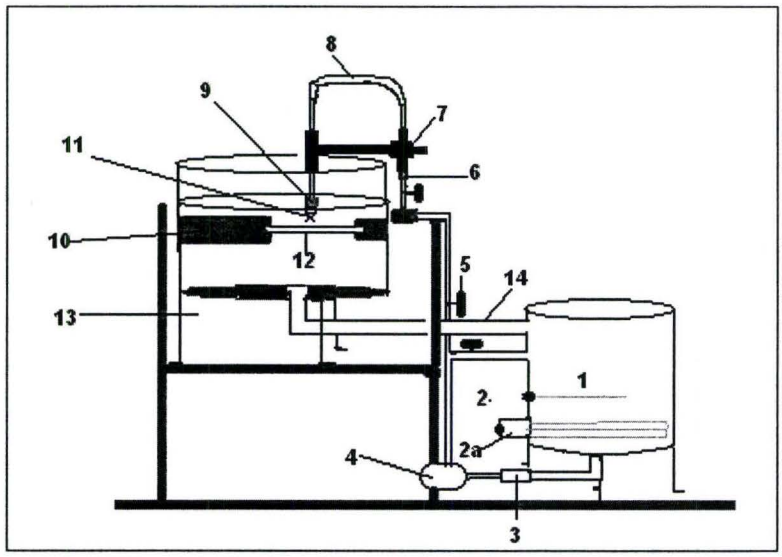

Figure 2.1:Components of fluid flow. 1-Main water reservoir, 2-T-type thermocouple, 2a-Immersion heater, 3-Strainer, 4-Water pump, 5- Control valve, 6-Turbine flow meter, 7-Nozzle positioning tool, 8-Flexible hose pipe, 9-Pipe probe thermocouple, 10-Specimen holding mechanism, 11-Nozzle, 12-Specimen, 13-Collecting tank, 14-Water return pipe.

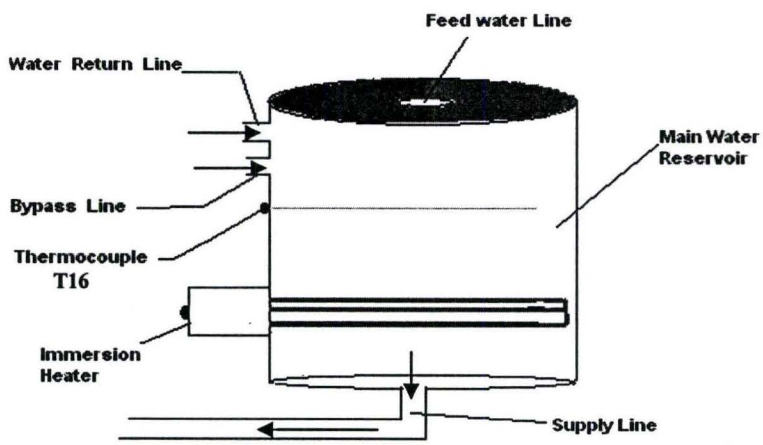

Figure 2.2- Water reservoir

2.1.2. Immersion water heater:

A 240 volts, single phase, 5kW; immersion heater with a thermostat range of -10 to 120 °C is installed in the water reservoir at 15.2 cm from its bottom. This position is chosen for uniform heating of water in the reservoir by the flow of heated water from the bottom of the water reservoir upwards due to density difference. Immersion heater has a screw plug with 1" NPT brass fitting and copper sheath. Length of the copper sheath is 43 cm. Immersion Heater sizing calculations are included in appendix -1.

2.1.3 Flow loop, pump, valves and fittings.

A pictorial representation of the flow of water from water reservoir through main components of the system is shown in figure 2.3.

Water pump suction and discharge area components are shown in figure 2.4. Two unions, one on suction side and other on discharge side are installed to add flexibility to the system. A Y-strainer of bronze construction with mesh screen no. 20 is used to protect the pump from solid particles etc. Mesh screen No.20 has the capability to block the particles as small as 5 microns.

Water pump employed is an SS centrifugal pump manufactured by EBARA International. This pump is ½ horse power pump with synchronous speed of 1725 RPM. Pump selection calculations are included in appendix -2 .The Performance curves of pump are also included in appendix-2.

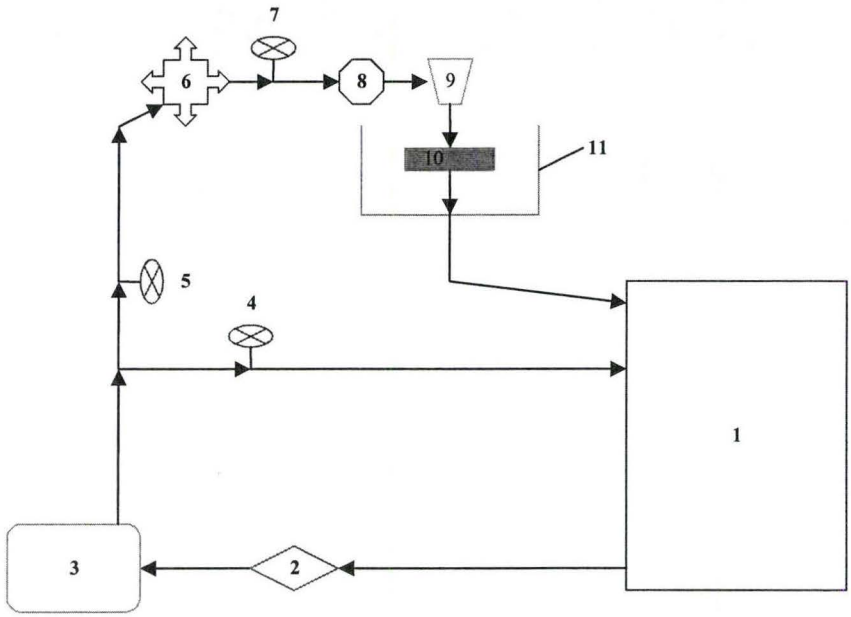

Figure 2.3. Flow loop 1- Water reservoir, 2- Y-strainer.3-Centrifugal water pump. 4-Bypass valve.5. Flow control valve. 6- 4way distributor. 7-Branch control valve. 8-Turbine flow meter. 9-Nozzle, 10- High temperature specimen. 11- Collecting tank.

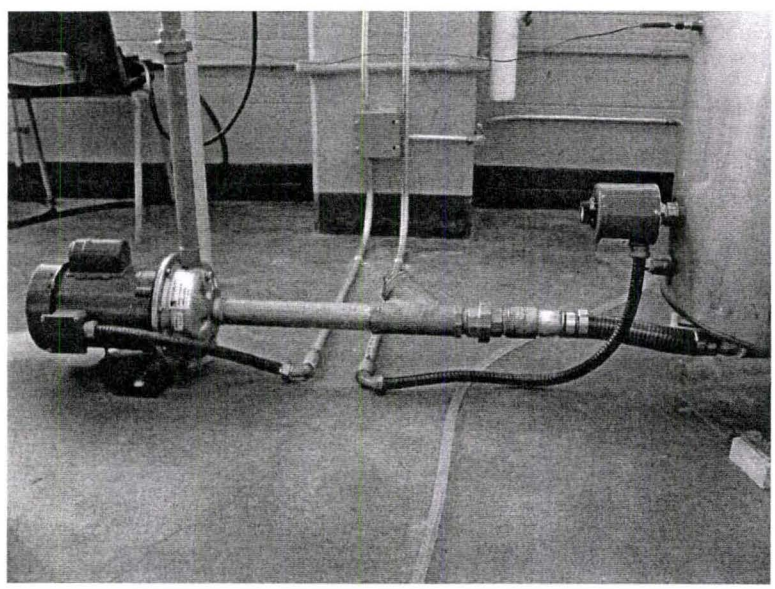

Figure 2.4 Water pump, pump suction and discharge area, unions, y-strainer and Immersion heater.

Water pump discharge pipe is a 2.54 cm nominal diameter schedule 40 pipe connected through a t-junction on one side to bypass line and flow control valve on other side. Flow control valve is a globe valve used in conjunction with bypass valve to control flow rate for changing jet velocity. Water then flows through a 4- way distributor shown in figure 2.5.

A wooden support is built in -house for supporting the water line and to absorb any vibrations due to working of water pump. These are two in number and are made to hold the water pipe snuggly by the use of an SS strap as shown in the figure-2.5

4-way distributor was designed keeping in view the expansion of the project from single impingement jet to 4 impingement jets. It is made from a 5 cm nominal diameter SS schedule 40 Pipe with one end sealed by welding with SS sheet and providing 4 equally spaced outlets (90°) for 1.3 cm nominal diameter SS schedule 40 pipes welded at its circumference. Three standard views and the isometric view of the 4-way distributor are given in the drawing i.e. figure 2.6. Figure 2.5 shows the 1.3 cm nominal diameter SS pipes welded on the circumference of 4-way distributor. 3 out of 4 of these pipes are closed by SS end caps as shown. The remaining one pipe is used to supply the water to the nozzle for impingement on specimen surface, through a globe valve. Water flows through a turbine flow meter which is used to measure the flow rate through data acquisition system.

2.1.4.Turbine flow meter:

A Turbine flow meter made by Simark Controls, model 5.05 H is used to measure water flow rate. It is of hexagonal body and has a Magnetic Pickup to sense the flow fluctuation

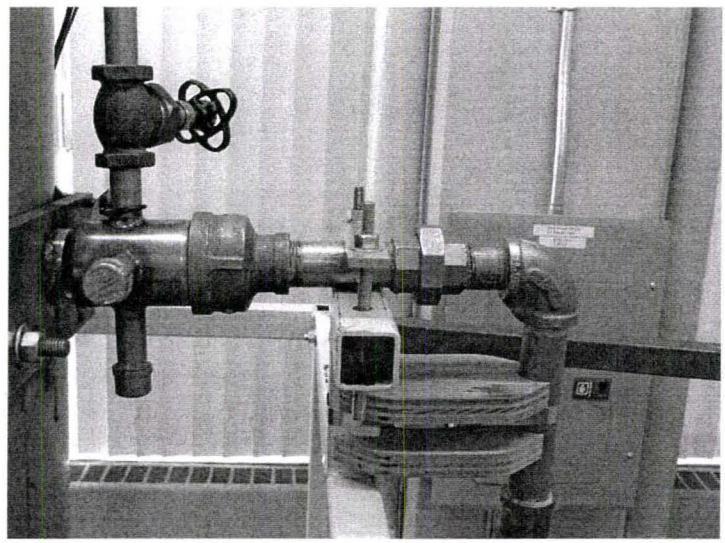

Figure 2.5: 4-way distributor and wooden support.

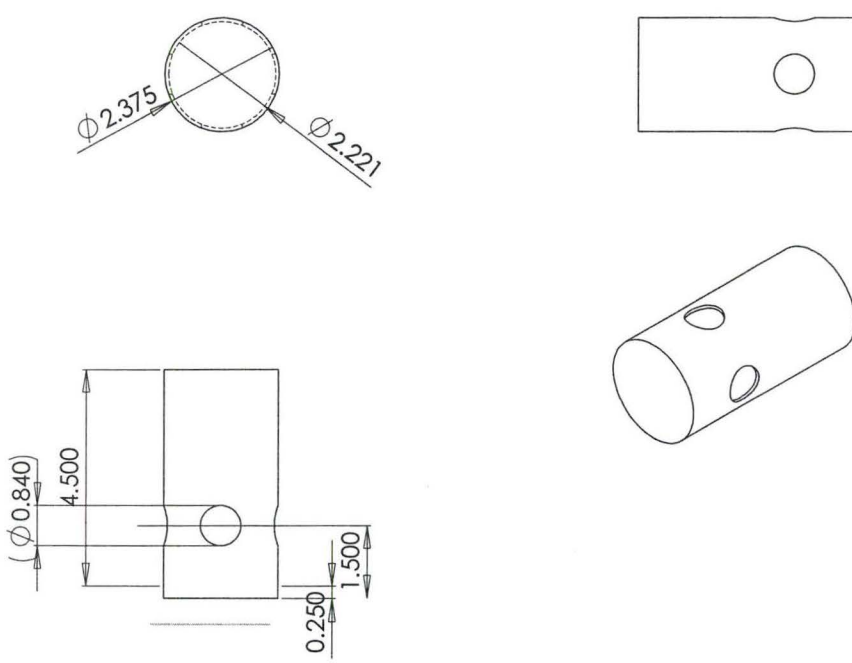

Figure 2.6. 4 way distributor drawing views

for measuring flow through a signal amplifier built in-house and subsequently reading of signal by connecting to the data acquisition system (explained later). Flow meter is provided with a shielded cable for reducing the noise effect etc. Flow meter has an accuracy of ±1 % of Indicated flow. Velocity of impinging jet (Vj) was thus calculated on the bases of following formula:

$$Vj = \frac{Qn}{An} \tag{9}$$

where Qn = Average flow through the nozzle (GPM) measured through DAQ by Turbine flow meter; An= Area of the nozzle = $\frac{\pi}{4} Dj^2$ and Dj= Diameter of the nozzle, i.e. 3mm and 4mm.Consequently jet impingement velocity (Vj) was maintained with ±3% accuracy.

2.1.5. Jet Positioning Setup.

Water from turbine flow meter passes through a flexible hose pipe assembly to enter 1.3 cm nominal diameter SS schedule 40 pipe held and positioned by a jet positioning tool which is used to position the pipe on the other end of which lies nozzle through which water flows to impinge on hot steel specimen during the experiment. Jet positioning tool is designed to add flexibility to the facility for adjustment of position of water Jet on the specimen surface. Due to this tool, jet nozzle has 4 degrees of freedom. Out of 4 degrees three are in planar directions and one is in azimuthal. A closer view of this tool is given in figure 2.7.It is composed of carbon steel pipes welded together perpendicular to each other. One is positioned on water pipe with set screws. Other pipe

position the water pipe with jet. This positioning tool is instrumental in positioning and repositioning of the nozzle.

Water pipe shown in Figure 2.7 is connected to a t-junction. This t-junction along with a K-type omega pipe probe thermocouple is used to measure the temperature of water just before its entering in the nozzle. This thermocouple is connected to data acquisition system through a 20 AWG fiberglass insulated stranded thermocouple wire with Stainless Steel over braiding.

2.1.6. Nozzles:

Nozzle is fitted on t-junction connected to water pipe. It is a unijet solid stream spray nozzle of brass body and tip. John Brooks nozzles with two different orifice diameters of 3mm and 4mm are employed for the experiments.

2.1.7 Collecting tank:

After jet impingement on the hot specimen surface, water is collected in a collecting tank, which is an SS tank with outside diameter of 0.7m, wall thickness 0.32 cm and height of o.6m. Its bottom is elevated to a height of 1.3m from the floor and its three welded legs are bolted onto the support structure. Collecting tank is connected with a flexible hose pipe to return water through return water line to water reservoir for re-circulation.

2.1.8 Water splash guard.

Keeping in view the splashing of water after impingement of water jet on hot specimen surface, a water splash guard was prepared in-house for protection of personal, electrical installations and equipments. This splash guard is made of the same material as of collecting tank and is mounted on it. Four equally spaced support brackets welded on int-

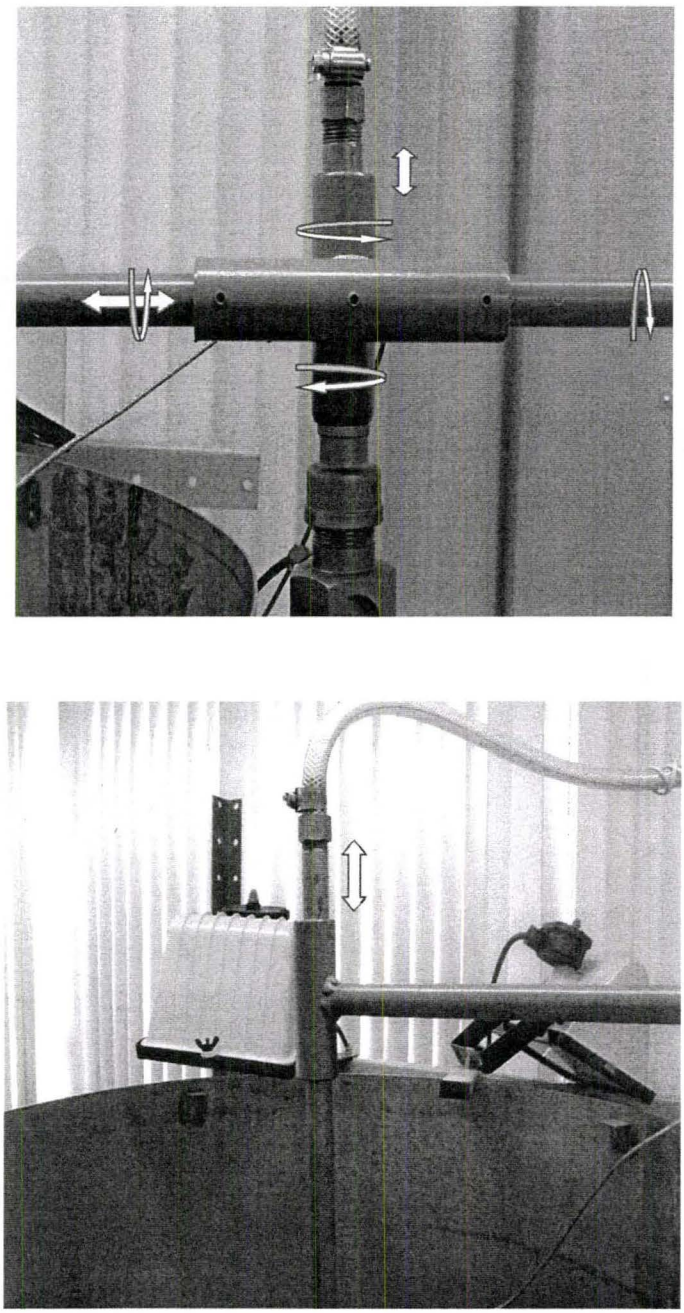

Figure 2.7: Two different views of the positioning tool with its degrees of freedom.

rnal diameter of the collecting tank are used to support the splash guard. It is provided with a rectangular {51 cm .x 19 cm x 1.3 cm} acrylic window to view the propagation of wetting front and also the condition of the sample. Acrylic window is bolted with the splash guard.

2.2. Specimen Handling and Instrumentation.

2.2.1. Moveable Specimen Cover Mechanism.

To view propagation of wetting front a specimen cover mechanism was designed and built in-house. This mechanism performs several important functions which facilitates the establishment of required experiment conditions and is instrumental in instantaneous start of experiment. Functions of this mechanism are discussed below:

- Isolates the specimen from ambient air and water to heat specimen surface to required temperature.
- Allows adjustment of water flow and consequently the jet velocity for experiment.
- Removes the cover instantaneously after achievement of required experimental conditions to establish instantaneous exposure of specimen surface to impinging water jet.

The Specimen cover mechanism is composed of a large number of parts, sub assemblies and major assembly.

2.2.1.1. Specimen Cover Assembly.

It is used to cover the specimen during heat up time and provide thermal insulation for it. It is composed of 4 identical SS plates with upper portion cut into V-shape. Two of these plates are joined together with a 23.5 cm long SS sheet fastened with set screws of 0.5

cm diameter, when pulled with attached spring loaded mechanism, cover slides on guide pipes. Specimen cover is shown in the figure 2.8. Rest of the two SS plates are joined together with a 10cm long SS sheet with set screws of 0.19 cm diameter, but not connected to the spring loaded mechanism to make it "stationary cover" of assembly shown in figure 3.8. Two guide rods are 1.3 cm nominal diameter schedule 80 SS pipes (length= 71 cm). The Ceramic tube shown here is used to isolate the specimen. It fully covers the specimen when both the "stationary cover" and "moving cover" are joined together before the start of heater for heating the specimen surface to the required temperature. The empty space between Alumina ceramic tube and SS sheet is stuffed with high temperature thermal insulation.

Two identical SS plates (20cm x 10cm x 1.3 cm) are welded on both sides of the collecting tank. These hold the guide rods and consequently keep both the specimen covers aligned. Two 3.8 cm nominal diameter schedule 80 SS pipes (length = 20 cm) welded with these SS plates on inside end of collecting tank. Other end of pipe is cut to form a "holding jaw" for the specimen. The specimen is held here in the two finger type jaws in the middle of the collecting tank. The ceramic tube in the "moveable cover" has enough clearance to slide back and forth without much resistance on the SS pipe on its end which acts as the guide for specimen along with thermocouples.

2.2.1.2 Spring Loaded Assembly:

Moveable specimen cover is attached to a spring loaded assembly which is used for its instantaneous pulling as experimental conditions are achieved and a test is desired to be run. It is composed of a SS rod bolted with "moveable cover" inside the collecting tank

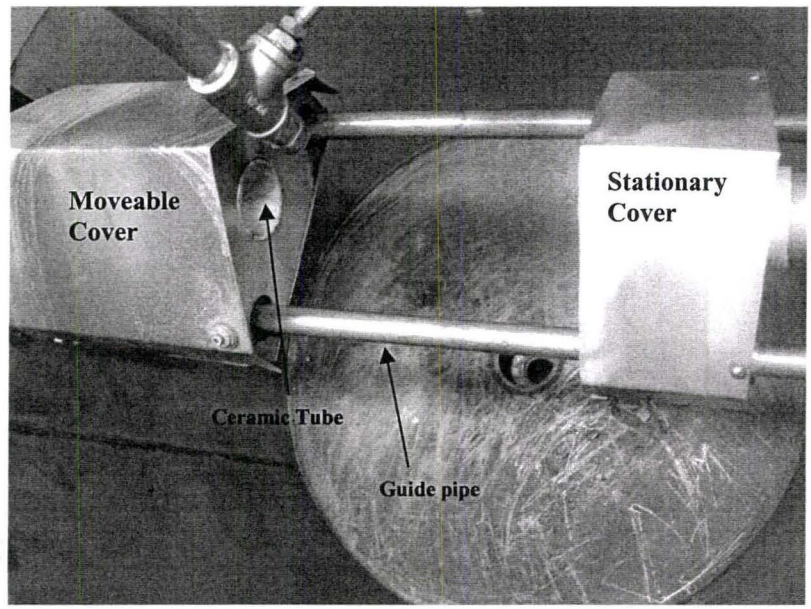

Figure 2.8: Specimen Covers

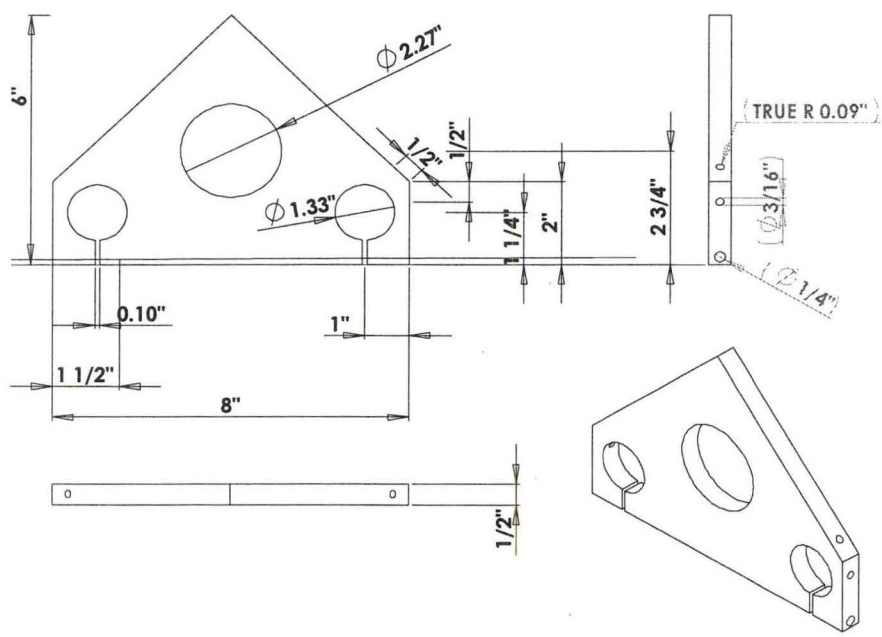

Figure 2.9: Details of specimen cover.

with SS bolt of 0.5 cm diameter. It is termed here as "cover placement rod" which is an SS Rod of 1cm outer diameter and length = 1.5m. Three standard views and one isometric view of the welded SS plate are given in figure 2.11

The cover placement rod is bolted on with a SS bracket which is bent and welded with SS steel plate of moveable cover shown in figure 2.10. Both the moveable and stationary covers are press fitted with brass bushings, made in the mechanical workshop for smooth movement of moveable cover on the guide rods. Outside the collecting tank, there is a spring loaded assembly shown in the figure 2.12.

It consists of two SS rods each with 1.9 cm diameter, two springs attached through custom made SS bushings. These SS bushings have press fitted nylon bushings for smooth movement of the "cover placement rod" with minimal friction. All the above stated bushings and rods were prepared and assembled in-house by the use of precision grinding , milling machines and special tools.

The SS bracket shown in figure 2.12 is a moveable bracket and performs three functions:

1. Keeps the support rods aligned.
2. Adjusts the stopping point by the adjustment of spike (retractable lever) and consequently the adjustment of "moveable cover".
3. "Mounted stopper lever" is used to keep the "spike" loaded with springs, during heating of the specimen while "moveable cover" is covering the specimen , and , release the "spike" to uncover the specimen for instantaneous start of jet impingement.

SS bracket is 1.3 cm thick SS plate cut into three pieces as shown by dotted lines in figure 3.15 and has four 1.3 cm diameter threaded holes for 3.8 cm long threaded bolts which are used to hold the support rods for their alignment. Stopper SS lever is attached loosely to SS plate through 0.6 cm diameter nut and bolt for its frictionless movement. Another similar SS bracket is used to keep the ends of the both the "support rods" and "cover placement rod" aligned.

2.2.2. Instrumentation.

2.2.2.1. Preparation and Instrumentation of Thermocouples in Specimen.

Specimen was made from a Stainless Steel pipe of 1.9cm(¾ in.) nominal diameter XXH SS316 of following dimensions:-

- Outer diameter = 1.05 in= 26.67mm
- Inner diameter = 0.434in= 11.02mm.
- Length = 12 in=304.8mm.

Two stainless steel pipes were used to get one specimen. Each one was cut longitudinally into two unequal portions; the one portion out of each specimen with bigger area (about 60% of the total specimen area) was then milled in the machine shop with an accuracy of ± 0.003 mm to get two identical half parts of the specimen as shown in figure 2.14.

One half section of specimen was then drilled precisely with 0.1cm diameter stainless steel drills from the internal diameter surface of the specimen's half part to a depth of 7.3mm (1mm from the surface of specimen). Eleven Holes were drilled at centre

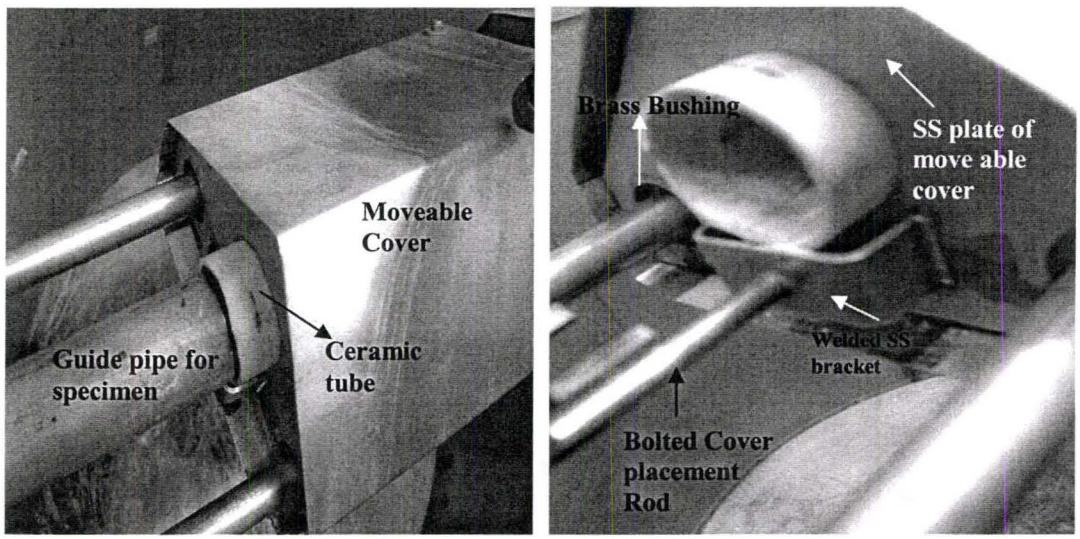

Figure 2.10: Specimen cover assembly.

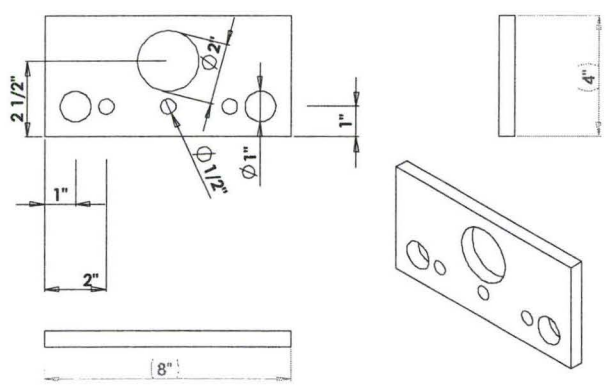

Figure 2.11: SS plate welded on collecting tank.

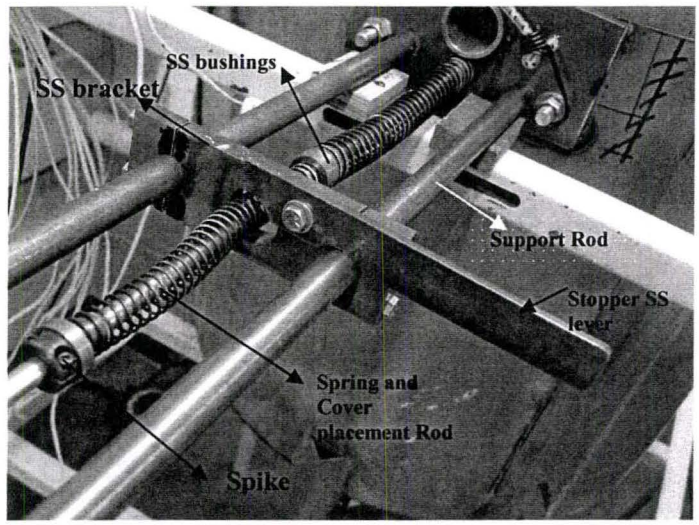

Figure 2.12: Spring loaded assembly.

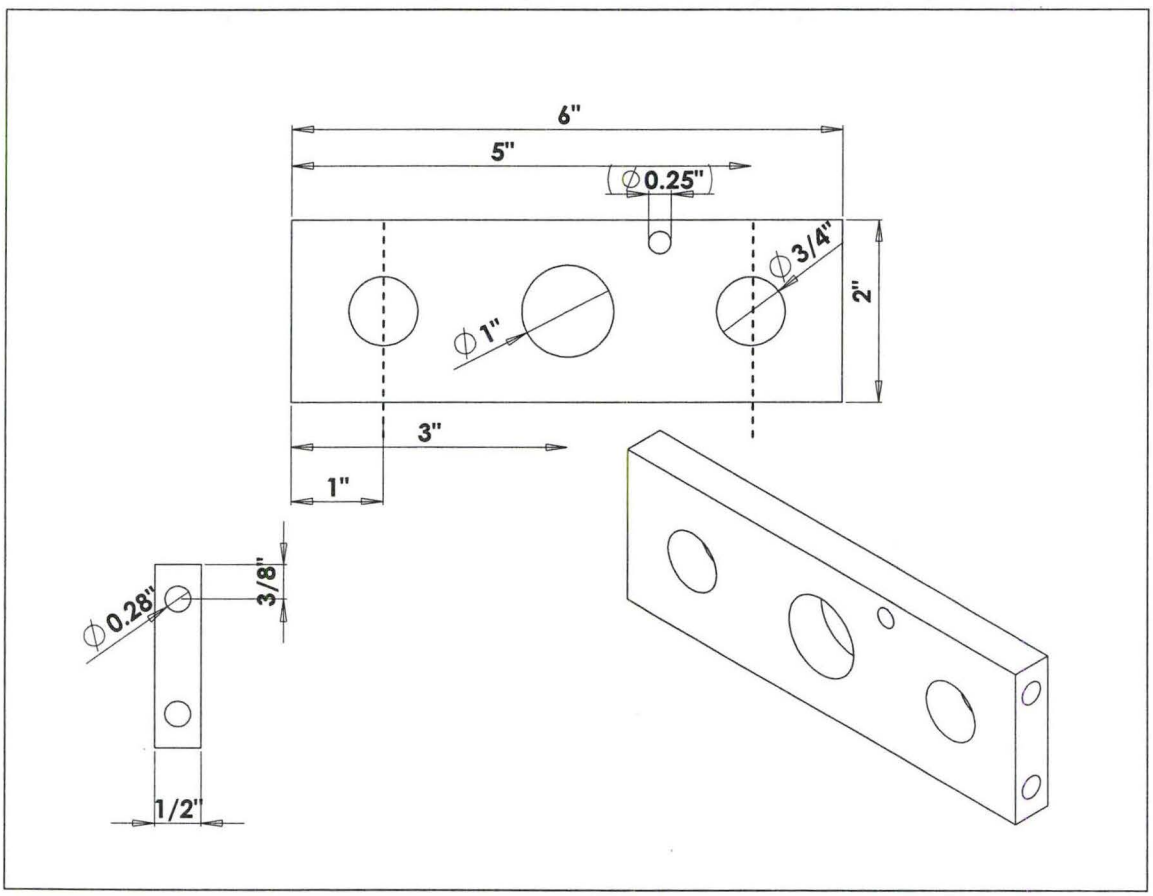

Figure 2.13: Front, side and isometric views of SS bracket.

line of the specimen in the axial direction and two holes at angles of 18.2° from vertical line at the centre of specimen. Both halves are clamped together tightly and outer surface was polished with emery paper # 500 for consistent surface finish.

The drilled holes in the half section of the specimen were used to precisely place the exposed junction K-type thermocouples with sheath diameter of 0.05 cm to measure the temperature of stainless steel specimen at 1mm from surface. Two thermocouples were placed at a distance of 41.3mm from the reference central thermocouple, one at the internal and other at the outer diameter of the specimen. The whole schematic of thermocouples' arrangement is shown in figure 2.15. This figure is not scaled; the area in the vicinity of thermocouples' location is enlarged in an attempt to clearly show the position of thermocouples within the specimen's half section.

It is important to note that:

- T1= Reference thermocouple placed at 15.2 cm from side of specimen. All the other thermocouples were placed with reference to this thermocouple. T11 and T12, thermocouples were placed in the drilled holes at angles of 18.2° (which gives a distance of 4mm from reference thermocouple), from the centre of specimen.
- T13 thermocouple placed at specimen internal diameter (ID) surface.
- T14 thermocouple not shown in the figure. It is placed at 41.3mm from the reference thermocouple at outer diameter (OD) surface of the specimen's half section.

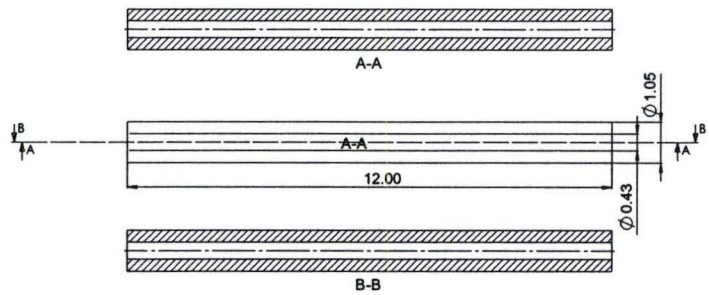

Figure 2.14- Sectional view of specimen.

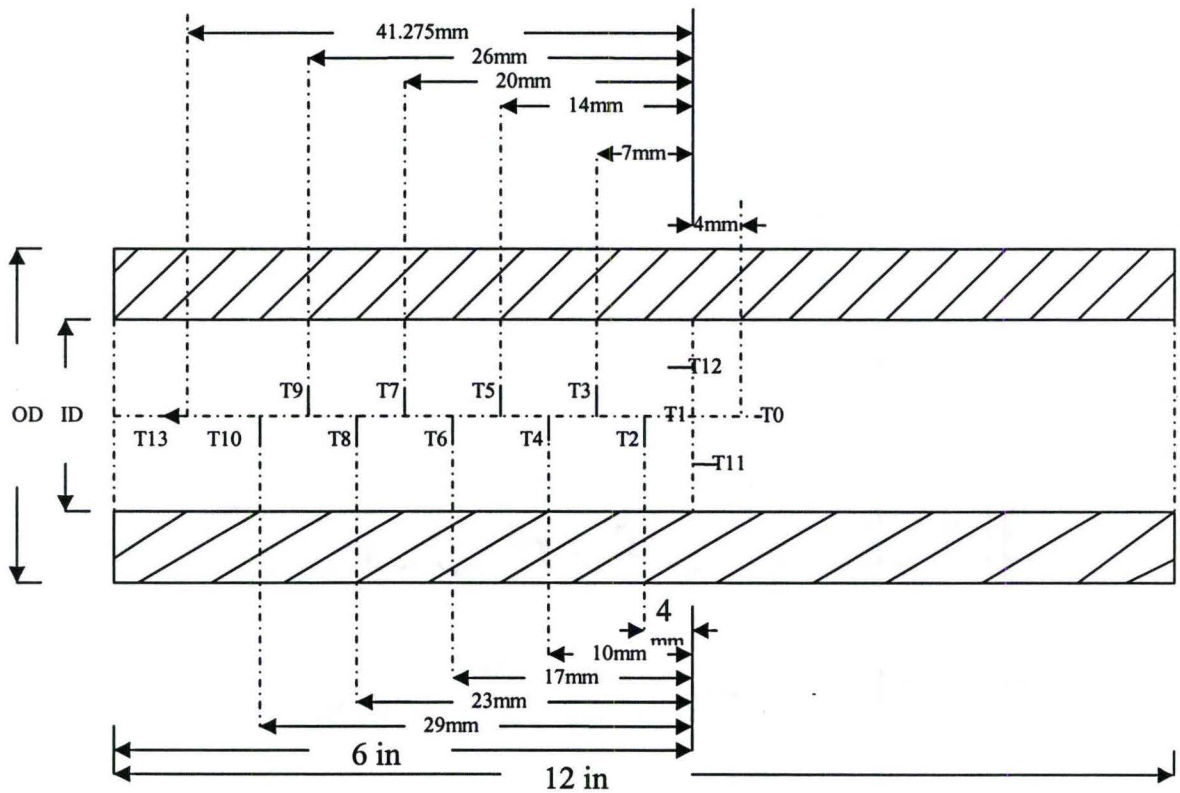

Figure 2.15: Placement of thermocouples in specimen.

The exposed junction thermocouples were selected because of their quick response time. Omega thermocouples have special limit of error of ± 0.4% of the reading. In an attempt to keep the thermocouples in their proper place, stainless steel shims were used. Figure 2.16 shows thermocouples and their fixation with shims on the internal half part of the specimen.

2.2.2.2. Data Acquisition System.

In order to get the data from thermocouples and flow meter, a Data acquisition system was built. All components of the Data acquisition system were acquired from M/s National Instruments. The main components are:

1. Built in PC cards:
    - PCI 6032E (for data from thermocouples)
    - PCI 6601 (for data from Turbine flow meter).
2. External Devices. (shown in figure 3.19)
    - SCXI chassis assembly.

      - A 32 channel isothermal terminal block SCXI-1303, directly connected on one end to the thermocouple extensions from the test section with other end mounted on module assembly SCXI -1102 fitted in 4 slot SCXI chassis 1000.

      - A SCXI-1349 connector assembly is directly connected with SCXI - 1102 at rear end of SCXI -1000.

      - Signal is transmitted to computer via PCI 6032 E through a shielded cable.

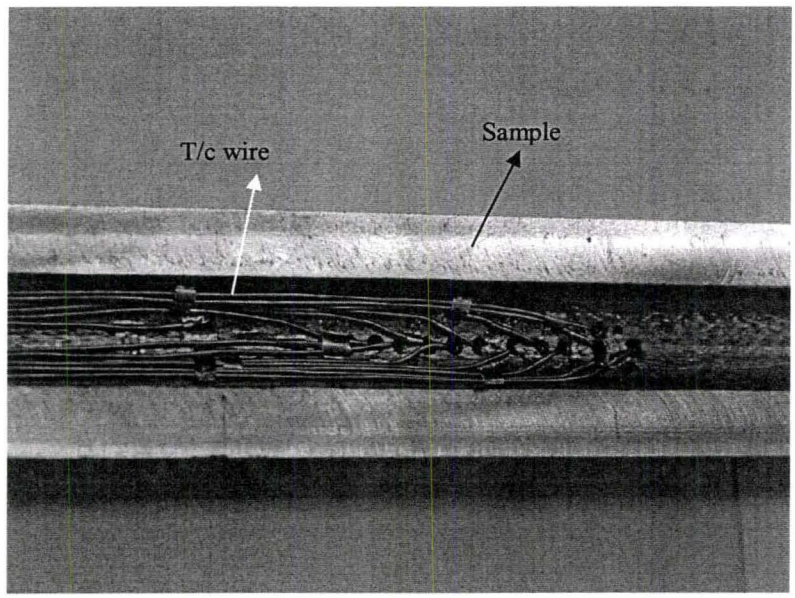

Figure 2.16-Instrumentaion in specimen.

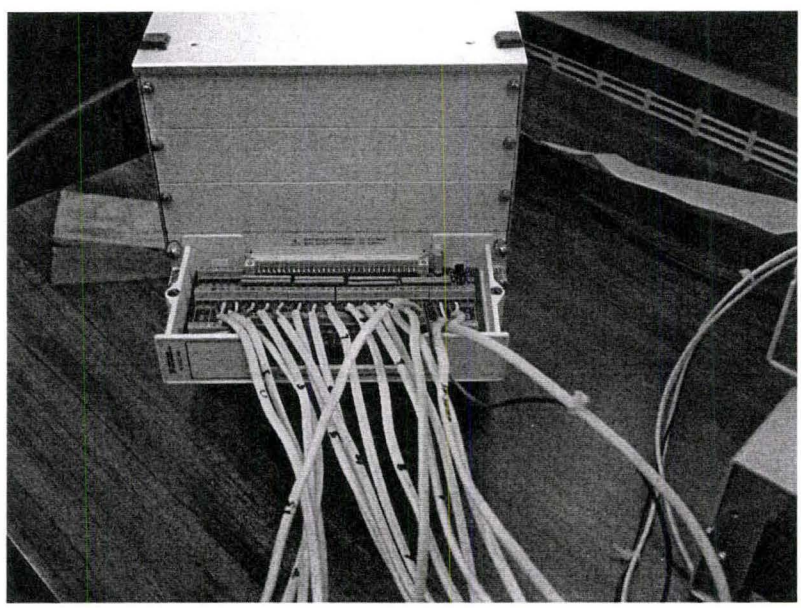

Figure 2.17-External parts of Data Acquisition system.

- An Omega signal amplifier for the Turbine flow meter signal amplification, directly connected on one end with the shielded signal cable from Turbine flow meter and other end to connector block CB-68LP. Signal is transmitted to computer via PCI -6601 through ribbon cable connector to the connector block.

Data from the 16 thermocouples at sampling rate of 1000 Hz and one turbine flow meter were acquired by the computer using Lab View 7.0. Two programs were used for collecting measurements from thermocouples and the flow meter.

2.2.2.3. Temperature Controller.

In order to protect the heater from burn out at high temperature experiments, a temperature controller was designed and built in-house. It has two display panels for desired temperature adjustment for the heater surface and specimen surface. It shutoff the power supply to the heater when the desired heater surface or specimen surface temperature is attained and turn on as temperatures fall below the required one. Two PID controllers No. E5CN, along with two solid state relays (SSRs) are used for this purpose. The heater controller circuit diagram is shown in figure 2.18.

2.3. High Speed Imaging and Support Structure.

2.3.1. Support Structure.

The support structure is comprised of 1.3 cm Stainless Steel square tubes and angles welded together to form the structure shown in figure 2.19.

2.3.1.1.Vibration Damper Assembly.

It is used to transmit vibrations due to various components of the facility to concrete wall as shown in the Figure 3.21. It is composed of 2 nos. 1.3 cm SS square tubes with wall thickness of 0.32 cm. The SS tubes are welded together on wall side to form a v-shape on the SS plate {15.2 cm x 7.6 cm x 1.3 cm}. It is bolted with concrete wall by 1.3 cm diameter bolts. Each SS tube of the assembly on support structure side is welded angularly to SS plate {10.2 cm x 3.8 cm x 1.3 cm}. Each SS plate is bolted with support structure with 1.3 cm diameter bolts. Figure 2.20 shows this assembly.

2.3.2 High speed imaging system.

In order to view the propagation of wetting front, a Redlake high speed imaging camera was utilized. Due to the emission of infra red radiations from hot specimen at high temperatures an IR cut off filter was used to obtain better images.

Since the specimen was placed inside the tank with a further 30 cm high cylindrical splash guard for protection, it was difficult to get a clearer image without glare. Three halogen lights were utilized for illumination purposes. The distribution of light was determined through various runs. Many experiments were repeated due to this problem.

All videos recorded have the following setup parameters:

Frame Rate: 500 Frames /sec.

Resolution: 240x210 pixels.

Total No. of Frames: 2048.

Total Record time : 4.1 seconds.

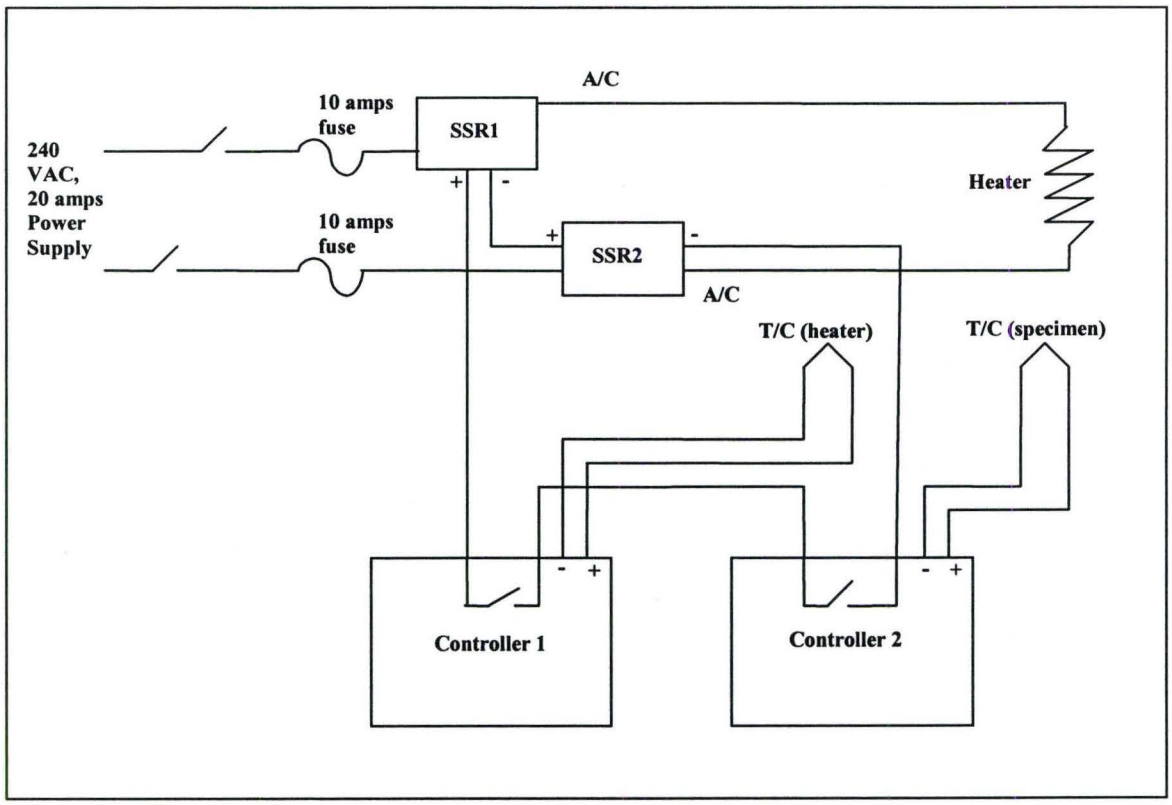

Figure 2.18: Electrical circuit diagram for temperature controller.

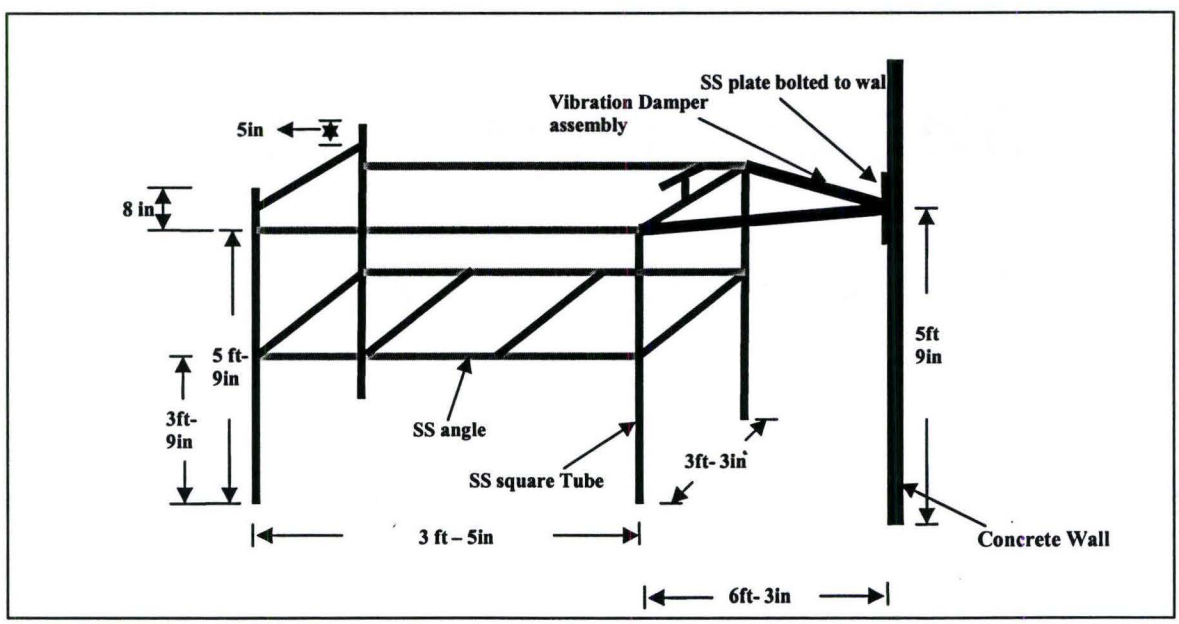

Figure 2.19. Support structure and vibration damper assembly.

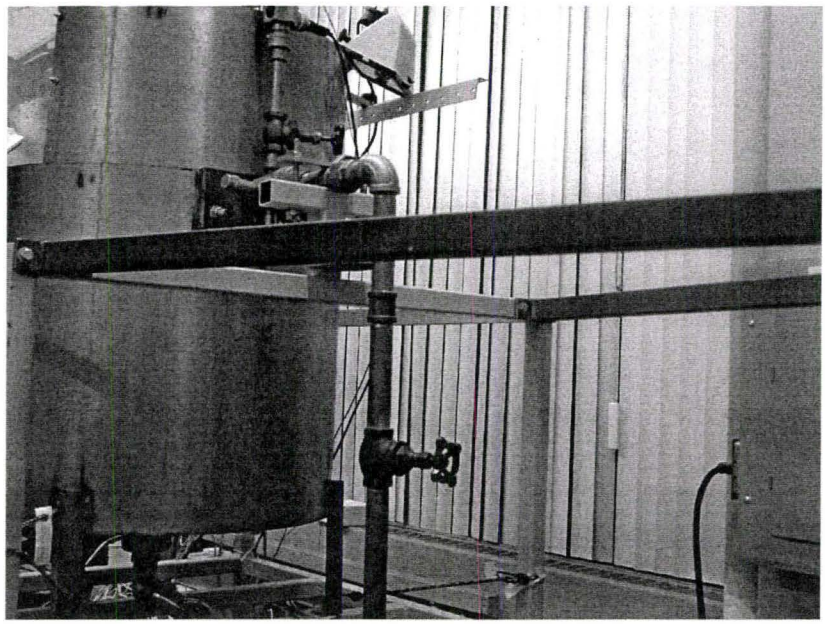

Figure 2.20: Vibration damper assembly.

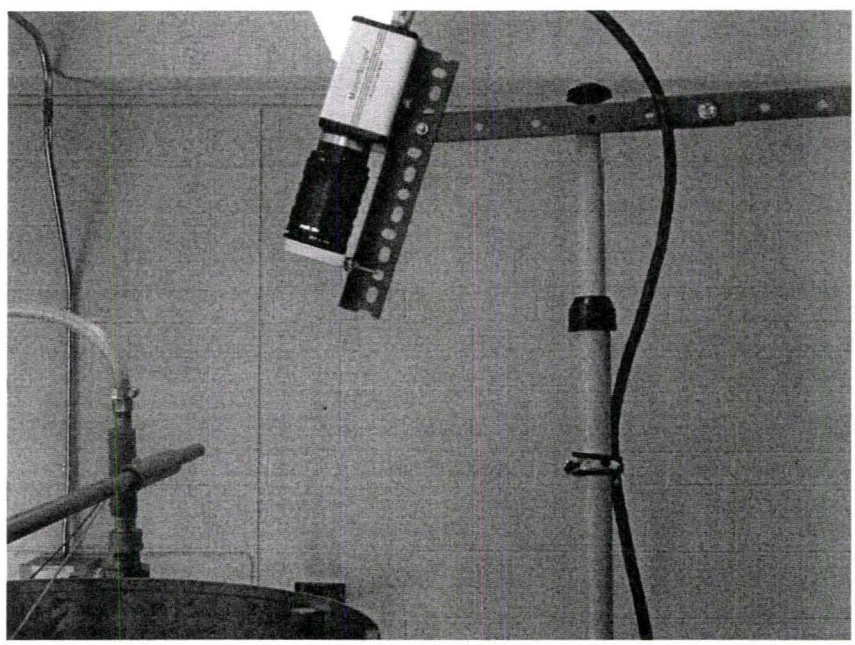

Figure 2.21: High speed video camera positioned on Specimen

Chapter 3.

Experimental Methodology

Experiments were performed to characterize the effect of jet velocity, jet diameter, water temperature and surface temperature on wetting of cylindrical stainless steel specimen surface by liquid jet impingement cooling. Following ranges of experimental parameters were selected to work with:

- Specimen surface temperature =250 °C, 500 °C, 800 °C.
- Jet velocity = 5m/sec & 7.75 m/sec. (Reynold's no. range =17,441 to 36,046)
- Jet diameter=3mm and 4mm.
- Water temperature at nozzle = 20 °C, 50 °C and 70 or 75 or 80 °C.

3.1.Induction of Mg O Powder and Heater in Specimen:

After placement of thermocouples in the specimen's half part as explained in chapter 3, the internal diameter surface of the specimen half part was pasted with a thin layer of MgO powder and tapped vigorously from the sides so that MgO powder should get into the tiny thermocouples holes and properly pack up for good conduction. Milled MgO powder with 99.8% purity was used for this purpose. MgO powder was then used to cover the holes and to create a layer before placement of the Specimen cartridge heater. The cartridge heater is used to heat the specimen. Specimen heater has the following specifications:-

- 0.31 in. outer diameter, Length= 12 in, 240 Volts, 1000 Watts.

In order to keep the heater in the centre of specimen, a stainless steel holder was built in-house which was used at one end of specimen.

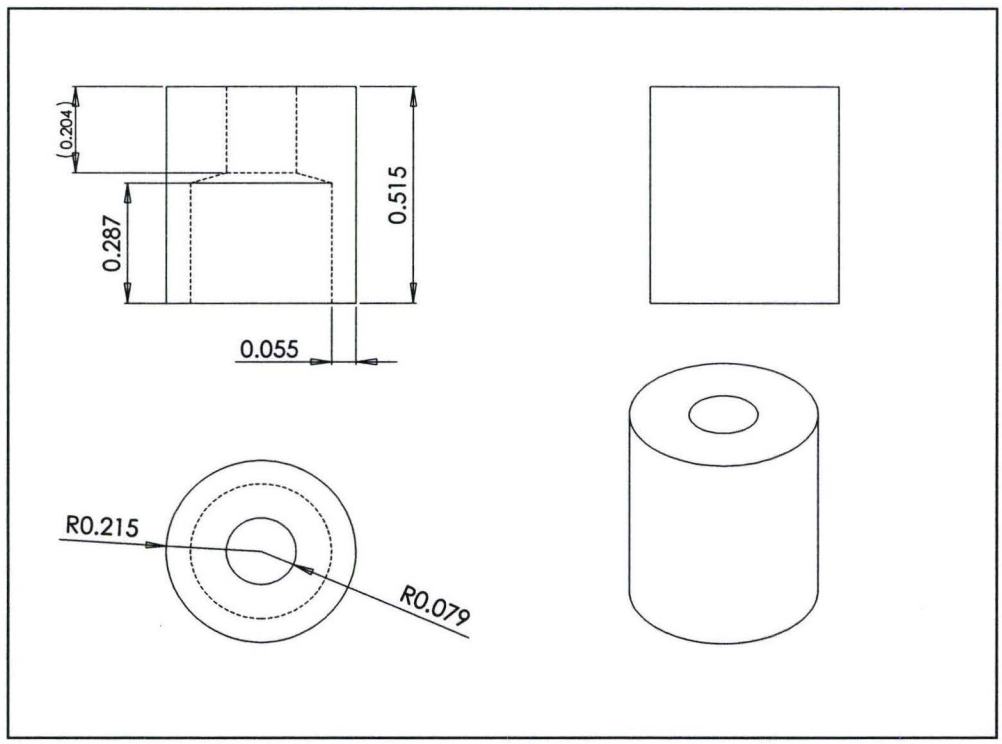

Figure 3.1- Heater Holder.

After placing the heater in the specimen one half, Mg O powder was poured on the heater and specimen half part to fill the gaps between specimen and heater. More MgO powder was used to cover the heater surface for possible covering of the space between the heater and specimen upper half part. The specimen second half was then placed and tightly clamped with the lower half part. A number of SS strap clamps were used to minimize the gap between the two half portions of the specimen. After tightening the strap clamps, two stainless steel holding cups were used on both the ends to hold the

specimen. One placed at the specimen end through which thermocouples and heater power cord passes via a hole in the holding cup. Drawings of the Specimen holding cup at Thermocouples' end are shown in figure 3.2:

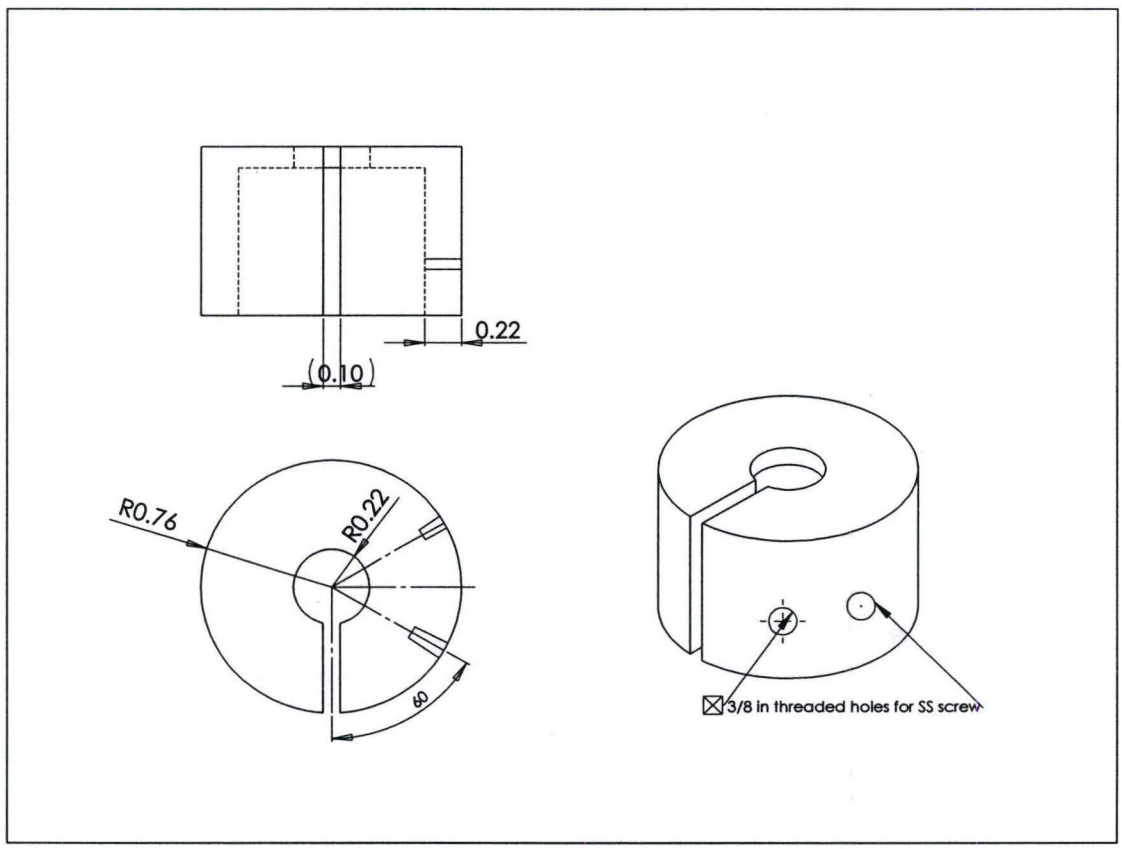

Figure 3.2. Specimen Holding Cup at Thermocouple End.

The other stainless steel specimen holding cup placed at the other end of specimen doesn't have any hole. These holding cups when tightened hold the specimen's two halves tightly as shown in figure 3.3.

After clamping of specimen as stated above, it was carefully tilted vertically and held in the vice jaw with soft edges (to prevent damage to the surface finish of the

specimen) with the "thermocouple end" held in upright position. More MgO Powder was then poured in the specimen through the hole of the "holding cup" and tapped from bottom for good compactness. Process of filling the specimen with MgO powder along with tapping it from bottom continued until there was no further room for compactness (visually determined).

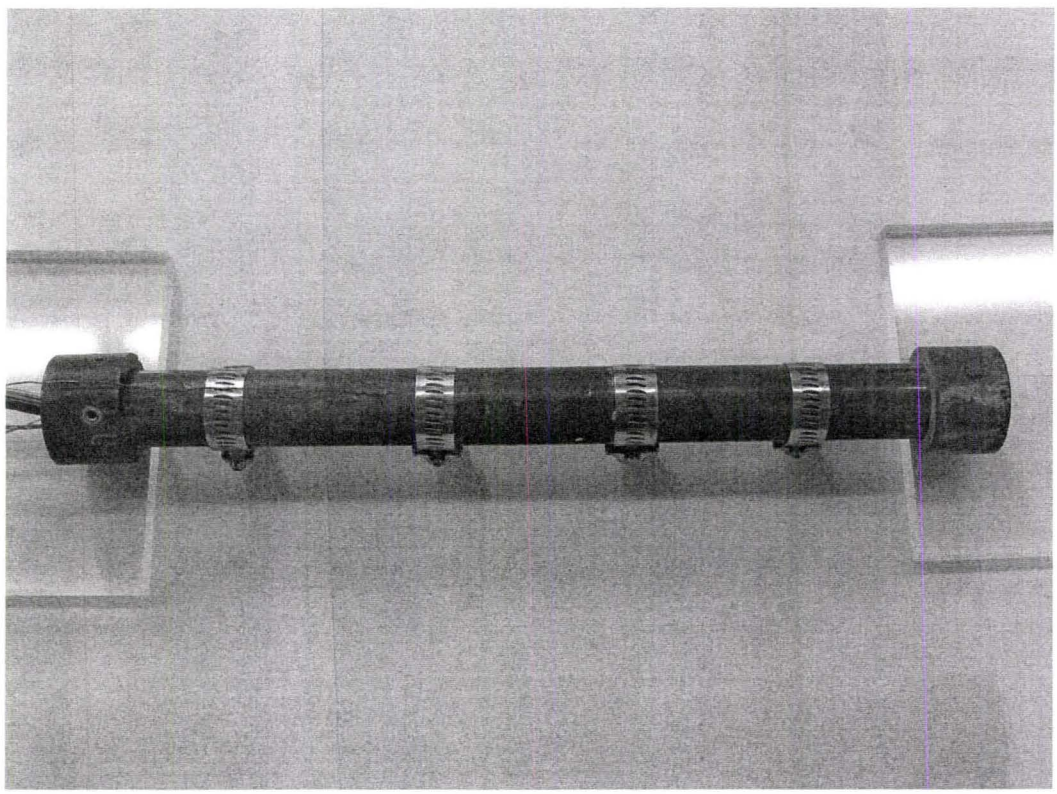

Figure 3.3. Specimen with heater inside.

3.2 Specimen Introduction inside Experimental Facility.

The specimen was then placed in the two finger type jaws through the guide pipe and held at the centre of collecting tank with Heater connection wire and thermocouple wires passing out of the guide pipe from "moveable cover" side of the "specimen cover

mechanism". The stainless steel straps used to hold the two half parts of specimen were then removed.

3.3. Connections.

Thermocouple wires were connected to the Data Acquisition System through extension wires. Heater wire was connected to the "Temperature Controller Box". Thermocouple wires from pipe probe thermocouple and water reservoir are connected to the Data Acquisition System. Moveable cover and immoveable cover are joined together to cover the specimen.

3.4. Experimental Procedure:

1. Data Acquisition System was turned on and working of Lab View programs was checked.
2. Water jet was sprayed and centered at thermocouple (T01). Temperatures at thermocouples adjacent to T01 (T0, T2,T11 and T12) were made approximately equal to centre the jet by adjusting the position of jet impingement position.
3. Intensity of video lights and focusing of high speed camera was adjusted.
4. Spring loaded cover mechanism was used to cover the specimen.
5. Heater controller was set up for the required specimen surface and heater surface temperature.
6. Immersion heater was powered up to heat the water in tank to the required temperature.
7. Heater was then powered up and specimen was heated to required temperature. As the surface temperature reaches the required temperature, the heater controller

automatically switch off the power supply to heater. In order to reach a steady surface temperature, specimen was heated approximately for 2 hrs for experiments with surface temperature of 250°C, 2-1/2 hours for specimen surface temperature of 500°C, and 3 hours for specimen surface temperature of 800°C.

8. As water temperature in tank becomes slightly above the required water temperature, water pump was turned on and jet was sprayed with specimen cover still covering the specimen. Jet velocity was then adjusted to the required water velocity by adjusting the water flow.
9. As water temperature at nozzle reached the required water temperature, and, specimen surface temperature seemed to reach the required steady state temperature, heater controller was turned off, video recording was started, specimen was uncovered and jet was impinged.
10. DAQ continue to monitor jet velocity by recording water flow through nozzle. Water temperature was also continuously monitored and recorded during each experiment.
11. DAQ was allowed to record the surface temperature of specimen at the impingement location and at stream wise locations until the surface temperature is approximately equal to water impingement temperature.
12. Lab View programs and video recording were then stopped.
13. Video was analyzed.
14. Surface temperature variation during experiment was analyzed.

3.5. Uncertainty analysis.

3.5.1. Direct measurements.

Propagation of wetting front was directly measured with a scale graduated in millimeters. The measurements were taken between two points, jet impingement centre (stagnation point) and wetting front. The uncertainty in direct measurements between two points was performed here using the approach outlined by Taylor [29]. Since scale measurements were 1mm apart so uncertainty in direct measurements for both points comes out to be ±0.5 mm. Hence total uncertainty in direct measurement is ±1mm.

3.5.2. Mass flow.

Jet velocity was measured on the bases of mass flow through nozzle. Mass flow was measured by Turbine flow meter through Data Acquisition system. Turbine flow meter was calibrated by bucket and stop watch experiment. The calibration curve is shown in figure 3.4. Relative uncertainty in mass flow was found to be in the range of ±0.01 to ±0.02.

3.5.3 Temperature.

Omega calibrated K-type thermocouples with special limit of error of 0.4% were used for the experiments.

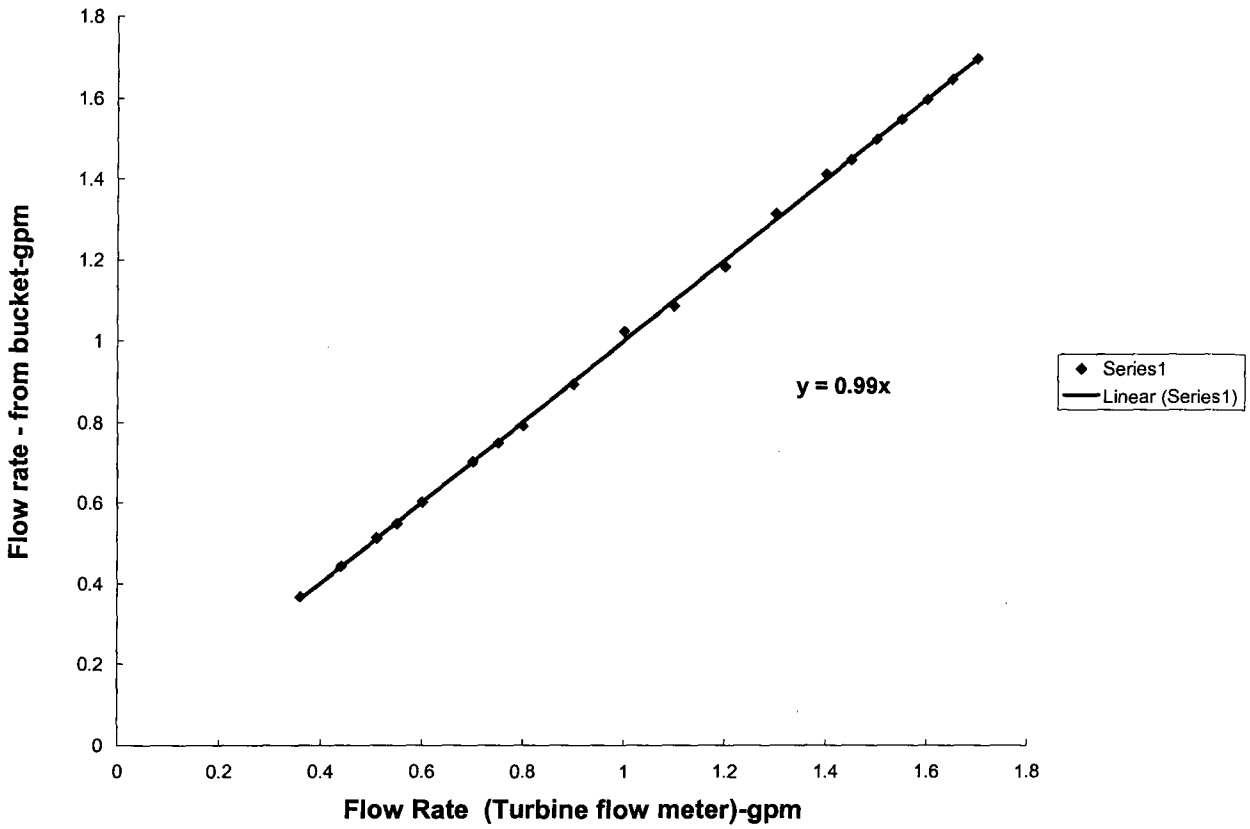

Figure 3.4. Turbine flow meter calibration curve.

Chapter 4.

Results and Discussion.

The main objective of the present study is to investigate the effect of jet velocity, jet nozzle diameter, water temperature and specimen surface temperature on the propagation of wetting front of water jets impinging on hot cylindrical specimens. Experiments were performed at transient mode by first heating the specimen to the required temperature and turning off the heater before the start of jet impingement.

Experiments were performed for three specimen surface temperatures of 250,500 and 800°C, and results are plotted and presented in the following sections.

4.1. Observation of boiling.

From observation of jet impingement on hot specimen surface, transient cooling process may be subdivided into three regions i.e. non-wetting region, spreading of wet front region and fully wetted region.

4.1.1. Non-wetting region.

This is the region which follows immediately after jet impingement on hot specimen surface and is marked by the initial non-wetting of the surface for small period of time. In this region water is completely splashed out as small droplets as shown in the representative figure 4.1. Even at stagnation point the solid liquid contact does not seem to be established. The time period for non-wetting region seems to be dependent on specimen surface temperature and degree of sub-cooling of water. The time period for

non-wetting region appears to increases with increase in surface temperature and water temperature.

After a small period of time water jet- specimen surface contact is established first at jet stagnation point as shown in figure 4.2.

4.1.2. Spreading of Wetting front region.

After the establishment of jet-surface first contact at stagnant point of jet, a wet region is seen spreading. As time passes this wet region spreads from centre towards the ends of circumferential specimen. In this region three heat transfer regions appear to coexist a)-single phase forced heat transfer region b)- nucleate boiling region c) –dry region as is shown in figure 4.3.An annular shape of width Δr_b appears as a white region. It seems nucleate boiling occurs in this region. This region expands circumferentially with time. Beyond the nucleate boiling region exists the non wetting region. This region shrinks with the passage of time as the wet front progresses outwards. This region is also shown in figure 4.3.

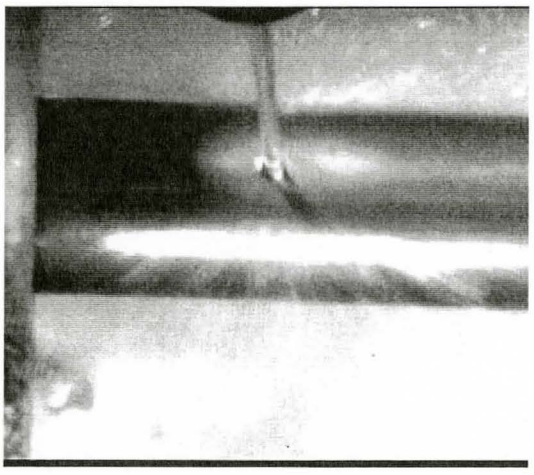

Figure 4.1 Existence of the non-wetting region for hot specimen surface

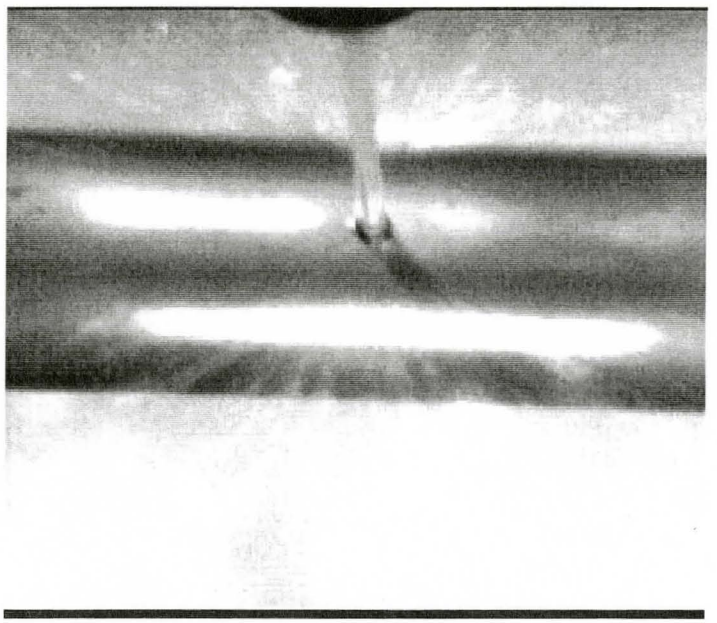

Figure 4.2. Solid –liquid first contact established at stagnation point.

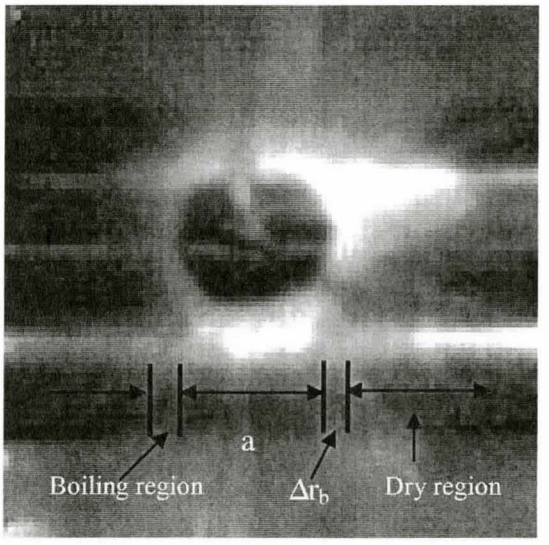

Figure 4.3.Typical photograph of flow boiling as seen during experiments. Where "a" is single phase flow region.

Value of width Δr_b is effected by specimen surface temperature, water temperature and jet velocity. It is hard to find out the size of Δr_b for the experiments conducted at specimen surface temperature of 250°C, but it is quite easily seen for specimen surface temperature of 500°C. The value of Δr_b is observed to be less than 0.5 mm for all experiments conducted at specimen surface temperature of 250°C and it is observed not to be changing for different parameters studied during experiments. For experiments conducted on specimen surface temperature of 500°C , width of Δr_b varies from less than 0.5mm to a maximum of 5mm. The value Δr_b changes continuously from maximum at initial stages of experiment to minimum as the wetting front propagates outwards.

4.1.3. Fully wetted region.

After the wetting front reaches the maximum size during experiment, usually the ends of the hot specimen, then the hot specimen is further cooled by continuous flow of water film through the nozzle.

Observations clearly indicate the effectiveness of nucleate boiling region limited in narrow annular region which spreads outwards in r-direction with time which causes the growth of wet region or in other words wetting front. Growth of this wetting front has greater role in the removal of heat from hot specimen.

4.2. Measurement of Radius of Wetting Front.

High speed imaging camera is utilized to record video of each experiment. After the experiment the video is analyzed to find the scale factor (L_s) of wetting front by equating the known outer diameter of the specimen to the diameter of specimen as observed on screen or in picture during experiment.

d_{sp}=diameter of specimen as seen in video image or picture.

d_{so}= Actual diameter of specimen=26.67mm.

$L_s = d_{so} / d_{sp}$

After determination of scale factor for each experiment, readings of propagation of wetting front are taken by measuring the distance from centre of impingement zone to the boundary of wetting front in the axial (R_{wa}) direction from different frames of video chosen based on the clarity of video images.

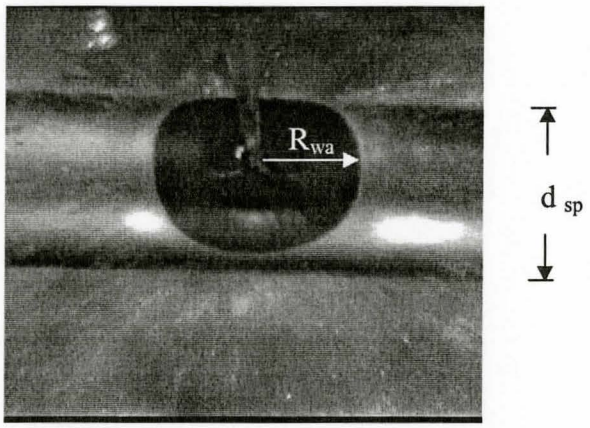

Figure 4.4: Measurement of wet front.

Then:

R= Radius of wet front in axial direction= $R_{wa} \times L_s$.

For each experiment the frame rate is 500 frames /sec. Time duration between two consecutive frames is 0.002 seconds. Hence on the bases of frame number Time lapsed between different frames was determined. Frame number for the first impact of water with the hot specimen was evaluated and experiment time starts from this frame, then consecutive frames were chosen, time lapse from first contact is calculated and radius of

wetting front (R) was recorded. This process is continued as long as the wetting front could be seen clearly. The results are plotted and analyzed for different set of parameters.

Visual observations during present study show that as water jet impinges on hot specimen surface a wet region is seen spreading after establishment of first contact between the specimen surface and water jet. The wetting front of this wet region initially propagates faster towards the ends of specimen. After some time it starts to slow down and continues to slow down until radius of wetting front reaches a maximum value and growth of wetting front afterward stops. This physical phenomenon of growth of wetting front can be expressed properly by power law. In previous studies, Mitsutake and Monde [6] showed that for flat surfaces the propagation of wetting front can be represented by a power law. They showed that for the case of flat surfaces the position, R, of the wetting front from the centre of impingement point is a power function of time as given by following equation:-

$$R = at^n \tag{1}$$

This proposed form of relation was also found suitable for expressing the physical phenomenon of propagation of wetting fronts on curved surfaces. Therefore, this equation was employed in the present study to approximate each curve for the position R as function of time.

4.3. Results with Specimen Surface Temperature of 250°C.

Experiments were performed for water temperatures of 20,50 and 80°C for initial specimen temperature of 250°C with jet velocities of 5m/sec and 7.75m/sec. The time between the jet being incident on the surface and the initiation of wetting (as seen visibly

through videos) is defined as wetting delay which was found to be negligible for all experiments conducted at initial specimen surface temperature of 250°C.

4.3.1. Effect of Water temperature, Jet velocity and Jet diameter.

Growth of wetting front with time strongly depends on water temperature. Figures 4.5 and 4.7 for jet diameter, Dj=3mm, and, figures 4.9 and 4.10 for Dj=4mm, indicate the comparative growth of wetting front "R" with time for Tw=20, 50 and 80°C for jet velocities of 5 and 7.75m/sec.

For Vj= 5m/sec and Dj= 3mm, the comparative growth of wetting front is shown in figure 4.5. Wetting front starts propagating immediately after impingement and radius of wetting front (R) after 0.002 seconds is 9mm, 6mm and 3mm for water temperatures of 20,50 and 80°C respectively. Increasing water temperature reduces the instantaneous size of the wetting front significantly. After 0.06 seconds "R" changes to 23mm (155% increase), 17mm(183% increase) and 12mm(300% increase) respectively. Propagation of wetting front is very high here.

After 0.12 seconds "R" increases to 28(21.7% increase), 22 (29.4% increase) and 17(41.6% increase) mm respectively. This represents the drastic slow down of the wetting front. It takes about 0.18 seconds for water at 20°C to attain Radius of wetting front of 32mm. The same radius of wetting front is attained by water temperatures of 50 and 80°C in much longer time of 0.36(100% delay) and 0.54(200% delay) seconds respectively.

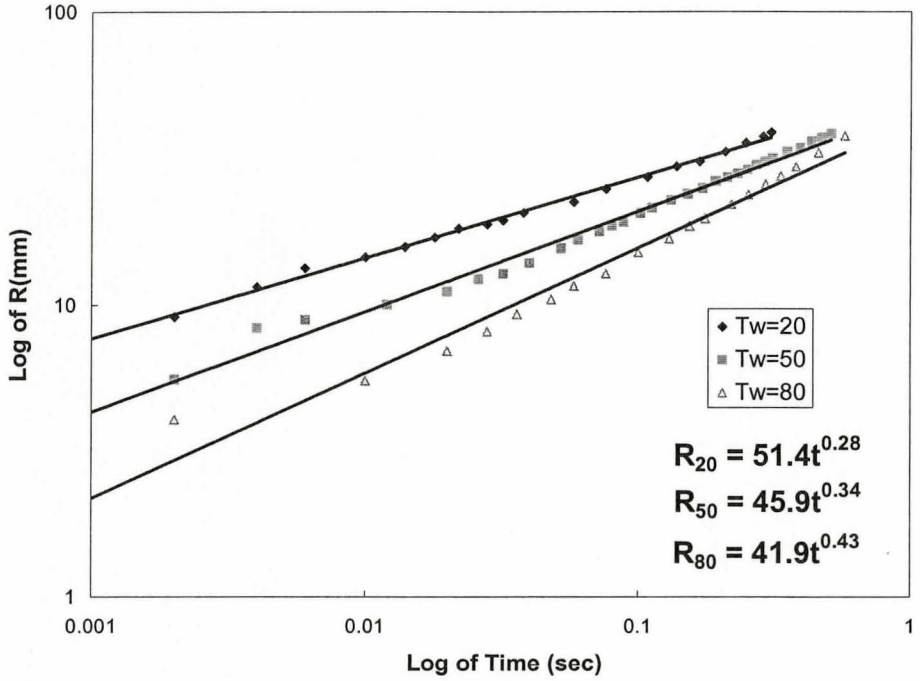

Figure 4.5: Radius of wetting front; as a function of time for Tw =20, 50, and 80°C and Dj=3mm, Tsp=250°C, and Vj = 5m/sec.

The sequences of an experiment with jet diameter=3mm, Tsp=250°C, Vj=5m/sec for water temperature of 50°C are given to demonstrate the propagation of wetting front.

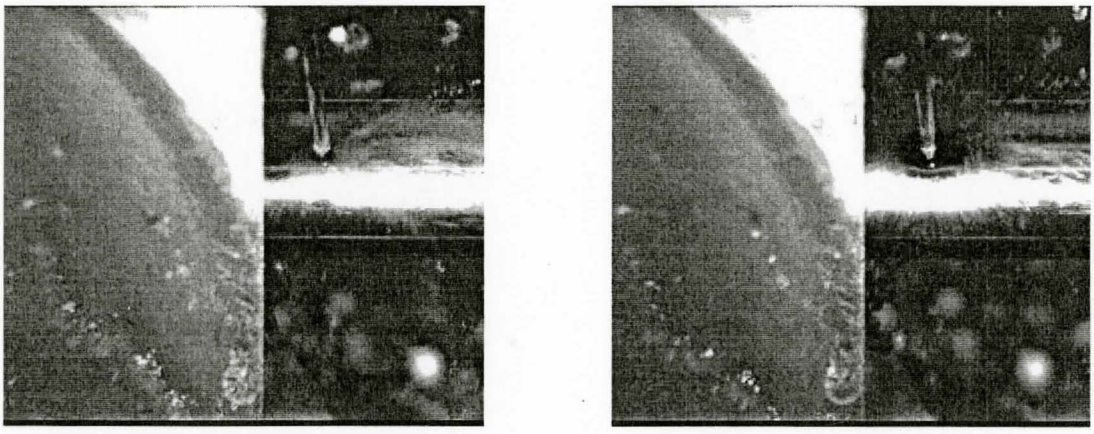

t=0 sec, R=0 t= 0.002 sec, R=5.55mm.

Figure 4.6: Sequences for experiment - Dj=3mm, Tsp=250°C, Tw=50°C, Vj= 5m/sec

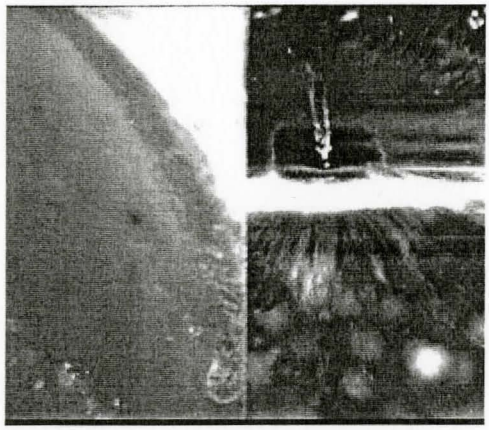

t= 0.006 sec, R=8.9mm

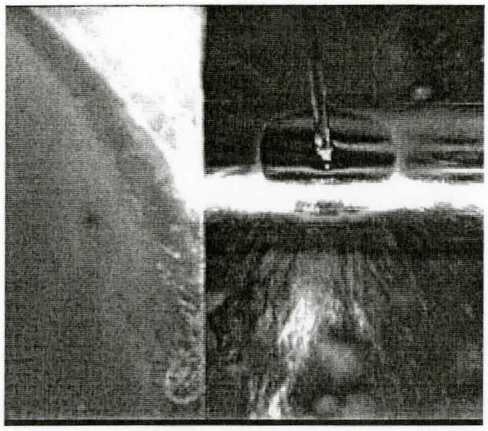

t= 0.02, R=11.1mm

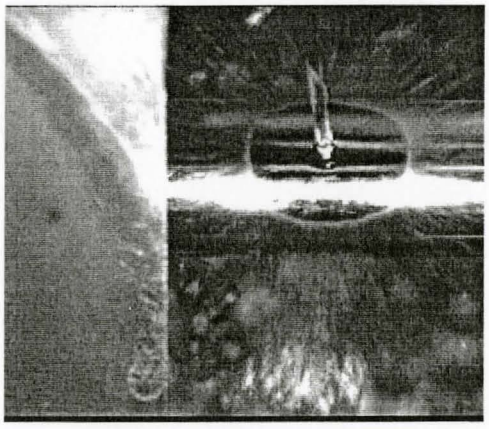

t= 0.032 seconds, R=12.8mm

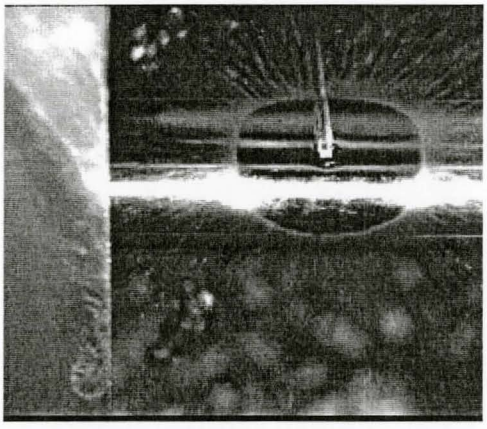

t= 0.052, R=15.6 seconds

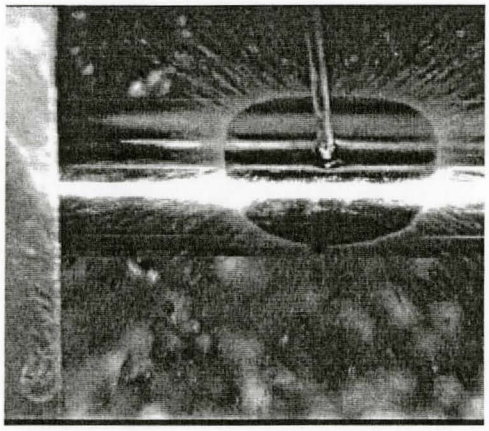

t=0.072 seconds, R=17.8 sec

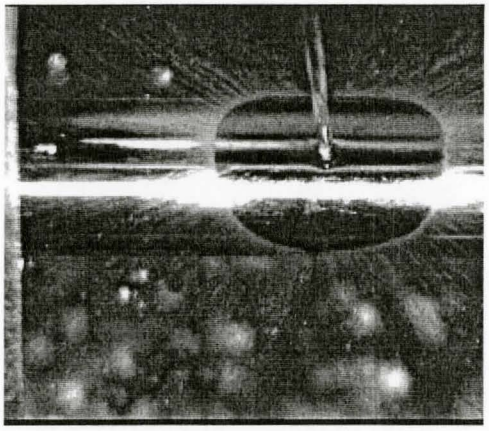

t= 0.088 seconds, R=19.2 seconds.

Figure 4.6: Sequences for experiment - Dj=3mm, Tsp=250°C, Tw=50°C, Vj= 5m/sec.

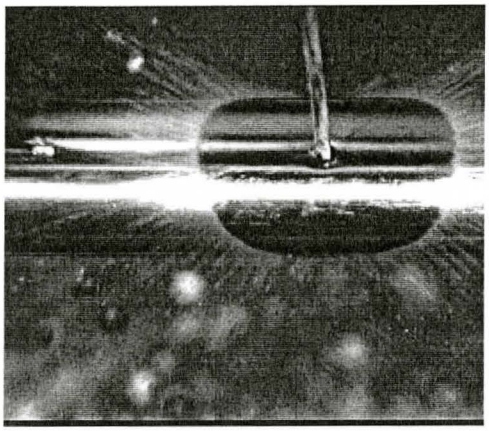

t= 0.112 seconds, R=21.4mm

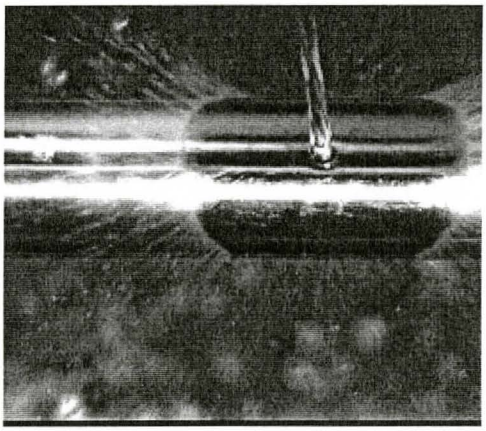

t= 0.152 seconds, R=23.9mm

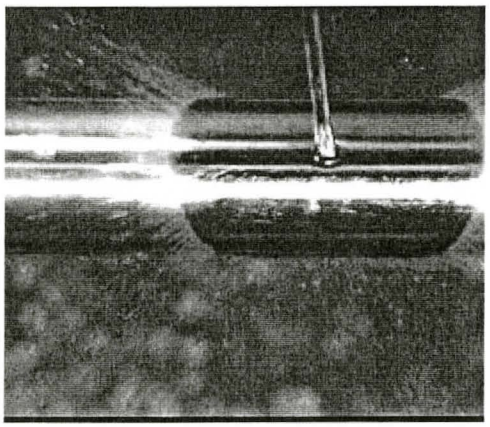

t= 0.192 seconds , R=26.4mm

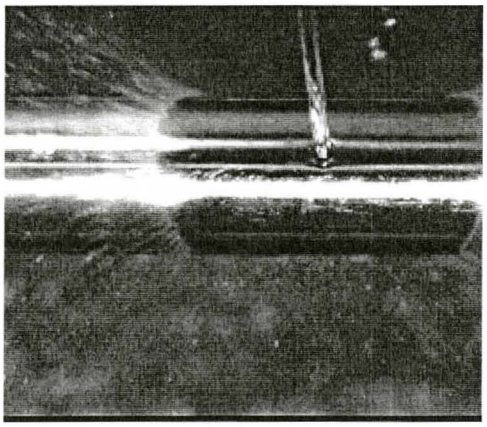

t= 0.232 seconds, t=28mm

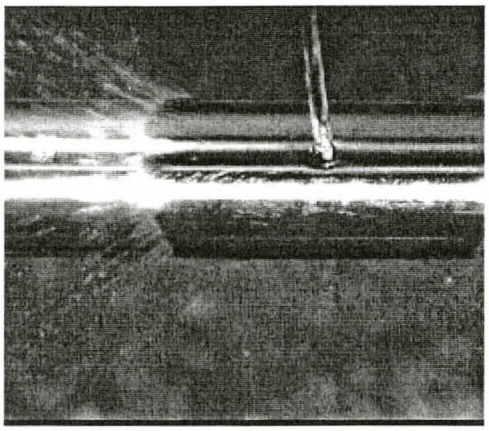

t= 0.272 seconds, R=30mm

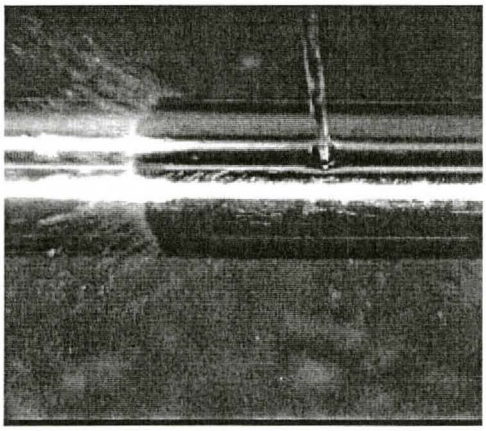

t= 0.312 seconds, R=31.7seconds

Figure 4.6: Sequences for experiment - Dj=3mm, Tsp=250°C, Tw=50°C, Vj= 5m/sec.

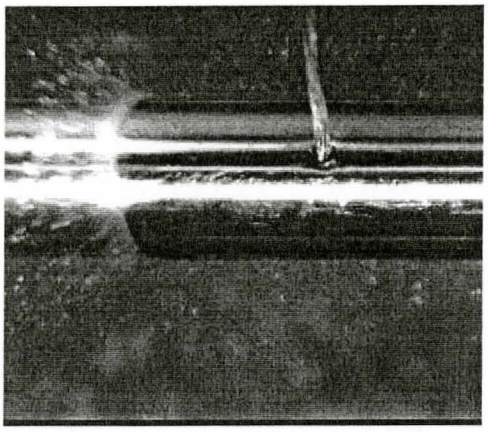

t= 0.392 seconds, R=34.5mm

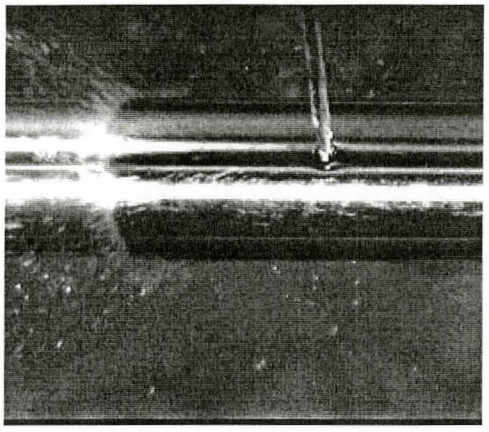

t= 0.472 seconds, R=37.23 seconds..

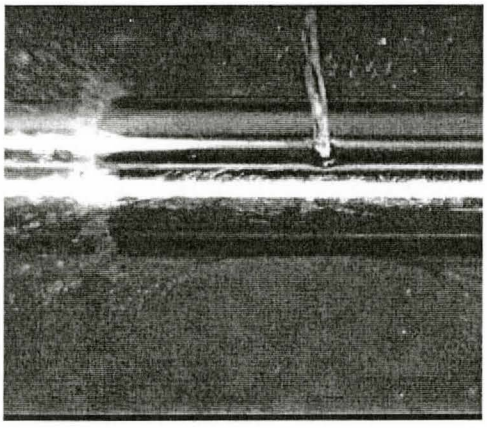

t= 0.512 seconds, R= 38.34 mm.

Figure 4.6: Sequences for experiment - Dj=3mm, Tsp=250°C, Tw=50°C, Vj= 5m/sec

The effect of water temperature is also evident for Vj= 7.75m/sec in figure 4.7. The wetting front after 0.002 seconds propagates a distance of 10.5mm for Tw=20°C which is 16% increase when compared with that of Vj= 5m/sec in figure 4.5. For Tw= 50 and 80°C, R increases to 3.6 and 3.3mm in 0.004 seconds. R increases to 27mm (157% increase), 16mm (344% increase) and 12mm (364% increase) in 0.06 seconds for Tw= 20,50 and 80°C respectively which when compared with figure 4.5 for Vj=5m/sec is an

increase by 17.4,0 and 0% . In 0.12 seconds "R" increases to 32(18.5% increase), 23(44%increase) and 17mm (42% increase) respectively and comparing it to Vj=5m/sec in figure 4.2, it is an increase by 14.3, 4.5 and 0%. In 0.18 seconds R further increases to 35(9.4% increase), 29(26%increase) and 21mm (23.5% increase) respectively. Wetting front takes about 0.18 seconds with water at 20°C to propagate to 35mm, 0.28 seconds (55.5% delay) for Tw=50°C but with water at 80°C could not propagate to 35mm during the maximum duration of video record of 4 seconds.

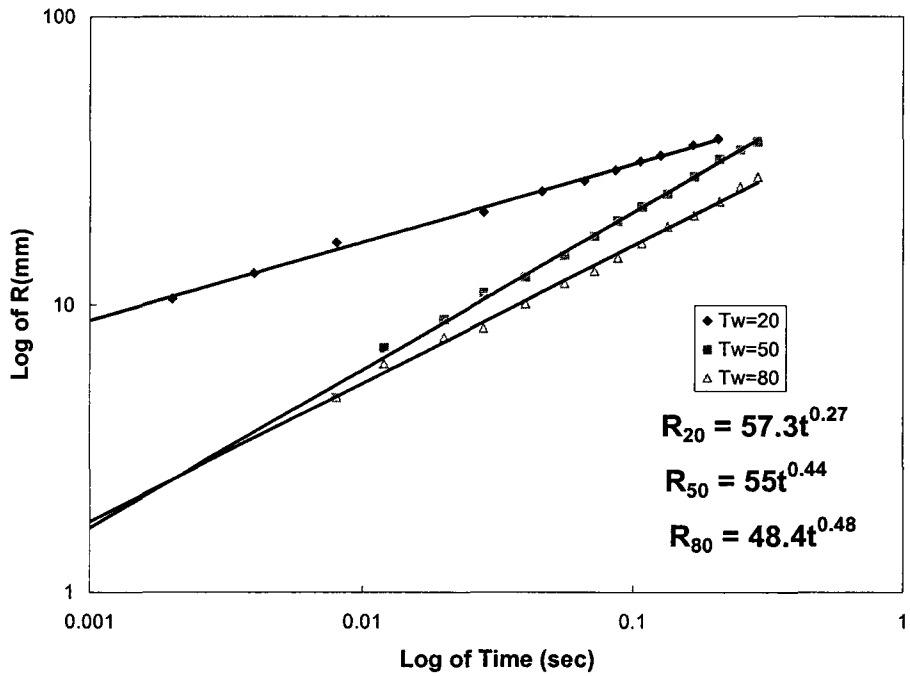

Figure 4.7: Radius of wetting front; as a function of time for Tw =20, 50, and 80°C and Dj=3mm, Tsp=250°C, and Vj = 7.75m/sec

This signifies that water with lower temperature enhances the rate of propagation of wetting front and thus increases the rate of cooling. This is due to high heat removal at

the surface at lower temperature of water which is inline with the findings of previous researchers for flat surfaces. Jet velocity seems to greatly influence the rate of propagation of wetting front at lower temperature of 20°C but it has little or no effect at water temperatures of 50 and 80°C which might be due to insufficient cooling capacity of jet at these water temperatures.

Sequences for an experiment with Dj=3mm, Tsp=250°C, Tw= 50°C and jet velocity of 7.75m/sec are shown in figure 4.8.

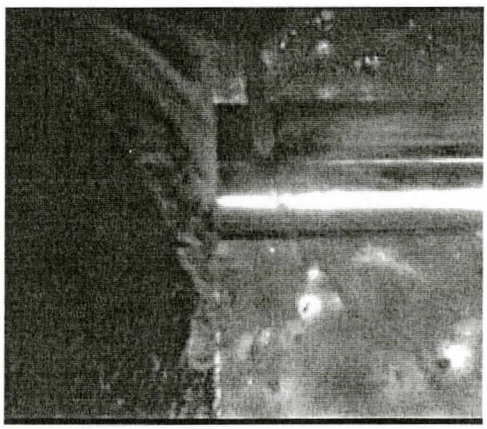

t=0 seconds, R=0mm

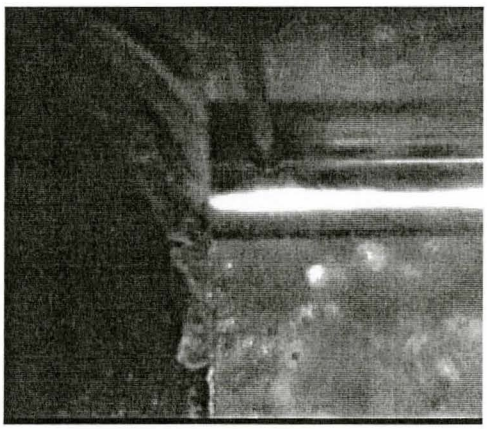

t= 0.004seconds, R=3.56mm

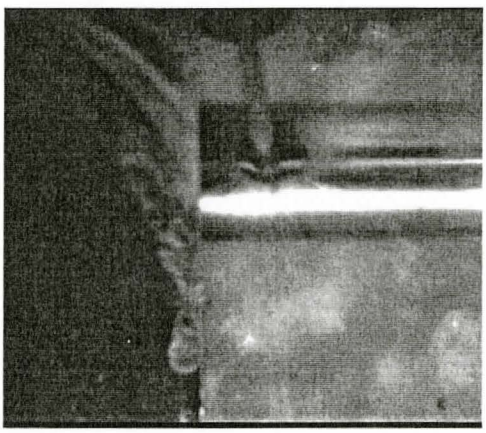

t= 0.008 seconds, R=4.7mm

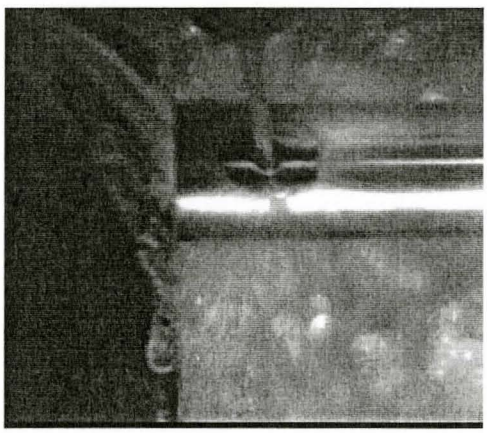

R= 0.02 seconds, R=8.9mm

Figure 4.8: Sequences for experiment - Dj=3mm, Tsp=250°C, Tw=50°C, Vj= 7.75m/sec

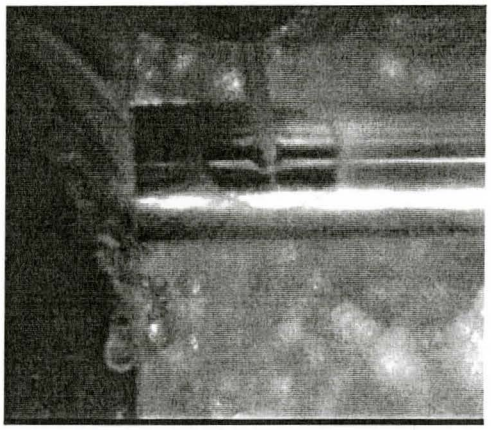

t= 0.04 seconds, R=12.5mm

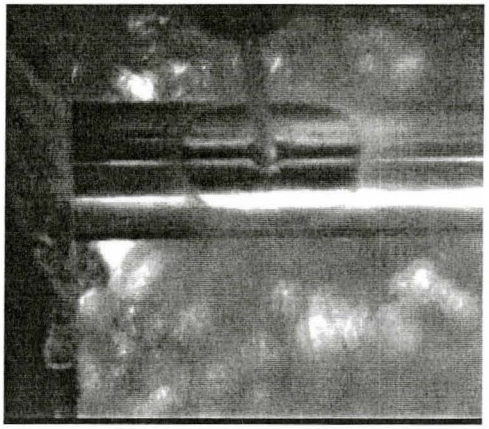

t= 0.072 seconds, R=17.2mm.

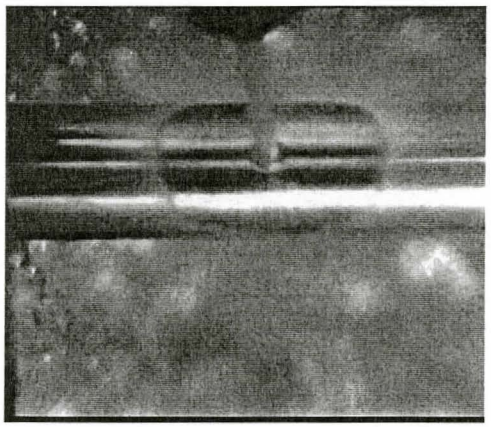

t= 0.108 seconds, R=22mm

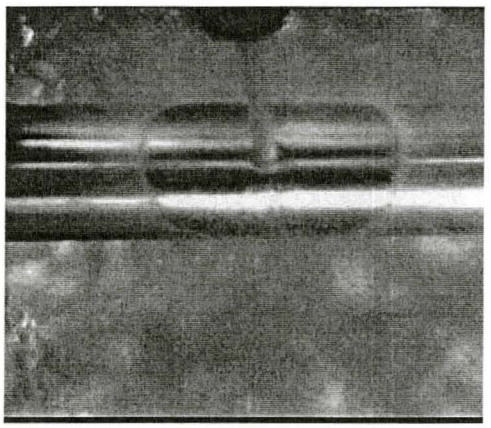

t= 0.134 seconds, R=24.3 mm

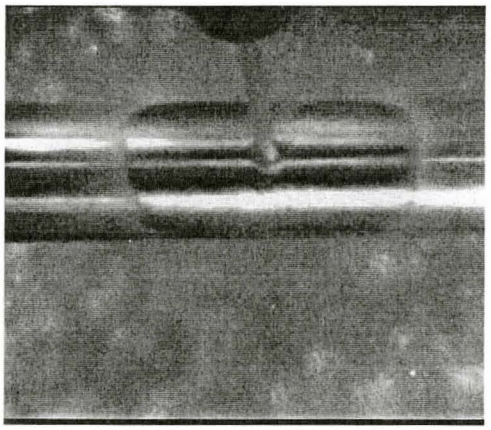

t= 0.168 seconds, R=27.9mm

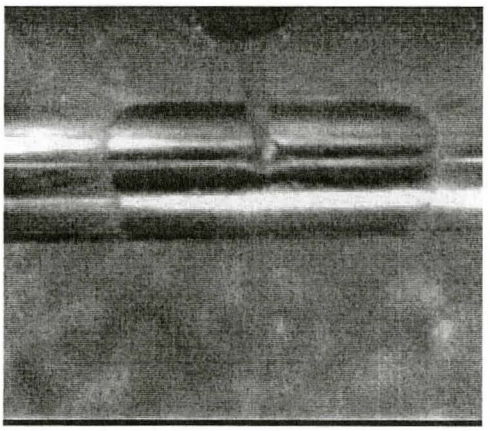

t=0.204 seconds, R=32mm

Figure 4.8: Sequences for experiment - Dj=3mm, Tsp=250°C, Tw=50°C, Vj= 7.75m/sec

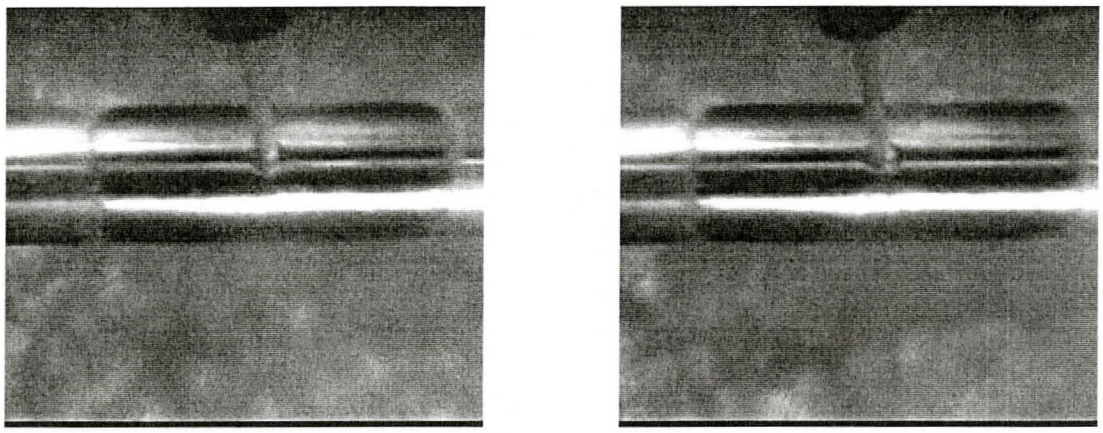

t= 0.248 seconds, R=34.4mm t=0.288 seconds, R=37.3mm

Figure 4.8: Sequences for experiment - Dj=3mm, Tsp=250°C, Tw=50°C, Vj= 7.75m/sec

Figure 4.9 shows the comparison of the propagation of wetting front with jet diameter of 4mm for jet velocity of 5m/sec. Table 4.1 shows effect of water temperature on values of R for the case of Dj=4mm and a comparison with the case of Dj=3mm.

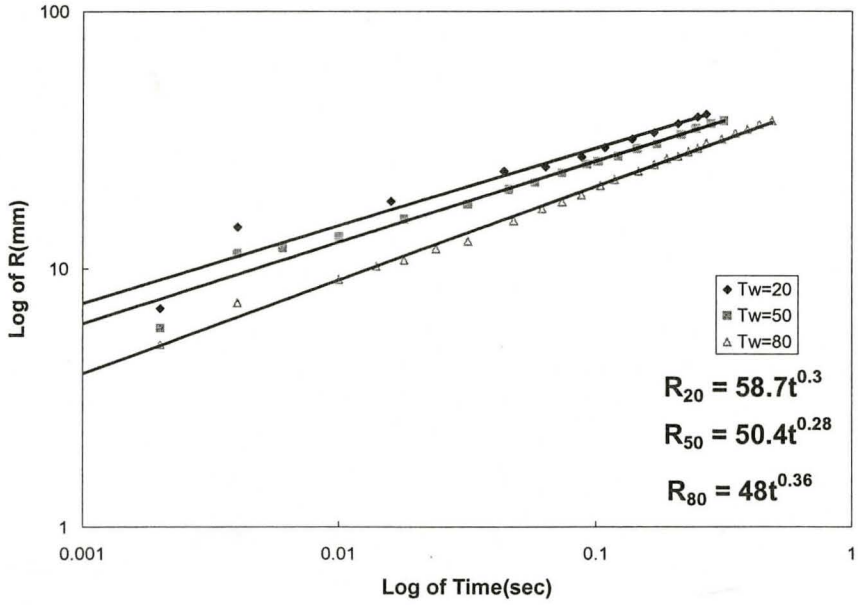

Figure 4.9: Radius of wetting front; as a function of time for Tw =20, 50, and 80°C and Dj=4mm, Tsp=250°C, and Vj = 5m/sec

As shown in Table 4.1 the increase in jet diameter has enhanced the propagation of wetting front. The radius of wetting front for R_{20} has increased to 35mm from 32mm in 0.18 seconds which when compared with that of Dj=3mm in figure 4.5 is an increase of 9.4%. Similarly delayed time for attaining the R_{50} = R_{20}=35mm has improved to 66.6% which was 100% for Dj=3mm and also the delayed time for attaining R_{80}= R_{20}=35mm has improved to 144% as compared to 200% for Dj=3mm. Hence Jet diameter has significant effect on propagation of wetting front. This might be attributed to the fact that increasing jet diameter and maintaining same jet velocity means higher flow rate. Experiments carried out with Dj=4mm, figure 4.9 had 77.8% higher flow rate than those reported in figure 4.5. It is worth noting that this increase in flow rate had its maximum impact on speed of wetting front at the highest water temperature, i.e. at Tw=80°C.

Table 4.1: Comparative analysis for Tsp=250°C, Dj=3mm and 4mm for Vj=5m/sec

	R_{20}		R_{50}		R_{80}	
Time(sec)	**mm(%age increase in comparison with initial value)**	**%age increase in comparison with Dj=3mm**	**mm(%age increase in comparison with initial value)**	**%age increase in comparison with Dj=3mm**	**mm(%age increase in comparison with initial value)**	**%age increase in comparison with Dj=3mm**
0.06	26	13	23	35	17	41.6
0.12	31(19.2%)	11	27(17.3%)	23	22(29.4%)	29.4
0.18	35(13%)	9.4	31(15%)	19	25(13.6%)	25
0.30	-	-	35(13%) delayed by 66.6%)	15.4	30(20%)	20
0.44					35(16.7%) delayed by 144%	

Figure 4.10 shows comparison of the propagation of wetting front with increase in water temperature for jet velocity of 7.75m/sec with jet diameter=4mm. The comparative analysis is presented in Table 4.2 which shows the effect of water temperature at Vj=7.75m/sec and comparison with results reported in figure 4.9 for Vj=5m/sec. The increase in jet velocity has increased the radius of wetting front in a given time. R_{20} in 0.18sec has increased to 37mm from 35mm when compared with that of Vj=5m/sec in figure 4.9 an increase of 6%. Similarly the time required for R_{50} = R_{20}=37mm has improved to 16.6% which was 66.6% for Vj=5m/sec and also the time required for R_{80}= R_{20}=37mm has improved to 30.7% which was 144% for Vj=5m/sec. Hence jet velocity has again shown to be strongly effecting the propagation of wetting front.

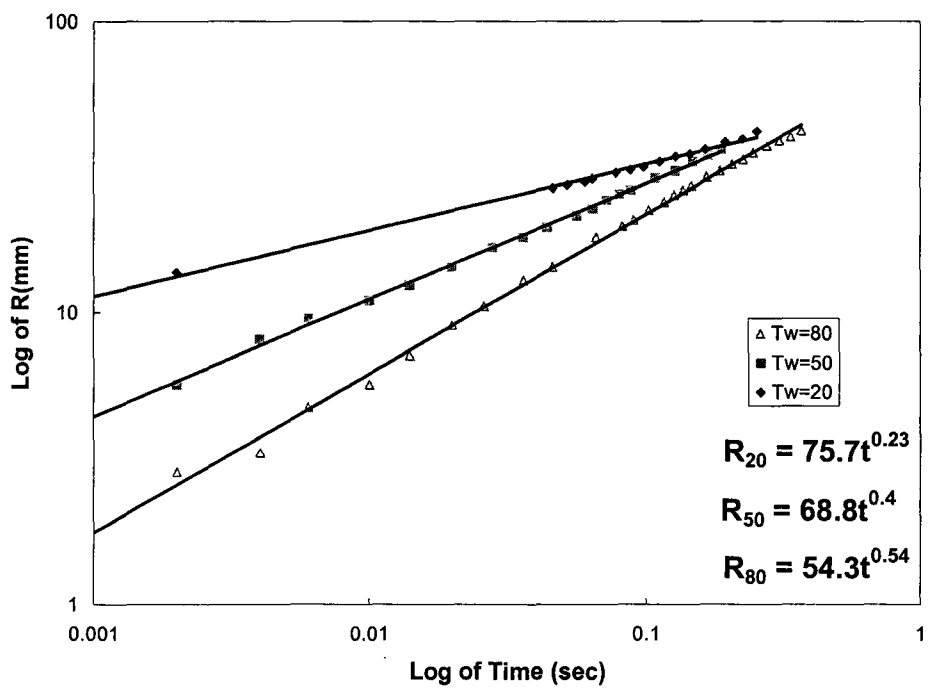

Figure 4.10: Radius of wetting front; as a function of time for Tw =20, 50, and 80°C and Dj=4mm, Tsp=250°C, and Vj = 7.75m/sec.

Table 4.2: Comparative analysis for Tsp=250°C, Dj=4mm for Vj=5 and 7.75m/sec

	R_{20}		R_{50}		R_{80}	
Time(sec)	**mm(%age increase in comparison with initial value)**	**%age increase in comparison with Vj=5m/sec**	**mm(%age increase in comparison with initial value)**	**%age increase in comparison with Vj=5m/sec**	**mm(%age increase in comparison with initial value)**	**%age increase in comparison with Vj=5m/sec**
0.06	29	11.5	23	0	17	0
0.12	34(17.2%)	9.6	30(17.3%)	11.1	23(44%)	4.5
0.18	37(13%)	6	35(15%)	13	29(26%)	16
0.21	-	-	37(6%) delayed by 16.6%)	17.5	32(10%)	15
0.26					37(16.7%) delayed by 30.7%	

Table 4.3: Comparative analysis for Tsp=250°C, Dj=3mm and 4mm for Vj=7.75

	R_{20}		R_{50}		R_{80}	
Time(sec)	**mm(%age increase in comparison with initial value)**	**%age increase in comparison with Dj=3mm**	**mm(%age increase in comparison with initial value)**	**%age increase in comparison with Dj=3mm**	**mm(%age increase in comparison with initial value)**	**%age increase in comparison with Dj=3mm**
0.06	29	7.4	23	44	17	33
0.12	34(17.2%)	6.2	30(17.3%)	30	23(44%)	35
0.18	37(13%)	5.7	35(15%)	20	29(26%)	38
0.21	-	-	37(6%) delayed by 16.6%)	17.7	32(10%)	15
0.26					35(16.7%) delayed by 30.7%	

Similarly Table 4.3 demonstrates the comparative effect on propagation of wetting front with variation in water temperature on the basis of figure 4.10 and also verifies the impact of jet diameter by comparing the propagation of wetting front for Dj=3mm with jet velocity of 7.75m/sec from figure 4.7.The increase in jet diameter has enhanced the propagation of wetting front. The value of R_{20} has increased to 37mm from 35mm in 0.18 seconds when compared with that of Dj=3mm in figure 4.7 is an increase of 5.7%. Similarly the time required for $R_{50} = R_{20}$=37mm has improved to 16.6%, which was 55.5 % for Dj=3mm and also the time required for attaining $R_{80}= R_{20}$=35mm has improved to 30.7%. Hence Jet diameter has significant effect on propagation of wetting front.

4.4. Results with Specimen Surface temperature of 500°C.

Although it has been shown that water temperature, jet velocity and jet diameter have profound effects on the propagation of wetting front for specimen surface temperature of 250°C but this needs to be verified for higher surface temperature of 500°C. During an experiment at specimen surface temperature of 500°C with water temperature of 80°C, propagation of wetting front with time could not be observed in the video because of vapors therefore for this surface temperature experiments were performed with a maximum water temperature of 75°C.

4.4.1. Effect of Water temperature, Jet velocity and Jet diameter.

Figures 4.11 and 4.13 for Dj=3mm, and, figures 4.14 and 4.16 for Dj=4mm, indicate the comparative growth of wetting front "R" with time for Tw=20, 50 and 75°C for jet velocities of 5 and 7.75m/sec.

Time delay in occurrence of wetting for experiment with Dj=3mm, Vj=5m/sec for Tw=20°C was found to be negligible but it was found to be 0.02 seconds for experiments with Tw=50 and 75°C. Results drawn in figure 4.11 show that the wetting fronts for water temperatures of 50 and 75°C have the same propagation speed after an initial transient period of 2 seconds. This might be due to the loss of momentum of water jet in which case the jet is unable to provide enough cooling for wetting front to propagate at different rates. Comparative analyses of the propagation of wetting front with time on the basis of figure 4.11 are shown in Table 4.4. Wetting front propagates faster with time for Tw=20°C as compared to Tw=50 and 75°C. In 1.6 seconds R_{20} reaches a value of 26mm which R_{50} and R_{75} take about 3.1 seconds to propagate to. This signifies about 100% delay for Tw=50 and 75°C.

Sequences for an experiment with jet diameter of 3mm, Tsp=500°C, Tw=20°C for jet velocity of 5m/sec are shown in figure 4.12 to demonstrate the propagation of wetting front.

Figure 4.13 shows the propagation of wetting front as a function of time for Tw=20, 50 and 75°C for jet velocity of 7.75m/sec. Wetting delay for experiment with Tw=20°C was found to be negligible but it was found to be 0.01 seconds for experiments with Tw=50 and 75°C. Table 4.5 presents the comparative effect on propagation of wetting front with variation in water temperature on the basis of figure 4.13 and also verifies the impact of jet velocity by comparing the propagation of wetting front for Vj=5m/sec for jet diameter of 3mm from figure 4.11.

The increase in jet velocity from 5 to 7.75m/sec has increased the radius of wetting front in a given time. R_{20} has increased to 31.5mm in 1.2 seconds which was 26mm in 1.6 seconds when compared with that of Vj=5m/sec in figure 4.6. This is an

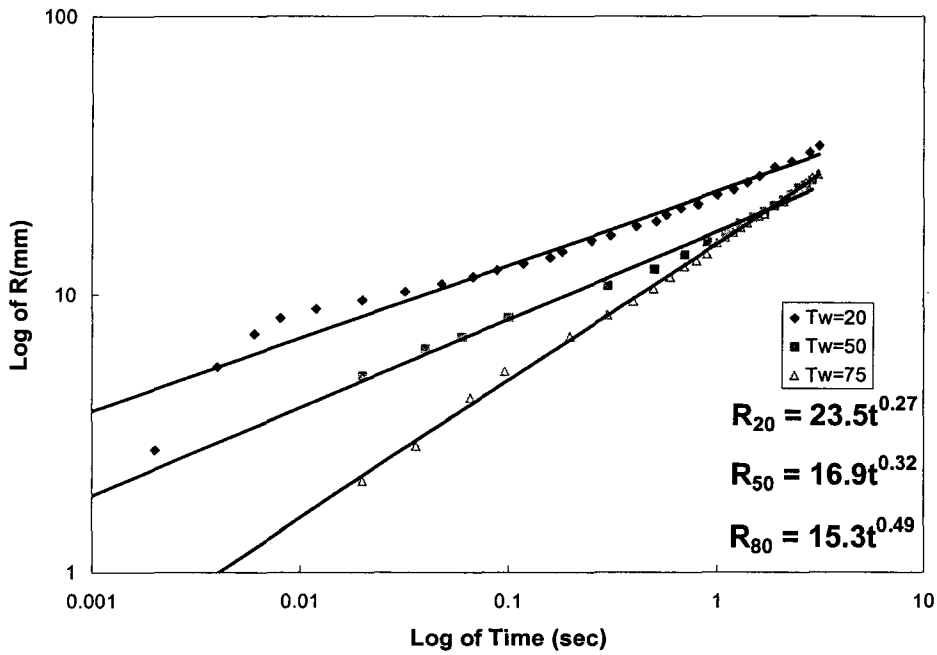

Figure 4.11: Radius of wetting front; as a function of time for Tw =20, 50, and 75°C and Dj=3mm, Tsp=500°C, and Vj = 5m/sec.

Table 4.4: Comparative analysis for Tsp=500°C, Dj=3mm and Vj=5m/sec

Time (seconds)	R_{20} mm (%age increase)	R_{50} mm (%age increase)	R_{75} mm (%age increase)
0.4	19	13	10
0.8	22(15.5%)	15.5(19.2%)	13.5(35%)
1.2	25(13.6%)	18(16.1%)	17(26%)
1.6	26(4%)	19(5%)	18(6%)
3.1		26(36.8%) delayed by 100%	26(36.8%) delayed by 100%

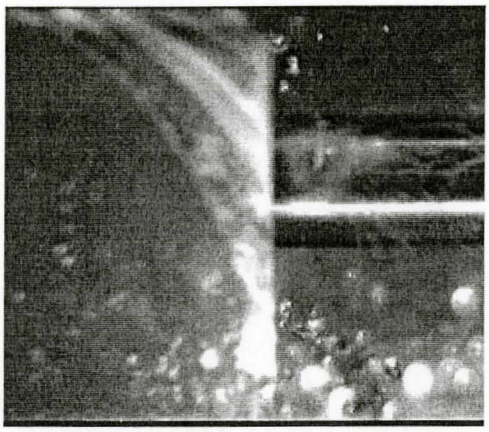

t=0 seconds, R= 0 mm

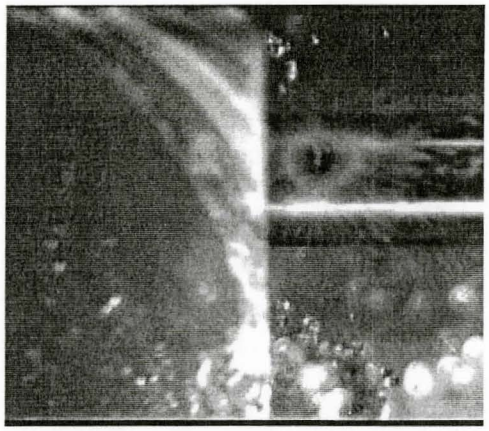

t= 0.002 seconds, R= 2.74mm

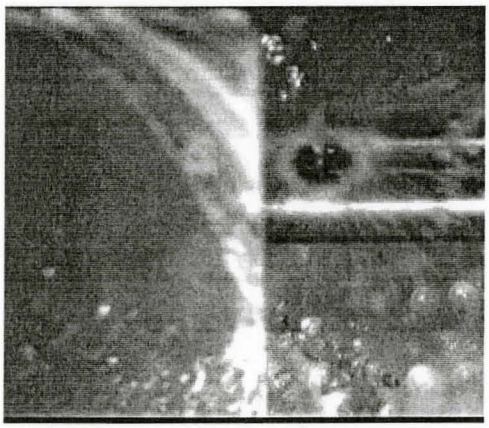

t= 0.004, R= 5.47mm

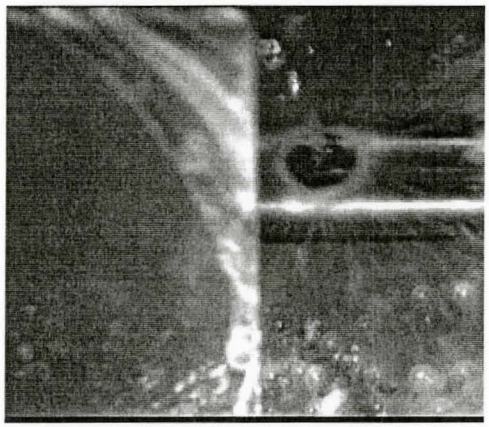

t= 0.006, R=7.2mm

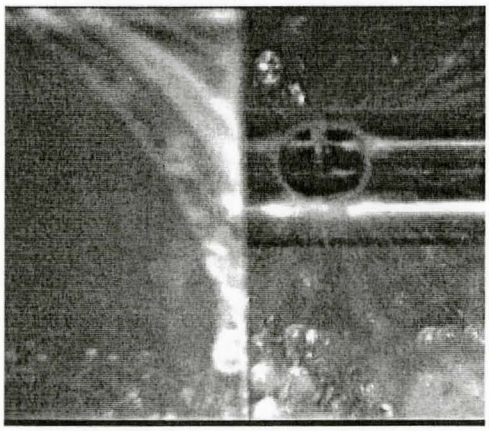

t= 0.012 seconds, R = 8.9mm

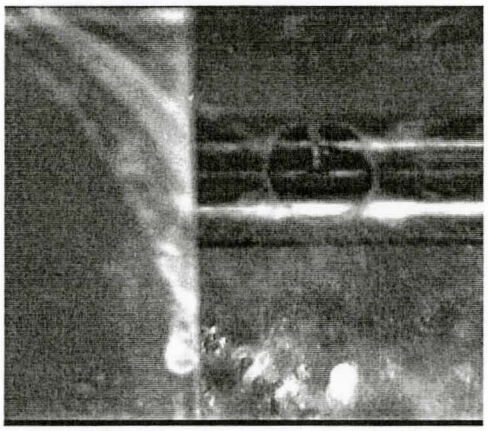

t= 0.032 seconds, R = 10.25mm

Figure 4.12: Sequences for experiment - Dj=3mm, Tsp=500°C, Tw=20°C, Vj= 5m/sec

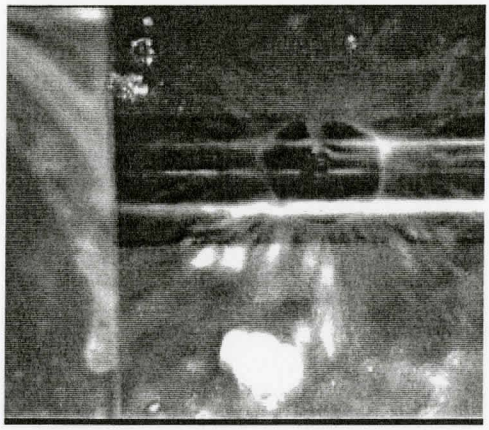

t = 0.068 seconds, R = 11.32 mm

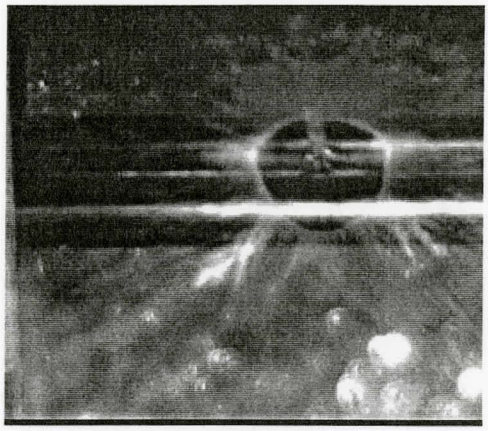

t = 0.118 seconds, R= 13mm.

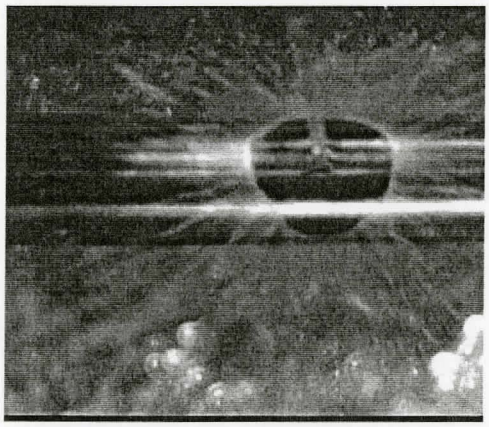

t= 0.18 seconds, R=14.36mm

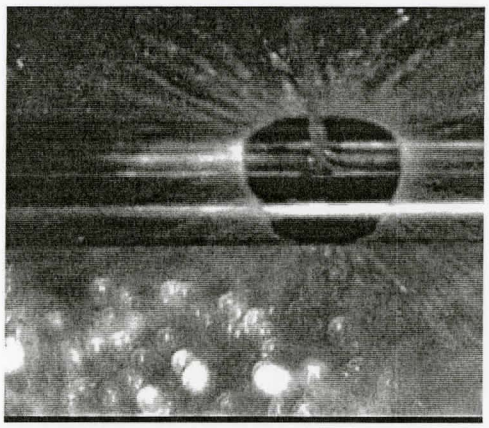

t = 0.308 seconds, R = 16.41mm

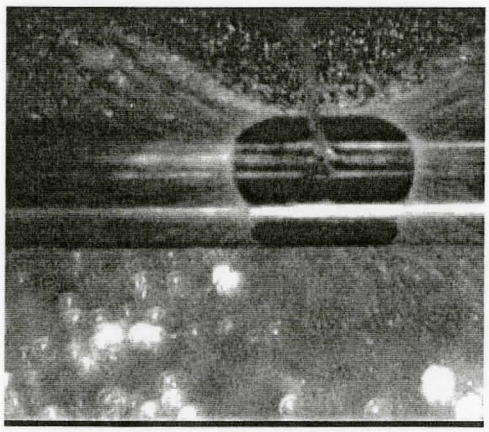

t = 0.508 seconds, R=18.46mm

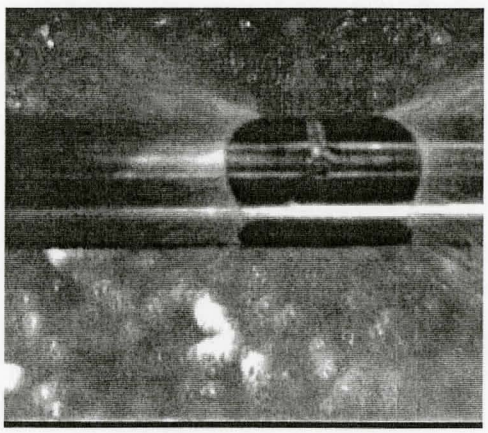

t = 0.668 seconds, R= 20.5mm

Figure 4.12: Sequences for experiment - Dj=3mm, Tsp=500°C, Tw=20°C, Vj= 5m/sec

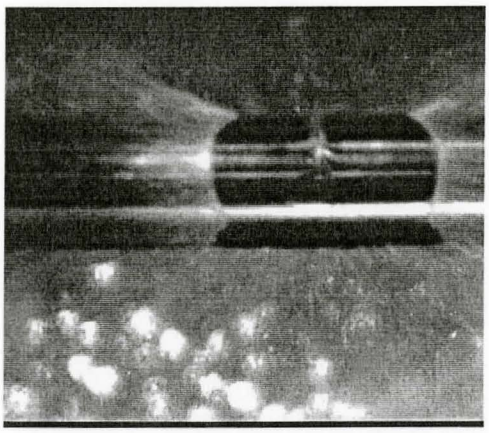

t= 1.008 seconds, R = 22.9mm

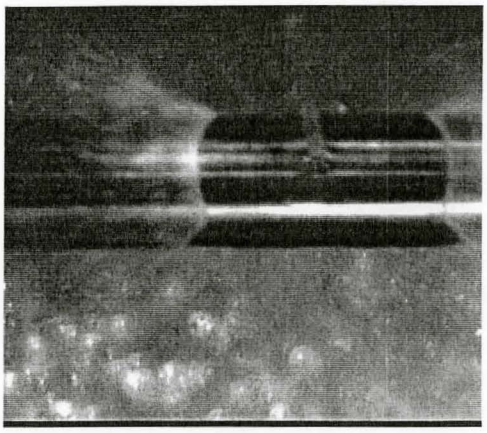

t = 1.408 seconds, R = 25.3mm

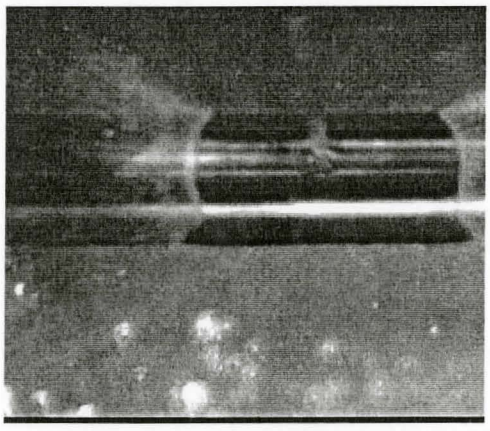

t = 1.608 seconds, R = 26.7mm

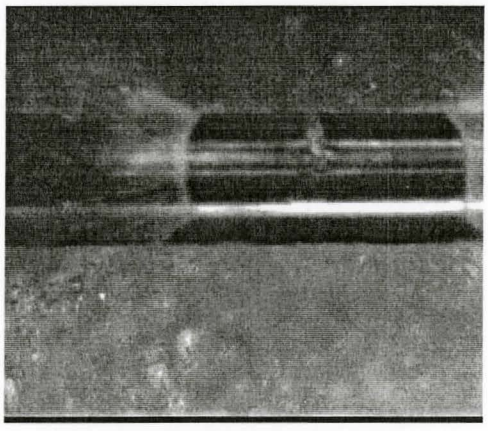

t = 1.908 seconds, R =28.7mm

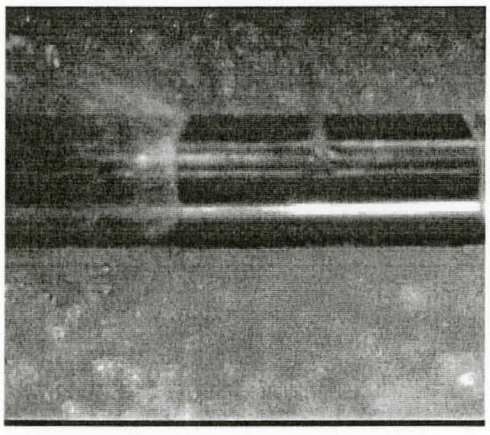

t = 2.308 seconds, R = 30.1mm

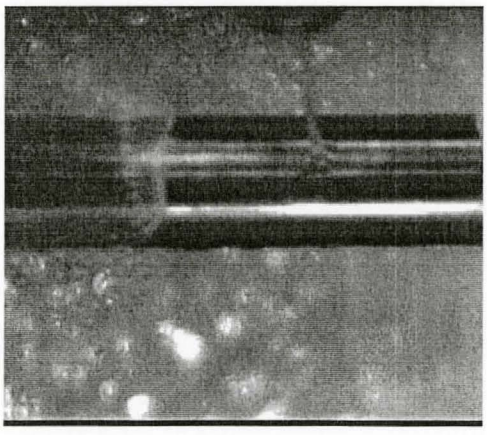

t = 2.808 seconds, R = 32.5mm

Figure 4.12: Sequences for experiment - Dj=3mm, Tsp=500°C, Tw=20°C, Vj= 5m/sec

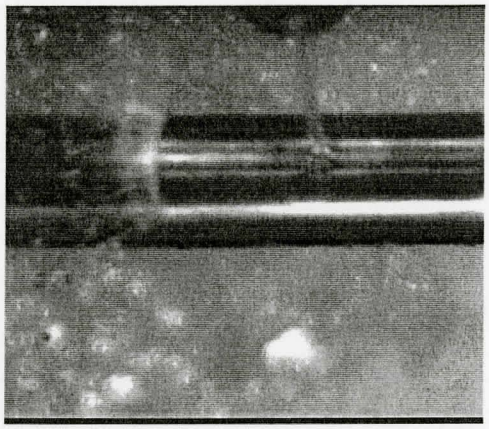

t = 3.12 seconds, R = 34.2mm

Figure 4.12: Sequences for experiment - Dj=3mm, Tsp=500°C, Tw=20°C, Vj= 5m/sec

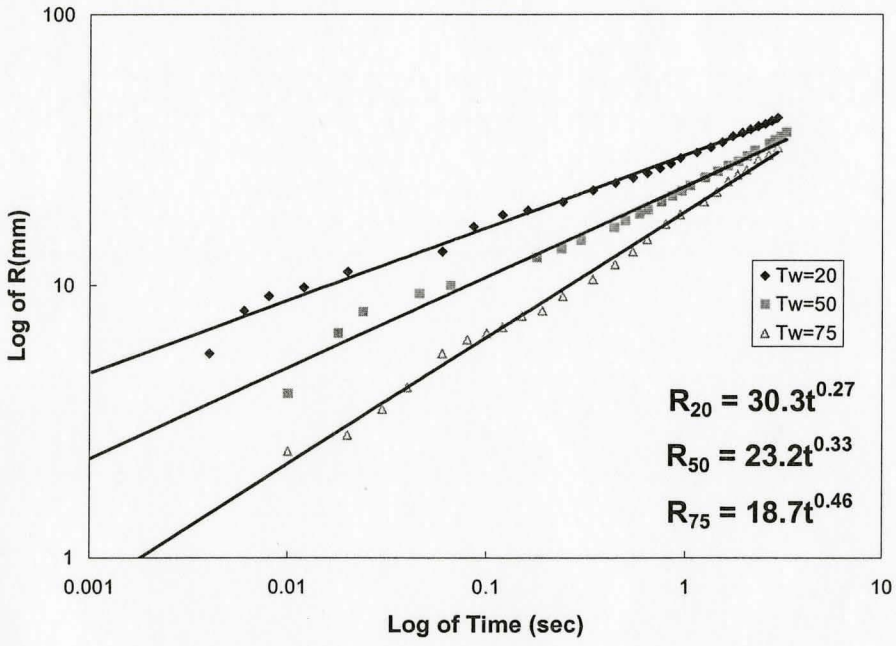

Figure 4.13: Radius of wetting front; as a function of time for Tw =20, 50, and 75°C and Dj=3mm, Tsp=500°C, and Vj = 7.75m/sec.

increase of 26%. Similarly the delayed time for attaining the R_{50} = R_{20}=31.5mm has increased to 125%which was 100% for Vj=5m/sec. It is important to note that this delayed time for jet velocity of 7.75m/sec is of 1.5 seconds while it is also 1.5 seconds for Vj=5m/sec. The delayed time for attaining R_{75}= R_{20}=31.5mm has increased to 158% (represent 1.5 sec) which was 100 %(represent 1.9 sec.) for Vj=5m/sec. Hence jet velocity has again shown to be strongly effecting the propagation of wetting front. The sequences for an experiment with Dj=3mm, Tsp=500°C, Vj=7.75m/sec and Tw=75°C, are shown in figure 4.14

Table 4.5: Comparative analysis for Tsp=500°C, Dj=3mm for Vj=5 and 7.75m/sec

	R_{20}		R_{50}		R_{75}	
Time(sec)	**mm(%age increase in comparison with previous value)**	**%age increase in comparison with Vj=5m/sec**	**mm(%age increase in comparison with previous value)**	**%age increase in comparison with Vj=5m/sec**	**mm(%age increase in comparison with previous value)**	**%age increase in comparison with Vj=5m/sec**
0.4	23.5	23.71	17.5	35	12	20
0.8	28(19%)	27.5	21(20%)	35	17(42%)	26
1.2	31.5(12%)	26	24(14.3%)	33.3	20(17.6%)	17.6
2.7	-	-	31.5(31.25%) delayed by 125%)	17.5	28(40%)	15
3.1					31.5(12.5%) delayed by 158%	

Figure 4.15 shows the effect of water temperature on propagation of wetting front with time for Dj=4mm and Vj=5m/sec. Wetting delay for experiment with Tw=20°C was found to be negligible but it was found to be 0.022 seconds for experiments with Tw=50 and 0.05 seconds for Tw=75°C. Consistent to what was observed in figure 4.11, the

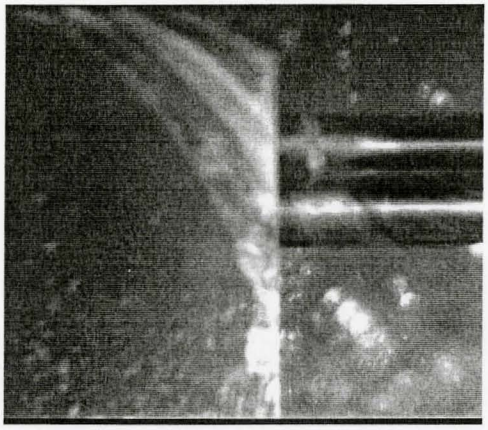

t=0 seconds, R=0 mm

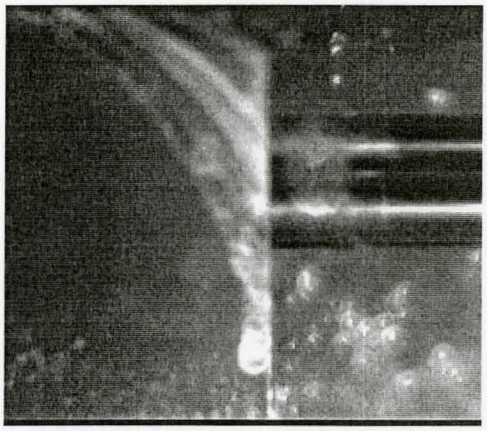

t = 0.004seconds, R= 0 mm

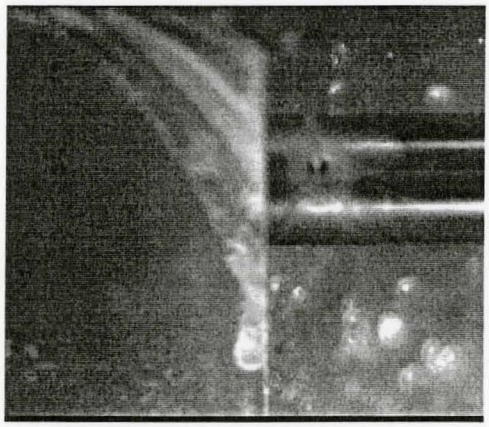

t = 0.01 seconds, R =2.45mm

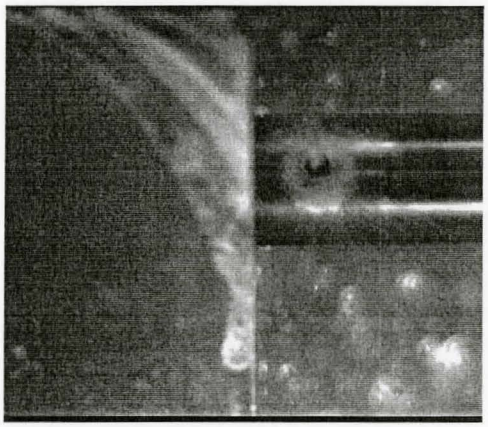

t = 0.02 seconds, R =2.8 mm

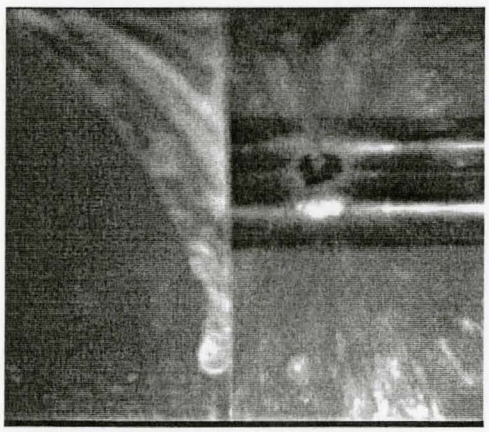

t = 0.04 seconds, R=4.2mm

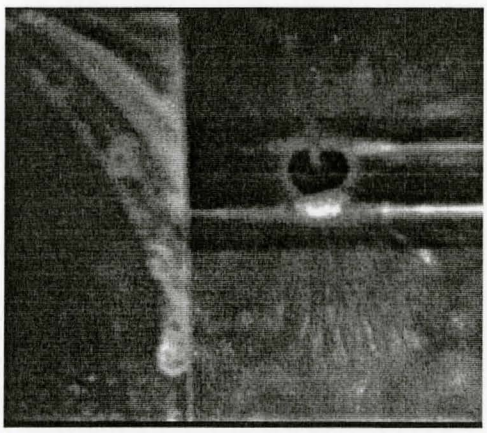

t = 0.08 seconds, R = 6.3mm

Figure 4.14: Sequences for experiment - Dj=3mm, Tsp=500°C, Tw=75°C, Vj= 7.75m/sec

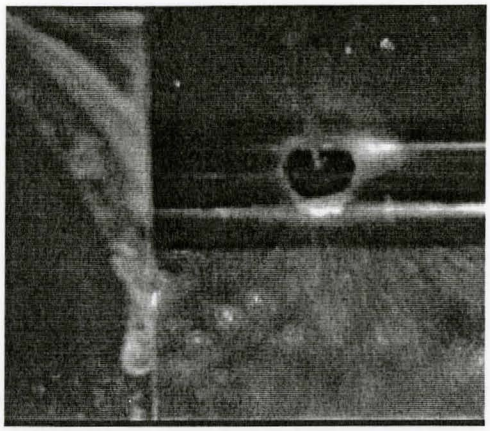

t = 0.12 seconds, R = 7mm

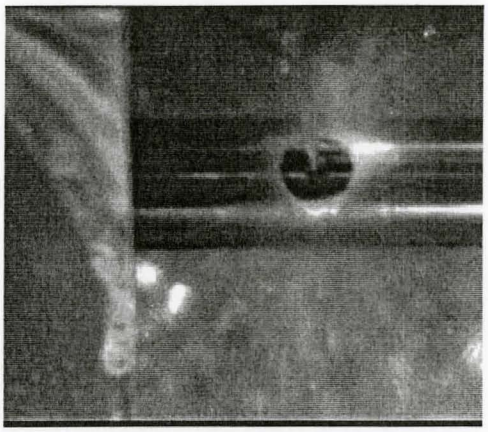

t = 0.15 seconds, R = 7.74 mm

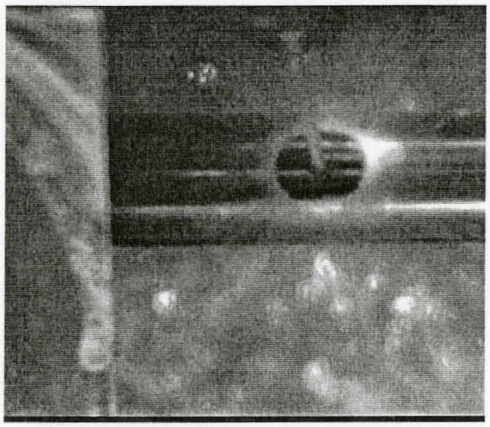

t = 0.24 seconds, R= 9.12 mm

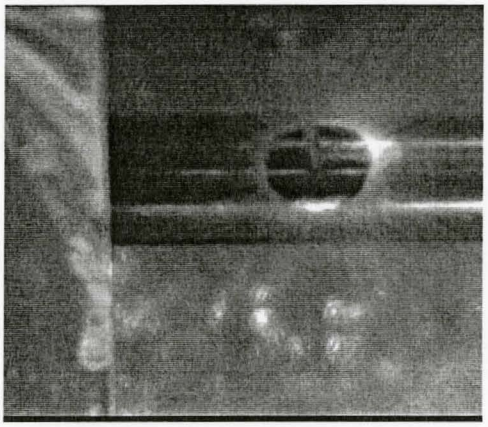

t = 0.34 seconds, R = 10.52mm

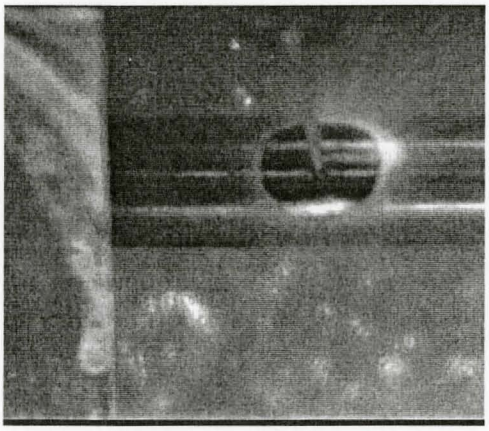

t = 0.44 seconds, R = 11.9mm

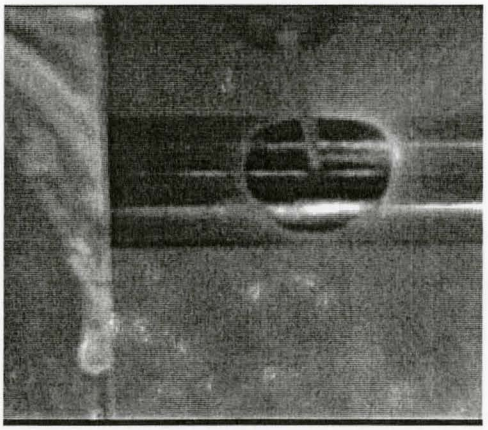

t = 0.64 seconds, R = 14.7mm

Figure 4.14: Sequences for experiment - Dj=3mm, Tsp=500°C, Tw=75°C, Vj= 7.75m/sec

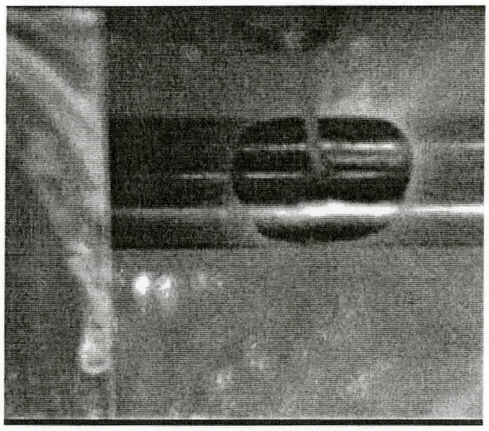

t = 0.94 seconds, R = 18.25 mm

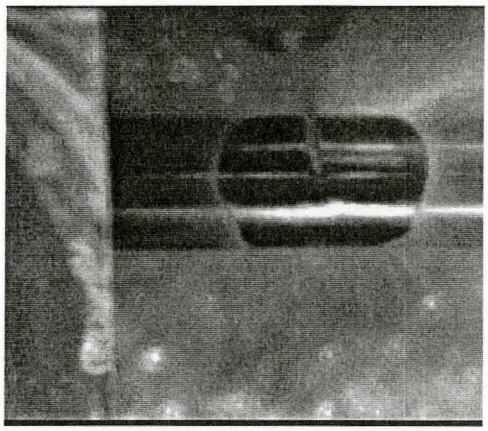

t = 1.24 seconds, R = 20.35 mm

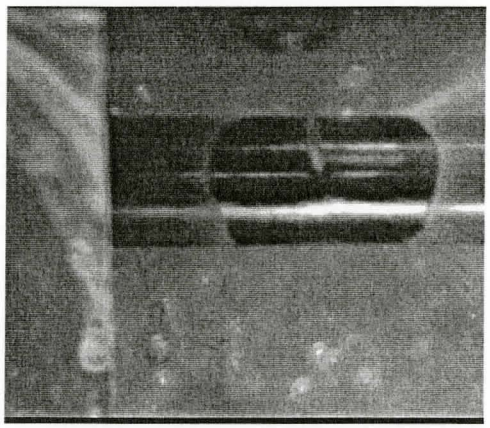

t = 1.44 seconds, R = 24.2 mm

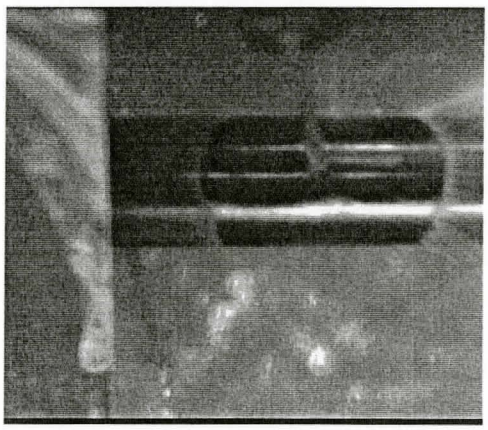

t = 1.64 seconds, R = 25.6 mm

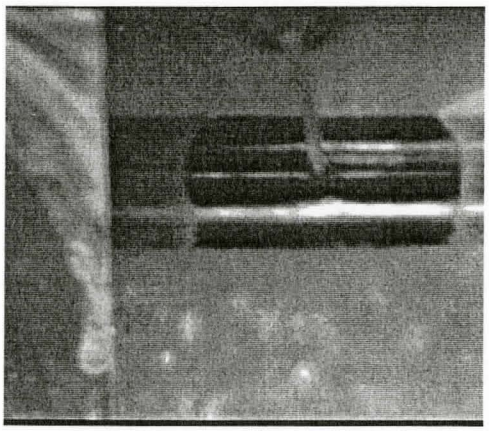

t = 2.04 seconds, R = 26.7mm

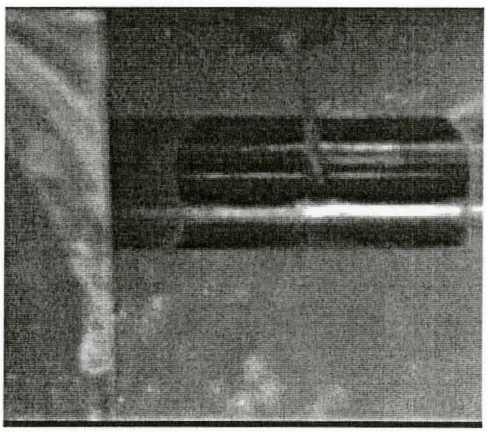

t = 2.34 seconds, R = 29.13

Figure 4.14: Sequences for experiment - Dj=3mm, Tsp=500°C, Tw=75°C, Vj= 7.75m/sec

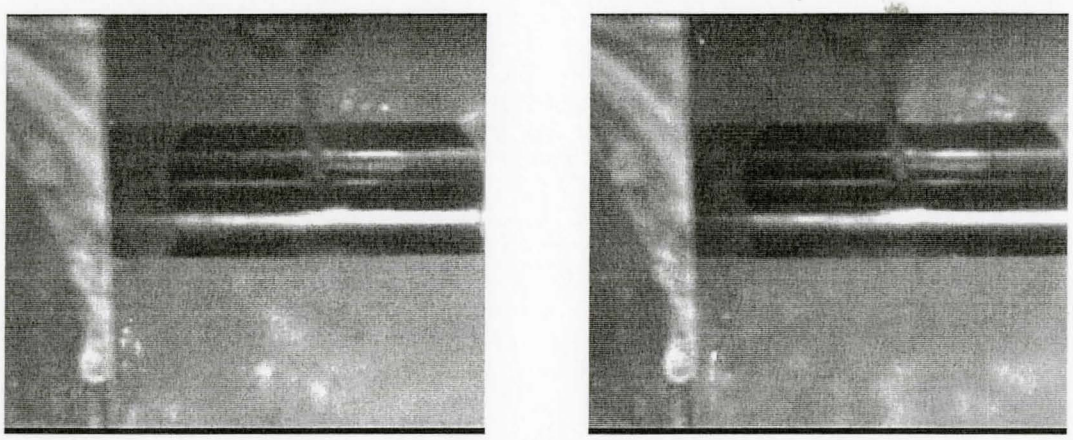

t = 2.64 seconds, R = 30.18 mm t = 2.94 seconds, R =32.3

Figure 4.14:Sequences for experiment - Dj=3mm, Tsp=500°C, Tw=75°C, Vj= 7.75m/sec.

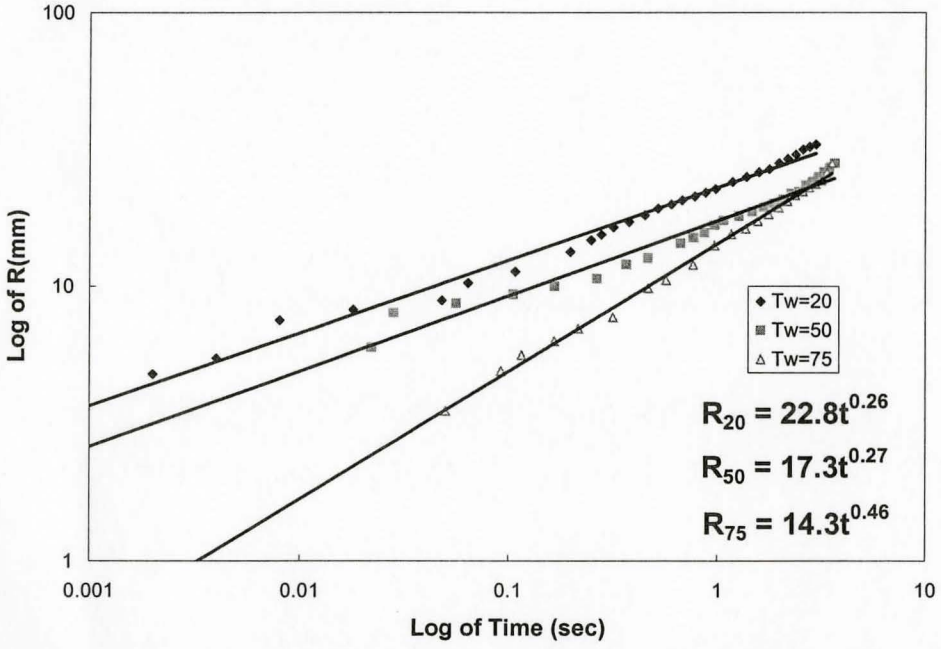

Figure 4.15: Radius of wetting front; as a function of time for Tw =20, 50, and 75°C and Dj=4mm, Tsp=500°C, and Vj = 5m/sec.

wetting fronts for Tw= 50 and 75°C appear to have the same propagation speed after 2.8 seconds and they seem very close to each other afterwards. This might be due to the loss of momentum of water jet due to which jet is unable to provide enough cooling for wetting front to propagate.

Table 4.6: Comparative analysis for Tsp=500°C, Vj=5 m/sec for Dj=3mm and 4mm

	R_{20}		R_{50}		R_{75}	
Time(sec)	**mm(%age increase in comparison with previous value)**	**%age increase in comparison with Dj=3mm**	**mm(%age increase in comparison with previous value)**	**%age increase in comparison with Dj=3mm**	**mm(%age increase in comparison with previous value)**	**%age increase in comparison with Dj=3mm**
0.4	18	0	14	7	10	0
0.8	22(15.7%)	0	16(14.3%)	3.2	13.5(35%)	0
1.4	25.5(13.6%)	2	19(19%)	3	18(38%)	3
3	-	-	25.5(34.2%) delayed by 100%)	17.5	25.5(46%) delayed by 100%)	0

Table 4.6 demonstrates the comparative effect on propagation of wetting front with variation in water temperature on the bases of figure 4.8 and also shows the impact of jet diameter by comparing the propagation of wetting front for Dj=3mm for jet velocity of 5m/sec from figure 4.6. Increase in jet diameter here seems to have no effect on the propagation of wetting front. The R_{20} has increased to 25.5mm from 25mm when compared with that of Dj=3mm in figure 4.6 which is a negligible increase Similarly the delayed time for attaining the R_{50} = R_{20}=25.5mm is the same which is 100 % for Dj=3mm and also the delayed time for attaining R_{75}= R_{20}=25.5mm remains the same.

This implies that increase in jet diameter shows no effect on propagation of wetting front when surface temperature is increased to 500°C which might be due to insufficient cooling capacity of water jet. Hence propagation of wetting front seems to be weakly affected by increase in jet diameter.

Figure 4.16 shows the effect of water temperature on propagation of wetting front with time for Dj=4mm and Vj=7.75m/sec. Wetting delay for experiment with Tw=20°C was found to be negligible but it was 0.014 seconds for experiments with Tw=50 and 0.018 seconds for Tw=75°C. Table 4.7 shows the comparative effect on propagation of wetting front with variation in water temperature on the basis of figure 4.16 and also shows the impact of jet velocity by comparing the propagation of wetting front for Dj=4mm for jet velocity of 5m/sec from figure 4.15.

Although wetting front initially propagates faster for all temperatures when compared with that of figure 4.13 but then slows down for Tw=50 and 75°C. Radius of wetting front for water temperature of 20 °C continue to propagate faster and attain a value of 34mm in 0.8 seconds which is attained by water temperatures of 50 and 75°C in 3 seconds. It is still better when compared with the radius of wetting front of 25.5 mm in 3 seconds for Tw=50 and 75°C for Dj=4mm and Vj=5m/sec from figure 4.15. This fact is tabulated in Table 4.7.

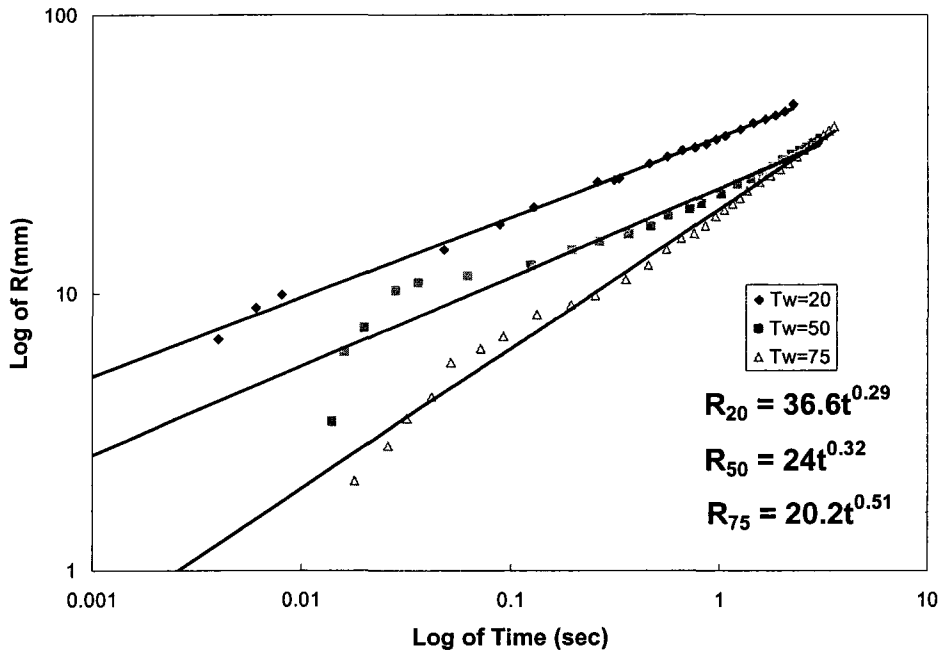

Figure 4.16: Radius of wetting front; as a function of time for Tw =20, 50, and 75°C and Dj=4mm, Tsp=500°C, and Vj = 7.75m/sec.

Table 4.7: Comparative analysis for Tsp=500°C, Dj=4mm for Vj=5 and 7.75m/sec

	R_{20}		R_{50}		R_{75}	
Time(sec)	**mm(%age increase in comparison with initial value)**	**%age increase in comparison with Vj=5m/sec**	**mm(%age increase in comparison with initial value)**	**%age increase in comparison with Vj=5m/sec**	**mm(%age increase in comparison with initial value)**	**%age increase in comparison with Vj=5m/sec**
0.4	29	61	18	22	22.22	35
0.8	34(17.2%)	9.6	23(28%)	44	18(33%)	33
3			34(48%) delayed by 275%		34(89%) delayed by 275%	

Table 4.8: Comparative analysis for Tsp=500°C, Dj=3mm and 4mm for Vj=7.75

	R_{20}		R_{50}		R_{75}	
Time(sec)	**mm(%age increase in comparison with initial value)**	**%age increase in comparison with Dj=3mm**	**mm(%age increase in comparison with initial value)**	**%age increase in comparison with Dj=3mm**	**mm(%age increase in comparison with initial value)**	**%age increase in comparison with Dj=3mm**
0.4	29	24	18	3	13.5	12.5
0.8	34(17.2%)	21	23(28%)	9.5	18(33%)	6
3			34(48%) delayed by 275%	8	34(48%) delayed by 275%	8

Table 4.8 shows the comparative effect of water temperature on the propagation of wetting front from figure 4.16 and also indicate the effect of increase in jet diameter by comparing the propagation of wetting front for Dj=3mm and Vj=7.75m/sec from figure 4.13. It shows increase in propagation of wetting front with increase in jet diameter to be higher for water temperature of 20°C when compared with increase in propagation of wetting front for 50 and 75°C. This might be due to the sufficient cooling capacity of water at 20°C as compared to that of water at temperatures of 50 and 75°C. This indicates that increasing jet diameter strongly affect the propagation of wetting front at lower water temperature of 20°C at jet velocity of 7.75m/sec.

Although it has been shown earlier that jet diameter has weak effect on propagation of wetting front at jet velocity of 5m/sec, but , this analysis also concludes that at higher jet velocity of 7.75m/sec and lower water temperature of 20°C jet diameter has strong effect on propagation of wetting front.

4.5 Effect of specimen surface temperature.

In order to investigate the effect of specimen surface temperature experiments were performed for water temperature of 20°C and 70 °C for specimen surface temperature of 800°C. Wetting delay for experiments with Tw=20°C and 70°C was found to be 0.02 and 0.084 seconds respectively. An experiment at water temperature of 80°C was performed but due to a lot of vapor it was impossible to study the wetting front at this temperature. The results were utilized for comparison with the results from surface temperatures of 250 and 500°C to assess the effect of surface temperature.

Figure 4.17 and 4.18 shows the comparison of propagation of wetting front at specimen surface temperatures of 250,500 and 800°C with jet diameter of 3mm at low water temperature of 20°C and higher possible water temperatures. These figures show that specimen surface temperature strongly influence the propagation of wetting front.

Results reported in figure 4.17 indicate that the propagation of wetting front is highest for surface temperature of 250°C. Wetting front propagates to 37mm in less than 0.2 seconds. The radius of wetting front at 500 and 800°C at 0.2 seconds seems to be 16mm and 10mm respectively, indicating significantly lower propagation speeds. It takes about 2.8 seconds for wetting front at specimen surface temperature of 500°C to propagate to 37 mm and specimen with surface temperature of 800°C reached a maximum value of 32 mm in 2.9 seconds.

Figure 4.18 shows the propagation of wetting front at high water temperatures of 70,75 and 80°C for surface temperatures = 800,500 and 250°C.Speed of wetting front is

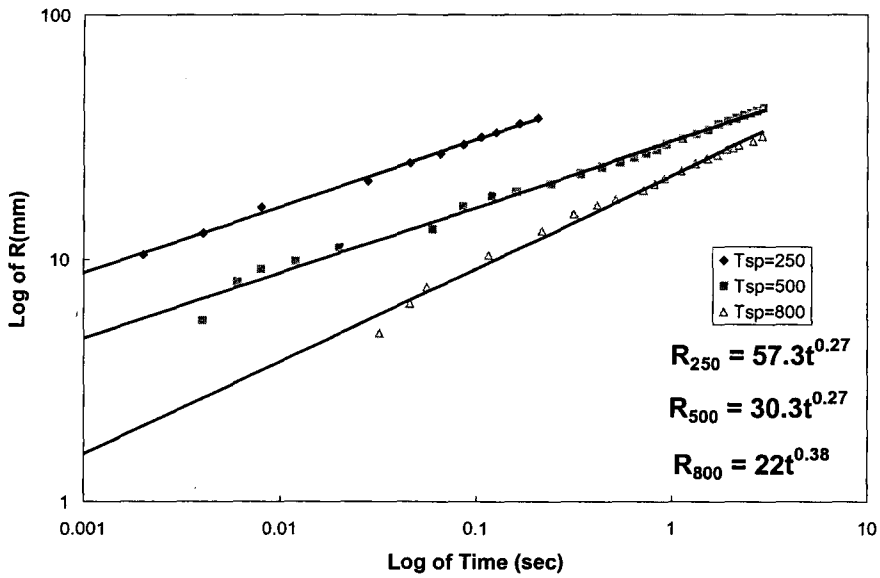

Figure 4.17: Radius of wetting front; as a function of time for Tw =20°C,Dj=3mm, Tsp=250,500 and 800°C, and Vj = 7.75m/sec.

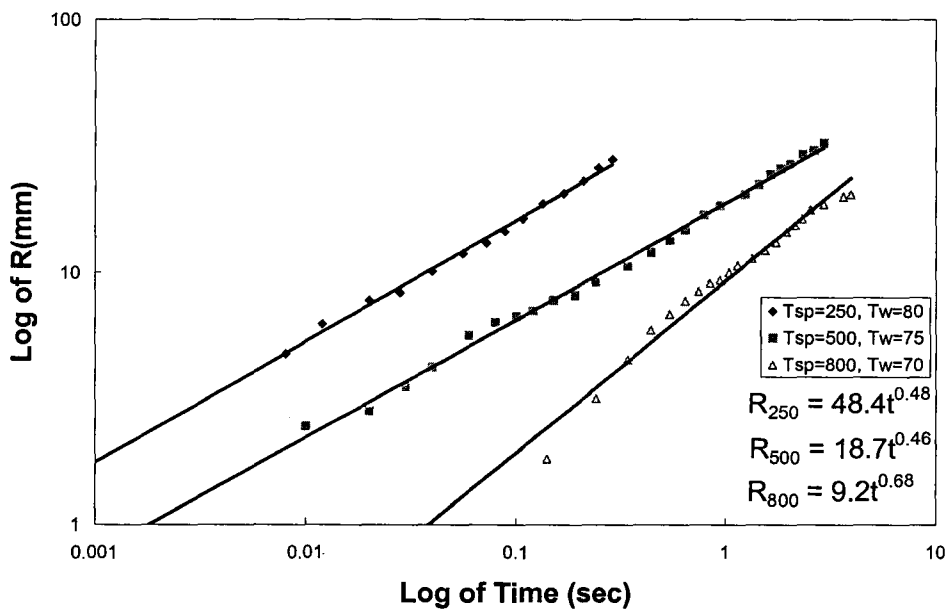

Figure 4.18: Radius of wetting front; as a function of time for Tw =70,75 and 80°C for Tsp= 800,500 and 250°C for Dj=3mm, and Vj = 7.75m/sec.

highest for surface temperature of 250°C. Wetting front propagates to 27mm in less than 0.3seconds which when compared with that of figure 4.18 is lower. The radius of wetting front at 500 and 800°C at 0.3 seconds seems to be 9.5mm and 2.5mm which comparably are very low. It takes about 2.2 seconds for wetting front at specimen surface temperature of 500°C to propagate to 27mm and specimen with surface temperature of 800°C reached a maximum value of 21mm in 4 seconds.

Hence specimen surface temperature strongly influences the propagation of wetting front. This influence increases with decrease in water temperature and decrease of specimen surface temperature. This might be due to higher cooling capacity of water at low water temperature.

4.6. Effect of jet velocity and degree of sub-cooling (ΔTsub) on constants:

In analysis of propagation of wetting front for each experiment, curves were approximated for position as the power function with respect to time as given by equation (1).

The values of constants "a" are plotted against degree of sub-cooling for different specimen temperature and jet velocities as shown in figures 4.19 and 4.20. Value of constant "a" has an increasing trend with increase in jet velocities but decreasing trend with increase in specimen surface temperature. Values of constant "a" are the lowest for specimen surface temperature of 800°C as shown in figure 4.21. Slopes of linear relationship between constant "a" and degree of sub-cooling are given in Table 4.9. The

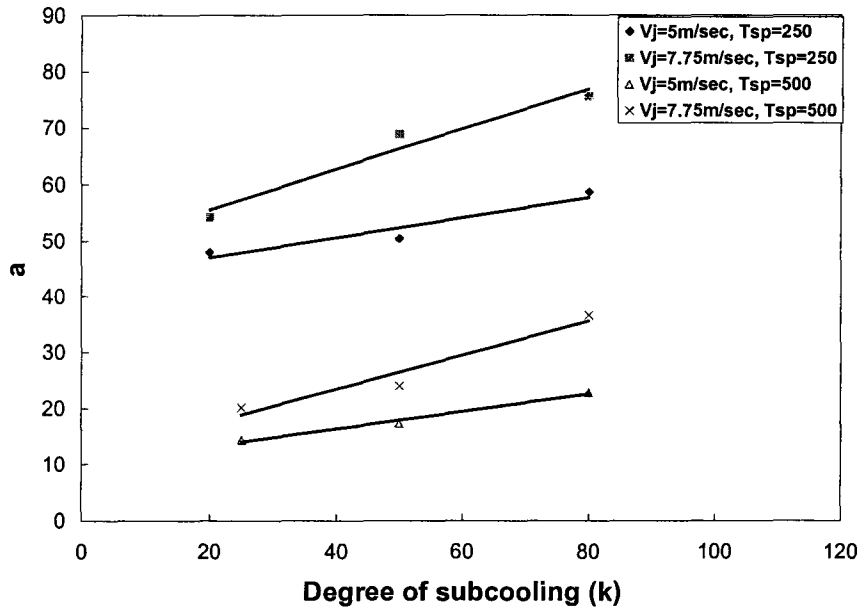

Figure 4.19: Relationship between constant "a" and degree of sub-cooling(ΔTsub) for jet diameter of 3mm.

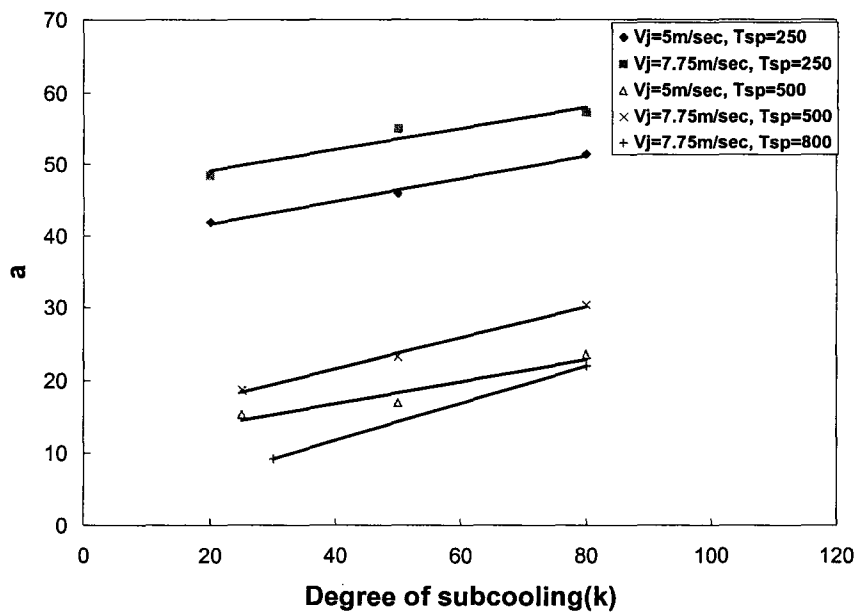

Figure 4.20: Relationship between constant "a" and degree of sub-cooling (ΔTsub) for jet diameter of 4mm.

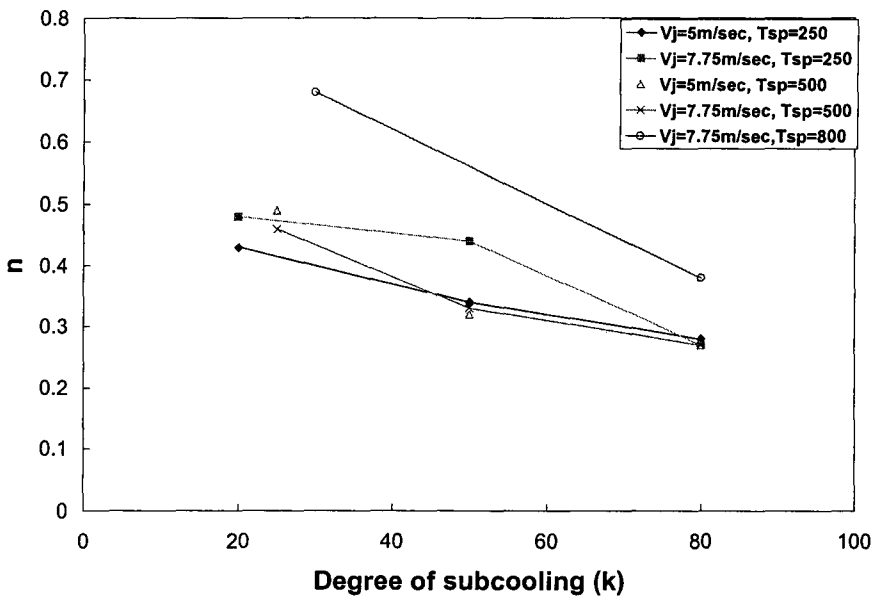

Figure 4.21: Relationship between constant "n" and degree of sub-cooling (ΔTsub) for jet diameter of 3mm.

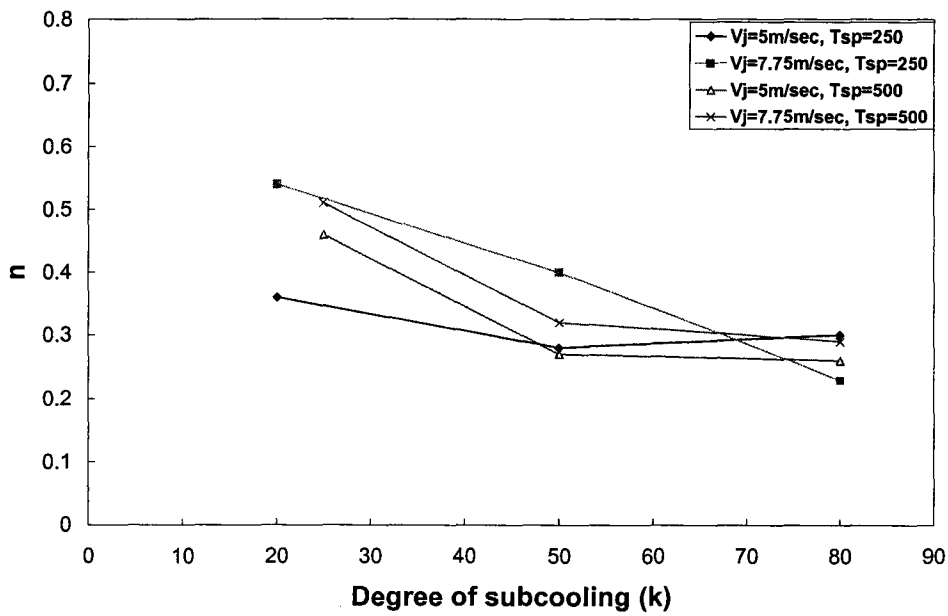

Figure 4.22: Relationship between constant "n" and degree of sub-cooling (ΔTsub) for jet diameter of 4mm.

Table 4.9: Slopes of linear relationship between constant "a" and degree of sub-cooling.

Parameters	Slope of constant "a"
Jet diameter=3mm.	
Tsp=250°C, Vj=5m/sec	0.16
Tsp=250°C, Vj=7.75m/sec	0.15
Tsp=500°C, Vj=5m/sec	0.15
Tsp=500°C, Vj=7.75m/sec	0.21
Tsp=800°C, Vj=7.75m/sec	0.26
Jet diameter=4mm.	
Tsp=250°C, Vj=5m/sec	0.18
Tsp=250°C, Vj=7.75m/sec	0.36
Tsp=500°C, Vj=5m/sec	0.16
Tsp=500°C, Vj=7.75m/sec	0.30

Table 4.10: Range of values of constant "a" for ΔT_{sub} = 20 to 80°C

Parameters	Range of value of "a"
Jet diameter=3mm.	
Tsp=250°C	41.9 to 57.3
Tsp=500°C	15.3 to 30.3
Tsp=800°C	9.2 to 22
Jet diameter=4mm.	
Tsp=250°C	48 to 75.7
Tsp=500°C	14.3 to 36.6

Table 4.11: Range of values of exponent "n" for ΔTsub = 20 to 80°C

Parameter	Range of value of "n"
Jet diameter =3mm.	
Tsp=250°C	0.27 to 0.48.
Tsp=500°C	0.27 to 0.49
Tsp=800°C.	0.38 to 0.68.
Jet diameter =4mm.	
Tsp=250°C	0.23 to 0.54.
Tsp=500°C	0.29 to 0.50.

range of values of constant "a" for range of degree of sub-cooling (ΔTsub) =20-80°C is presented in Table 4.10.Relationship between exponent "n" and degree of sub-cooling is shown in figures 4.21 and 4.22. The exponent "n" appears to be independent of jet velocity but weakly dependent on degree of sub-cooling. The range of values of exponent "n" for range of degree of sub-cooling (ΔTsub) =20-80°C is shown in table 4.11.

4.7. Transient Temperature in hot specimen.

Transient temperatures were recorded by thermocouples embedded in the specimen at a depth of 1mm from the specimen surface by the help of data acquisition system. Although there was one thermocouple at the specimen surface at 41.75mm from impingement centre, which gives surface temperature to start the experiment but there was no thermocouple installed at the surface in the vicinity of impingement area to avoid disturbance to the propagation of wetting front.

Hence, there was delay time in transmission of cooling by impinging jet to the embedded thermocouples. This delay time was calculated by using the following semi-infinite 1-D heat conduction equation :-

$$\frac{T(x,t)-T_0}{T_i-T_0}=erf\left(\frac{x}{2\sqrt{\alpha t}}\right) \quad (2)$$

Where: $T(x,t)$ is Temperature at time "t" at 1mm from surface, T_0 is Specimen surface temperature and T_i is initial temperature of 1mm thick stainless steel between position of thermocouple and specimen surface.

Delay time was found to be 0.047 to 0.076 seconds.

4.7.1. Propagation of Wetting Front as indicated by Transient Temperature Measurements.

The curves for the propagation of wetting front for all experiments were evaluated from the videos. An analysis of temperature readings of selected experiment is done in an attempt to examine the possibility of predicting the propagation of wetting front by using temperature readings of embedded thermocouples.

As wetting front reach thermocouple locations the temperature at that location will start dropping quickly and thus a sudden temperature drop in the cooling curve will be evident. The propagation of wetting front on the basis of estimated power relation for one of the experiments reported in figure 4.11 is shown in figure 4.23. Transient temperature curves recorded for this experiment are shown in figure 4.24. Temperature drop experienced by the thermocouple located at the impingement point (IP) signify the start of experiment as this is the point which will first experience the impingement, was used therefore to determine the starting time for these temperature measurements indicating beginning of wetting. Only the first 5.6 seconds are shown in figure 4.25 corresponding to R-t relation shown in figure 4.23.

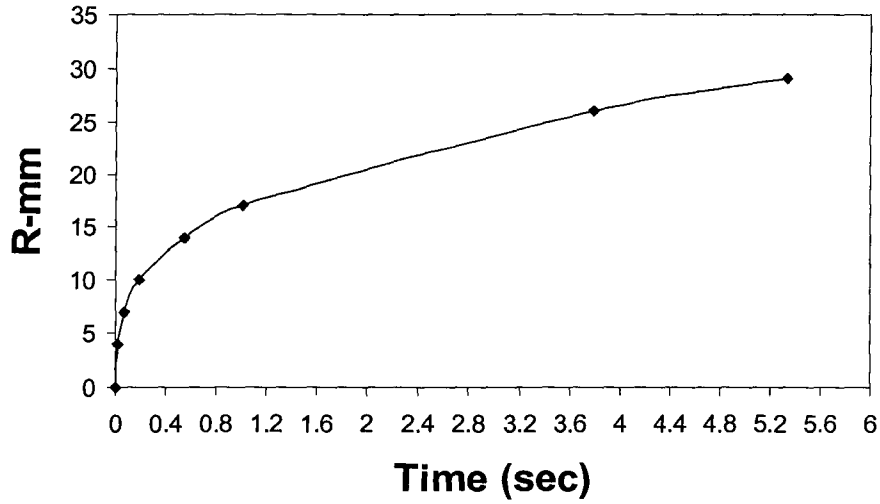

Figure 4.23. Estimated propagation of wetting front on the basis of power relation shown in figure 4.11 for Dj=3mm, Tsp=500, Tw=50, Vj=5m/sec.

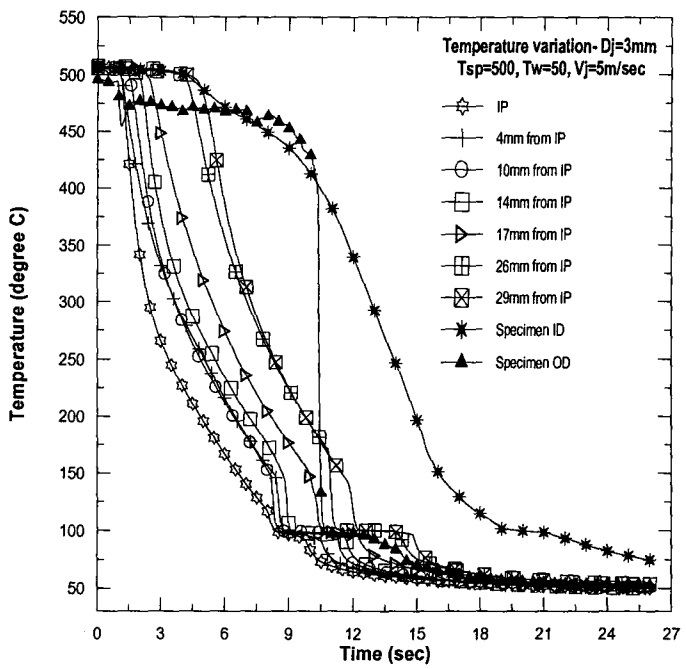

Figure 4.24. Transient cooling curves - Dj=3mm, Tsp=500, Tw=50, Vj=5m/sec.

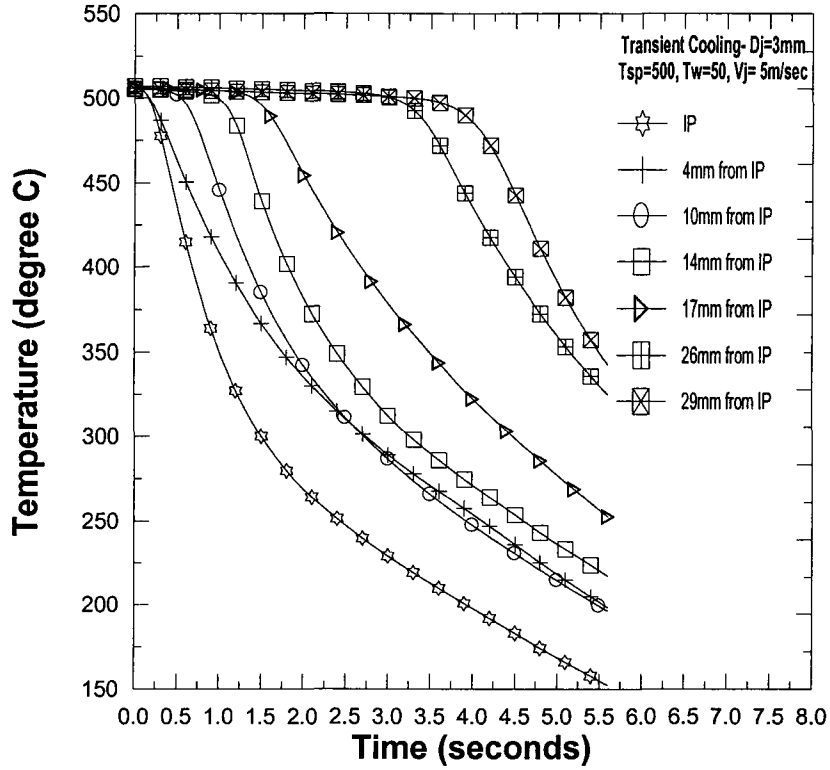

Figure 4.25: Transient temperature profiles for first 5.6 seconds - Dj=3mm, Tsp=500, Tw=50, Vj=5m/sec

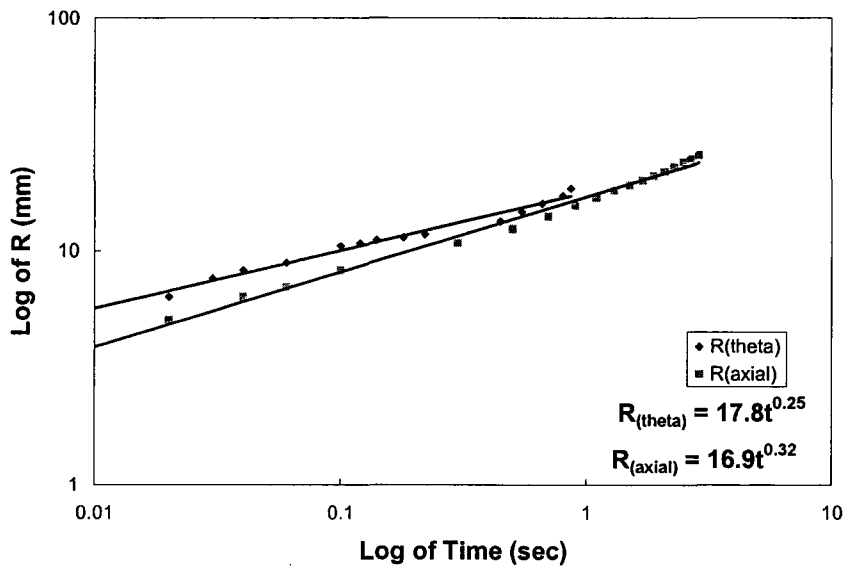

Figure 4.26: Comparison of propagation of wetting front – Dj=3mm, Tsp=500°C, Tw=50°C, Vj=5m/sec

Wetting front propagates to 4mm in 0.01 seconds, 10mm in 0.2 seconds according to figure 4.23 . It seems the boundary of wetting front reach at a distance of 4mm from IP in 0.073 seconds and at 10mm in 0.24 seconds according to figure 4.25 and from related data of thermocouple readings. According to figure 4.25, the wetting front propagates to 10mm in 0.24 seconds and thermocouple located at this point experiences a sharp decline in temperature. Temperature shown by thermocouple located at 4mm from IP at 0.24 seconds is 493.4°C.

Table 4.12 shows the comparison of the times the wetting front seems to reach a thermocouple location according to figures 4.23 and 4.25 .Time difference is low for thermocouples located within 10mm from the impingement point but is quite high for thermocouples located beyond that. Figure 4.26 shows a comparison of the propagation of wetting front in axial direction (R_{axial}) and that along the theta direction (circumferential) (R_{therta}) which indicates that propagation of wetting front along the theta direction is faster than that along the axial direction. Hence more water is directed in the theta direction and therefore higher heat transfer is attained in that direction which might explain the time difference observed by thermocouples shown in Table 4.12.

Table 4.13 shows the change in surface temperature at various thermocouple locations as wetting front propagates from IP towards thermocouple locations. Results reported in Table 4.13 show that as the wetting front reaches a location the temperature at that location drops sharply starting from 500°C (initial surface temperature) as the wetting front passes through.

Table 4.12: Comparison of times wetting front reaches location of thermocouples- Dj=4mm, Tsp=800°C, Tw=20°C, Vj=7.75m/sec.

Thermocouple distance from Impingement point (mm)	Time wetting front reaches according to figure 4.23(sec)	Time wetting front reaches according to figure 4.25(sec)	Time difference
4	0.01	0.073	0.063
10	0.2	0.24	0.04
14	0.55	0.75	0.2
17	1	1.2	0.2
26	3.6	3.25	0.35
29	5.3	3.9	1.4

Table 4.13 : Variation in Thermocouple readings from IP as wetting front propagates.

Stream wise location of thermocouple from IP (mm)	Temperature at times					
	0.073sec	0.24sec	0.75sec	1.2sec	3.25sec	3.9sec
4	500	493.4	433.5	390.3	279.5	201
10	-	500	480	418.9	280	257
14	-	-	500	483.6	300.2	250
17	-	-	-	500	363.4	274
26	-	-	-	-	500	444
29	-	-	-	-	-	500

Keeping in view the time difference as shown in Table 4.12, it can be concluded that the prediction of propagation of wetting front by using temperature readings is possible for a distance of up to 10 mm from the impingement point.

4.8. Effect of Surface Curvature.

In order to asses the effect of surface curvature on velocity of wetting fronts, present results were compared with those reported by Mitsutake and Monde [6] who investigated propagation of wetting fronts on flat surfaces as shown in figure 4.27 which shows:

- According to present study average velocity of wetting front reaching 38.4mm distance from Impingement point in 0.512 seconds with Dj=3mm, Tsp=250°C, Tw= 50°C as per figure 4.5 is.

  $V_1 = 38.4/0.512 = 75$ mm/sec.

- Average velocity of wetting front reaching 40 mm distance from impingement point in 4.6 seconds with Dj=2mm and under the same parameters reported in [6] on a flat surface is.

  $V_2 = 40/4.6 = 8.7$ mm/sec.

Hence ratio of the velocity of wetting fronts is given below:

$$\text{Velocity Ratio} = V_1 / V_2$$

$$= 8.62 \qquad (2)$$

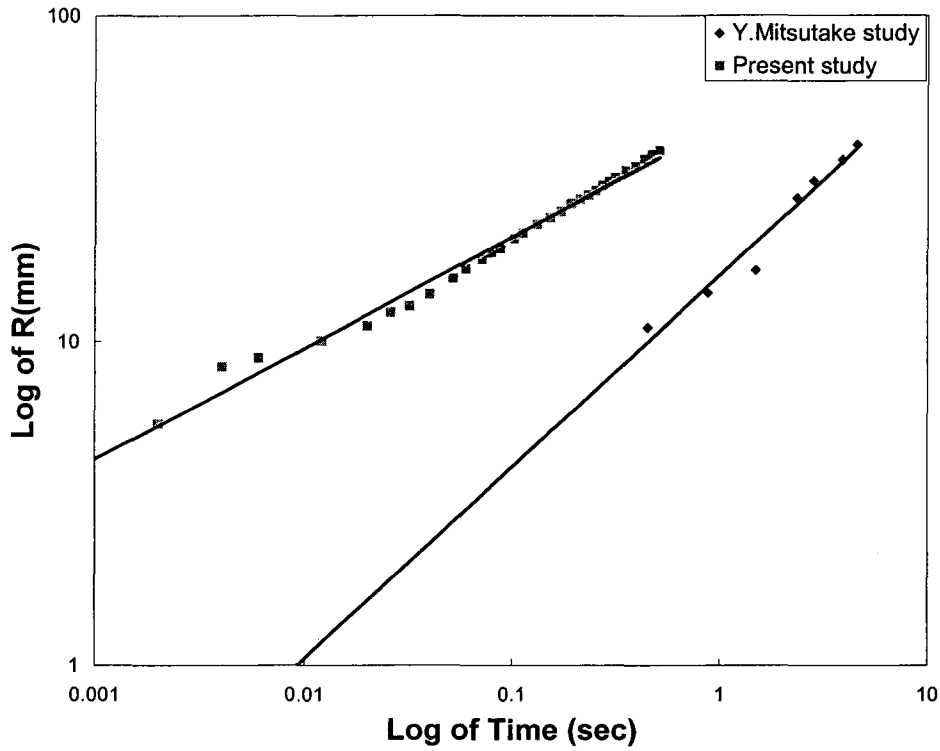

Figure 4.27: Comparison of Propagation of wetting fronts. (Present study and study by Y.Mitsutake).

Equation (2) indicates that the speed of wetting front in present study is very high as compared to that of experiments reported in [6]. Since the experiments are unsteady, the difference in velocity of wetting front might be attributed to two factors : size (mass) of specimen; and surface curvature. The effect of size of specimen can be examined by looking at the mass ratio. The mass ratio of the samples used in the present study and that used in [6] are given below:

$$\text{Mass ratio} = M_1 / M_2$$

$$= 1.4/4.2$$

$$= 0.33.$$

Mass ratio indicates that the specimen used during present study is one third of that used in[6].Applying the equation of lumped capacitance analysis for present study and [6]:-

$$\frac{T - T_\infty}{T_i - T_\infty} = \exp\left(-\frac{\tau}{\tau_c}\right) \tag{3}$$

Where: $\tau_c(\text{time constant}) = \frac{\rho CV}{hA}$, and ρ is specimen density, C is specific heat., V is specimen volume , h is heat transfer coefficient, T is surface temperature, T_i is Initial surface temperature, T_∞ is water temperature and A is specimen surface area (taken here as jet nozzle area).

Assuming that T_i, T, ρ, C and T_∞ are the same and applying equation (3) for both cases of present study and that of [6], the ratio of cooling time can be expressed as:

$$\text{Ratio of Cooling Times} = \frac{\tau_1}{\tau_2} = \frac{\tau_{c1}}{\tau_{c2}} = \frac{M_1}{M_2}.\frac{A_2}{A_1} \tag{4}$$

$$= 0.33 \text{ x } \left(\frac{2}{3}\right)^2$$

$$= 0.147.$$

$$\text{then} \quad \frac{\tau_2}{\tau_1} = 6.8 \tag{5}$$

In determining the above ratio of cooling times in equation (5) the difference in jet diameter used in the present study and jet diameter used in [6] has been taken into consideration by using the respective jet nozzle diameters for determining the respective specimen areas to be cooled. Thus, value given by equation (5) is an

indication of the ratio of velocities of wetting front of present study and that of [6] taking into account the difference in specimen areas and specimen masses.

Ratio given by equation (2) indicates the ratio of velocities of wetting front taking into consideration the difference in specimen area, specimen mass and specimen surface profile used in the present study and that used in [6]. Hence, the difference between values in equations (2) and (5) i.e. 8.6 and 6.8, can therefore be used to evaluate the effect of surface curvature. The difference between these shows that surface curvature has resulted in an increase in propagation of wetting front by about 26%.

Chapter 5

Conclusions

An experimental work to study the effect of jet velocity, jet water temperature, jet nozzle diameter, specimen surface temperature and specimen curvature on propagation of wetting front of hot cylindrical specimen surfaces of stainless steel pipe was conducted. Transient temperature drop of thermocouples located at stream wise locations were used in an effort to predict the propagation of wetting front. Power law correlating radius of wetting front and time was found to be valid for curved surfaces. Results and analytical discussions are presented in chapter 4. A summary of these investigations is given.

Effect of Water temperature, Jet Velocity and Jet Diameter:

Propagation of wetting front is strongly affected by changes in water temperature, jet velocity and jet diameter. Average velocity of wetting front increases by 10 to 300% with decrease in water temperature from 80 or 75 to 20°C depending upon jet velocity, jet diameter and specimen surface temperature.

Effect of Specimen Surface Temperature:

Initial specimen surface temperature has strong effect on propagation of wetting front. Average velocity of wetting front increases from 6 to 190mm/sec (3000% increase) as initial specimen surface temperature is decreased from 800 to 250°C.

Effect of surface curvature:

Effect of surface curvature on propagation of wetting front was determined by comparing the results of presented study with those reported in [6] for flat surface. Surface curvature was found to have a significant effect on propagation of wetting front. The velocity of wetting front increased by 26% (8.7 to 75mm/sec) depending on difference of specimen mass, specimen area and surface curvature.

Prediction of Propagation of Wetting Front with Transient Temperature Measurements:

The temperature readings from thermocouples embedded in the specimen were used to predict the propagation of wetting front which was found to be valid for a distance of 10mm from impingement point. Beyond 10mm from impingement point the prediction of propagation of wetting front does not hold good due to decrease in the rate of heat transfer associated with loss of momentum, increase in water temperature and high heat transfer rate in circumferential direction.

Chapter 6

Recommendations

In order to further study the propagation of wetting front, effect of various other parameters should be studied and the range of existing parameters should be increased in a systematic way, like:

- Angle of jet inclination to vertical line of specimen surface.
- Effect of more than one jet.
- Effect of jet-surface distance.
- Effect of jet or specimen rotation.
- Increase in range of Jet velocities.
- Increase in range of Jet diameters.
- Change of surface curvature by using specimens of different sizes.
- Effect of thermal conductivity by using specimens of different materials.

Bibliography

1. Line, S., and Sefiane,K., "Prospects of confined flow boiling in thermal management of microsystems", Journal of Applied Thermal Engineering, Vol.22, pp.825-837, 2002.
2. Liu, X., and Lienhard, J.H.V., "Extremely high heat flux removal by subcooled Liquid Jet Impingement", Journal of American Society of Mechanical Engineers, Heat Transfer Division, Vol.217, pp.11-20, 1992.
3. Wolf, D.H., Incropera, F.P., and Viskanta, R., "Local jet impingement boiling heat transfer", International journal of Heat Mass Transfer, Vol. 39, pp.1395-1406, 1996.
4. Liu, Z.D., Fraser, D., Samarasekera, I.V., and Lockhart, G.T., "Experimental observations and modeling of thermal history within a steel plate during water jet impingement", Journal of Canadian Metallurgical Quarterly, Vol.41, No.1, pp. 75-86, 2002.
5. Carbajo, J.J., "A study on the rewetting temperature", Journal of Nuclear Engineering & Design, Vol. 84, pp.21-52, 1985.
6. Mitsutake Y., and Monde, M., "Heat transfer during transient cooling of high temperature surface with an impinging jet", Journal of Heat and Mass Transfer, Vol.37, pp. 321-328, 2001.
7. Mudawar, I., and Wadsworth, D.C., "Critical heat flux from a simulated chip to a confined rectangular impinging jet of dielectric liquid", International Journal of Heat and Mass Transfer, Vol.33,No.6, pp.1465-1479,1991.

8. Faggini, S., and Grassi, W., "Round liquid jet impingement heat transfer: local nusselt numbers in the region with non zero pressure gradient", Proceedings of International Heat Transfer conference, pp. 197-202,1990.
9. Anno, J.N., "The Mechanics of liquid jets", D.C. Health and Company ,Massachusetts, USA, 1977.
10. Nevins, R.G., "Cooling Power of an Impinging Jet", Ph.D.dessertation, 1953.
11. Copeland, R.J., "Boiling heat transfer to a water jet impinging on a flat surface", PhD. dissertation, Southern Methodist University, 1970.
12. Ruch, M.A., and Holman, J.P., "Boiling heat transfer to Freon -113 jet impinging upward onto a flat heated surface", International journal of heat and mass transfer, Vol.18, pp: 51-60, 1974.
13. Piggott, B.D., White, E.P., and Duffey, R.B., "Wetting delay due to film and transition boiling on hot surfaces", Journal of Nuclear Engineering and Design, Vol.36, pp.169-181,1976.
14. Pais, M.R., and Chow, L.C., "Multiple jet impingement cooling", Journal of thermo-physics and heat transfer, Vol.7, No.3, pp.435-440, July-Sept.1993.
15. Liu, Z., and Zhu, Q., "Prediction of critical heat flux for convected boiling of saturated water jet impinging on the stagnation zone", Journal of heat transfer, Vol.124, No.6, pp.1125-1130, December 2002.
16. Liu, Z., Tong, T., and Qiu, Y., "Critical heat flux of steady boiling for sub-cooled water jet impingement on the flat stagnation zone", Journal of heat transfer, Vol.126, No.2, pp.179-183, April 2004.

17. Akimenko, A.D., "Features of film boiling in surface water cooling", NASA report T-T-F-10184, N66-33689, 1966.

18. Ishigai, S., Nakanishi S., and Ochi, T., "Heat transfer to impinging plane water jet", Proceedings of International Heat Transfer Conference, Vol. 1, pp. 444-450, 1978.

19. Miyaska, Y., Inada, S., and Owase, Y., "Critical Heat flux and sub-cooled nucleate boiling in transient region between a two-dimensional water jet and a heated source", Journal of chemical engineering of Japan, Vol.13, No.1, pp.29-35, 1980.

20. Ochi, T., Nakanishi,S., and Ishigai, S., "Cooling of a hot plate with an impinging circular water jet", Proceedings of multi-phase flow and heat transfer*III,* pp. 671-681, 1983.

21. Tseng, A.A., Chen, S., and Westgate, C.R., "Determination of local heat transfer coefficients for modeling rolling process", Journal of ASME Material division Vol.3, pp.51-64, 1987.

22. Han, F., Chen, S., and Chang, C., "Effect of surface motion on liquid jet impingement heat transfer", Journal of ASME Heat Transfer division, Vol.180, pp.73-81, 1991.

23. Chen, S., Kothari, J., and Tseng, A.A., "Cooling of a moving plate with an impinging circular water jet", Journal of Experimental Thermal and Fluid Science, Vol. 4, No.3, pp.343-353, May 1991.

24. Kumagai, S., Suzuki, S., and Sano, Y., "Transient cooling of a hot metal slab by an impinging jet with boiling heat transfer", Proceedings of the ASME-JSME Thermal engineering joint conference, Vol.2, pp. 347-352,1995.

25. Liu, Z., and Wang, J., "Study on film boiling heat transfer for water jet impinging on high temperature flat plate", International Journal of heat and mass transfer, Vol.44, pp:2475-2481,2001.

26. Hall, D.E., Incropera, F.P., and Viskanta, R., "Jet impingement boiling from a circular free surface jet during quenching: Part 1-single phase jet", Journal of heat transfer, Vol.123, pp.901-910, 2001.

27. Mondey, M., "Critical heat flux in saturated forced convective boiling on a heated disk with an impinging jet", Journal of Heat Transfer, Vol.109, No.4, pp 398-401, 1987.

28. Hauksson, A.T., Fraser, D., Prodanovic, V., and Samarasekera, I., "Experimental study of boiling heat transfer during sub-cooled water jet impingement on flat steel surface", Journal of Ironmaking and Steelmaking, Vol.31,No.1, pp.51-56,2004.

29. Taylor, J.R., "Introduction to Error analysis - A study of uncertainties in physical measurements", Mill Valley, California, University Science Books,1982.

Appendix- 1
Immersion Heater Sizing

C_p *(steel)* = 0.12 BTU/lb-°F, C_p *(water)* = 1 BTU/lb-°F

t_h= Water heat up time = 5 hrs

Exposed surface area of the tank =A_{st}= $\left(\pi DH + 2\pi r^2\right)$

D= Diameter of water tank. = 22in= 1.833 ft

H= Height of water tank= 3 ft

r = Radius of water tank= 11 in. = 0.9166 ft.

Hence: A_{st} = 22.52 ft^2.

Approximate initial ambient temperature of water inside the tank =T_{in}=21°C= 70°F.

Max. required temperature of water inside water tank= T_{req}= 80°C= 176°F.

ΔT = Temperature difference for heating = T_{req} - T_{in}

= 106°F.

= approx. 110°F.

Mass of water in Tank = M_w= Density of Water/Volume of water. = d_w/V_w

V_w= $\frac{\pi}{4} D^2 H$ =7.916 ft^3 =59.22 Gallons.

d_w = 8.33 lbs/Gallons

M_w =493.33 lbs.

Q_w= Energy required to heat up the water = $\frac{M_w C_p(water)\Delta T}{3421}$ = 15.86 kWh. (1)

Mass of steel tank = M_{st} = Density of steel /Volume of steel tank. = d_{st}/V_{st}

d_{st} = 0.286 lbs/in^3 .

Appendix- 1(Continued)
Immersion Heater Sizing

$V_w = \frac{\pi}{4}(D_{out}^2 - D_{in}^2)H = 164.16$ ft^3.

M_{st} =46.22 lbs.

Q_{st} = Energy required to heat up the steel tank = $\frac{M_{st}C_p(steel)\Delta T}{3421}$ =0.178 kWh. (2)

Tank surface heat loss at 80°C (176°F) = T_{hl} = 71 watts/ft^2. (From Caloritech. Inc Hand book Page 89. Figure- 2).

Average Tank surface loss = $\frac{A_{st}T_{hl}t_h}{2x1000}$ = 3.997 kWh (3).

Safety factor = 0.20x (15.86+0.178+3.997) = 4 kWh (4).

Total Heat Energy Requirement = (1) + (2) + (3) + (4)

= 24 kWh.

Power Required = 24/5 = 4.8 kW.

Appendix -2
Pump sizing for the System

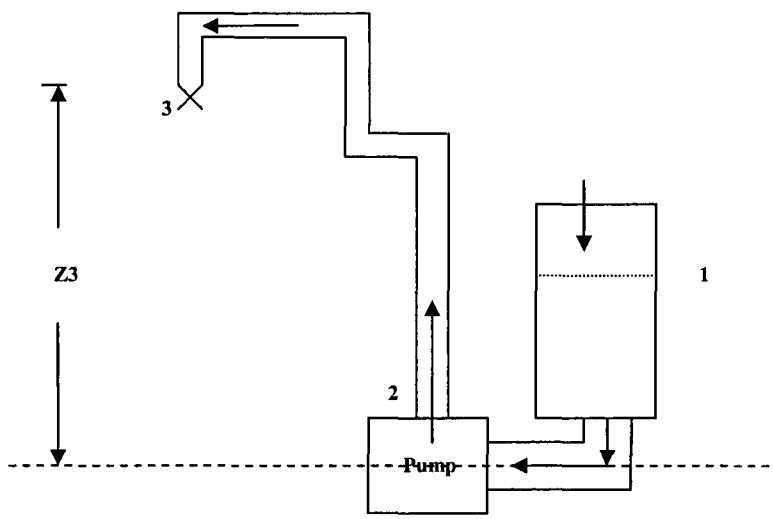

Simplified system diagram.

The simplified form of Energy equation for steady flow from points 2 and 3 is given below taking the Inlet of Water Pump as the reference:

$$\frac{P_2 - P_3}{\rho} = h_{major} + h_{minor} + gz_3 \qquad (1)$$

P_3 = Atmospheric Pressure.

h_{major}= Major losses = $h_{major1} + h_{major2} + h_{major3}$ (2)

h_{major1} = Losses due to 1in. Nominal diameter Schedule 40 SS pipe. (d_{p1}= 0.0266m)

h_{major2} = Losses due to ½ in. Nominal diameter Schedule 40 SS pipe. (d_{p2}= 0.0158m)

h_{major3} = Losses due to the Nozzle (Nozzle diameter= d_n =3mm)

Minimum Flow = 0.557 GPM = 3.5×10^{-5} m^3/sec.

V_{p1}= Velocity in pipe 1 = Q/A_{p1} = 0.06298 m/sec.

V_{p2}= Velocity in pipe 1 = Q/A_{p2} = 0.178 m/sec.

Re= Reynolds No. = $\frac{V_p x d_p}{\upsilon}$, where υ = Kinematic Viscosity = 1 x 10^{-6} m^2/sec.

Re_{p1}= Reynolds No. in Pipe 1 = 1675.268 < 2000 --- Flow is laminar in dp1= 0.0266m.

Re_{p2}= Reynolds No. in Pipe 2 = 2812.4 > 2000- Flow is in Critical zone in d_{p2}= .0158m

L_{p1} = Length of Pipe 1 = 77in = 1.9558 m.

L_{p2} = Length of Pipe 2 = 77in = 1.88 m.

f_{p1} = Friction Factor for pipe 1= 64/ Re_{p1} =0.038.

f_{p2} = Friction Factor for pipe 2= 0.045 (from Page A-25, Flow of Fluids by M/sCRANE).

K_3 = Resistance Coefficients for Nozzle.

Loss Coefficient for pipes = $K_p = \frac{f_p x L_p}{d_p}$

K_{p1} = 2.8 & K_{p2} = 5.35 .

$K_3 = \frac{1-\beta^2}{C^2\beta^4}$, (from Page A-20, Flow of Fluids by M/s CRANE).

Diameter of pipe before entering the converging are of nozzle = d_{p3}= 0.4635 in.

Where $\beta = d_n/d_{p3}$ = 0.1898,

C for ½ in nominal diameter pipe with Reynolds no. of 2812.4 = 0.94.

K_3 = 840.67

$h_{major} = K_p \frac{V_p}{d_p}$, therefore : h_{major1} = 5.55 x 10^{-3} , h_{major2} = 0.0848.

$h_{major\,3} = 13.3.$

$h_{major} = h_{major1} + h_{major2} + h_{major\,3} = 13.39.$

Minor Losses:

$$h_{minor} = = K_{minor} \text{ x } \left(V_p^{\,2} / 2 \right)$$

h_{minor1} = Loss at entrance from Pump to d_{p1}

$K_{minor\,1} = 0.5$ (from Page 324, Principles of Fluid Mechanics by Alexandrou).

$h_{minor1} = 9.9 \text{ x } 10^{-4.}$

h_{minor2} = Loss at T-junction on d_{p1}.

$K_{minor\,2} = 20 f_t = 20 \text{ x } 0.023 = 0.46$ (from Page A-26, Flow of Fluids by M/s CRANE)

$h_{minor2} = 9.122 \text{ x } 10^{-4.}$

h_{minor3} = Loss due to Ball Valve on d_{p1}

$K_{minor\,3} = 3 f_t = 3\text{x } 0.023 = 0.069$ (from Page A-26 & A-28, Flow of Fluids by M/s CRANE)

$h_{minor3} = 1.36 \text{ x} 10^{-4}.$

$h_{minor\,4}$ = Loss due to 90° bend on d_{p1}

$K_{minor\,4} = 30 f_t = 30 \text{ x } 0.023$ (from Page A-26 & A-29, Flow of Fluids by M/s CRANE).

$h_{minor\,4} = 1.36 \text{ x} 10^{-3}.$

$h_{minor\,5}$ = Loss at the entrance in the 4 way distributor.

d_{pd} = diameter of 4-way distributor pipe = 0.0525 m.

$K_{minor\ 5} = \left(1 - \frac{d_{p1}^{\ 2}}{d_{pd}^{\ 2}}\right)^2 = 0.5525.$ (From Page 2-11, Flow of Fluids by M/s CRANE)

$h_{minor\ 5} = 1.09 \times 10^{-3}$.

$h_{minor\ 6}$ = Loss at the exit from the 4 way distributor pipe.

$K_{minor\ 6} = \left(1 - \frac{d_{p2}^{\ 2}}{d_{pd}^{\ 2}}\right) = 0.455.$ (From Page 2-11, Flow of Fluids by M/s CRANE)

$h_{minor\ 6} = 7.2 \times 10^{-3}$.

$h_{minor\ 7}$ = Loss due to Globe Valve on d_{p2}.

$K_{minor\ 7} = 340 f_t = 340 \times 0.027 = 9.18$ (from Page A-26 & A-27, Flow of Fluids by M/s CRANE).

$h_{minor\ 7} = 0.145$

$h_{minor\ 8}$ = Loss due to T-junction on d_{p2}.

$K_{minor\ 8} = 20 f_t = 20 \times 0.027 = 0.54$ (from Page A-26, Flow of Fluids by M/s CRANE)

$h_{minor\ 8} = 8.5 \times 10^{-3}$.

Total Minor Losses = $h_{minor} = 0.165$.

From equation (1);

$\frac{P_2 - P_3}{\rho} = h_{major} + h_{minor} + gz_3$, where z3 = 78 in = 1.98 m.

$\frac{P_2 - P_3}{\rho} = 13.39 + 0.165 + 19.404 = 32.959$ m2/sec^2.

Let W_t = Theoretical Power of Pump.

W_a = Actual Power of Pump.

Efficiency = $\acute{\eta} = W_t / W_a$

$W_a = \frac{\rho Q}{\eta}\left(\frac{P_2 - P_1}{\rho}\right)$ where $P_1 = P_3$, then,

$W_t = \rho Q\left(\frac{P_2 - P_3}{\rho}\right)$, $W_t = 1.15$ Watts.

W_a = ½ HP= 0.373 kW.

The Actual Power of the Pump is very high as compared to theoretical required Power, which is understandable for the possible expansion of the project to multiple nozzles etc.

Performance curves for Centrifugal Pump.

CDU4 200/5-½HP Synchronous Speed: 1725 RPM Size: 1 x 1½ x 5 11/16